



CHALMERS



Realtime estimation of tyre-road friction for vehicle state estimator

Master's thesis in Automotive Engineering

JAKUB PROKEŠ

MASTER'S THESIS IN AUTOMOTIVE ENGINEERING

Realtime estimation of tyre-road friction for vehicle state estimator

JAKUB PROKEŠ

Department of Applied Mechanics
Division of Vehicle Engineering and Autonomous Systems
CHALMERS UNIVERSITY OF TECHNOLOGY

Göteborg, Sweden 2015

Realtime estimation of tyre-road friction for vehicle state estimator
JAKUB PROKEŠ

© JAKUB PROKEŠ, 2015

Master's thesis 2015:11
ISSN 1652-8557
Department of Applied Mechanics
Division of Vehicle Engineering and Autonomous Systems
Chalmers University of Technology
SE-412 96 Göteborg
Sweden
Telephone: +46 (0)31-772 1000

Chalmers Reproservice
Göteborg, Sweden 2015

Realtime estimation of tyre-road friction for vehicle state estimator
Master's thesis in Automotive Engineering
JAKUB PROKEŠ
Department of Applied Mechanics
Division of Vehicle Engineering and Autonomous Systems
Chalmers University of Technology

ABSTRACT

Tyre-road interaction is the major source of forces by which the road vehicle can be controlled in its speed and direction. These forces are generated by either steering the wheels (lateral tyre force), applying driving or braking torque on wheels (longitudinal tyre force), or both. These forces are limited in magnitude and crossing this limit can in the worst case lead to the loss of control. Therefore it is of highest interest to keep the tyre forces below the limit. The limit is commonly denoted as the tyre-road friction coefficient, and it relates the maximal achievable resulting horizontal tyre force (lateral, longitudinal or their combination) with the actual vertical load on the respective tyre. Knowledge of the tyre-road friction coefficient would thus allow to limit the requested control forces so that the loss of control is avoided. The goal is thus to estimate the tyre-road friction coefficient in realtime during operation of the vehicle.

In this thesis some of the possible ways to estimate the friction coefficient, that has been published earlier, are reviewed. In this thesis the possible methods are limited to those that use in-vehicle measurements and observation of the dynamic behaviour of vehicle and its tyres. Models of dynamic behaviour of tyre to either lateral or longitudinal load is in particular used to identify the friction coefficient. As a model to match the real tyre response a brush tyre model is used and no *a priori* knowledge of tyre parameters is used.

The operation of the vehicle is described as a state machine of specific driving situations, hereafter called driving modes. In this case the vehicle under investigation is the Volvo FMX rigid truck in 8x4 configuration. Cornering and pure longitudinal acceleration driving modes have been briefly evaluated using a simulation model for possibility of friction estimation. The pure longitudinal acceleration driving mode proved to be more viable option at the time, especially due to rollover tendency of trucks. A recursive estimation algorithm based on an Extended Kalman Filter (EKF) was developed. Tuning of the EKF is discussed with respect to necessity of sufficient excitation of the tyre in order to extract information about the friction. The performance of the estimator was evaluated in a simulation model of the whole vehicle with added noise on the input signals to the estimator. In these conditions the estimator is able to successfully predict the tyre-road friction coefficient with sufficient tyre excitation.

Experimental tests were performed using the investigated vehicle to gather real input data for the estimator. The processing of the real vehicle measurements is discussed with respect to the estimator functionality. The real data does not match the expected tyre response characteristics which prevent the estimator from predicting the tyre-road friction coefficient. The estimator can however still indicate the low tyre-road friction within a short time interval after saturation of the tyres. Testing of the estimator implemented as a realtime solution in the embedded hardware has not been done due to the issues with in-vehicle measurements and signal processing.

The uncertainty of the inputs to the estimator based on experimental data has been evaluated and a sensitivity of the inputs has been analysed.

The sensitivity of the estimator to the excitation conditions is discussed and conditions for when the estimator can update the estimates are introduced. A process to identify the sufficient excitation is developed and tested in the simulation model. This process can serve as a base for adaptive tuning of the EKF estimator. The functionality of this process has not been evaluated in the conditions of real inputs.

Keywords: tyre-road friction, estimation, realtime

PREFACE

This thesis report is a documentation of a master project, which is a final requirement to complete a master study program Master in Automotive Engineering (MAE). MAE is international joint master program organized by Czech Technical University (CTU) in Prague in collaboration with different universities around the world. This thesis completes the specialisation specialisation Vehicle Dynamics and Clean Driveline Control Systems, where first year has been taught at CTU in Prague and the second year at HAN University of Applied Sciences (HAN) in Arnhem, The Netherlands.

The last semester of MAE master program is entirely devoted to a master project, which shall be in the best case conducted within an automotive OEM/supplier company or research institute. In this case the project was proposed by Volvo Group Trucks Technology (Volvo GTT) located in Gothenburg, Sweden, that extensively cooperates with local Chalmers Technical University. The master thesis project is therefore officially organised by Chalmers, Volvo GTT provided the assignment and most of the resources needed for working on the project. The project has to meet the requirements of Chalmers, Volvo GTT and HAN.



For formal purposes this thesis is published in two variants:

- with Chalmers cover and title page published by Chalmers under number 2015:11
- with HAN cover and title page published by HAN

Content-wise both versions are exactly the same.

ACKNOWLEDGEMENTS

I would like to express my gratitude to my supervisors, Leo Laine from Volvo GTT, Anton Albinsson from Chalmers University of Technology and Karel Kural from HAN University of Applied Sciences. I am happy for having the all-time positive support and motivation from Leo. Weekly discussions with Anton then helped me to explore new ideas where the development shall go and how. Karel helped me to keep things aligned with the requirements of HAN. Thanks to all for careful reading and feedback that helped me improve my report.

Special thanks goes to Tom Bell and FISITA organisation, for awarding me with the FISITA Travel Bursary support.

Thanks to all the great people - specialists in Volvo GTT, especially Carl-Johan Hoel, who helped me keep on track and think about problems from different perspective. Thanks Johan Eklöv for answering a lot of questions I had during my thesis. And there are others from Volvo GTT who gave me insight into specific fields - thank you Niklas, Fredrik, Kristoffer, Mats, Markus and Martin. My thanks also goes to the other Master thesis students who I met in the department at Volvo GTT. Our talks helped me see things from a different perspective. I am also glad that we have found the time to have fun together. Thank you Abhishek, Andrea, Petr, Robert and Syarifah for being there.

For the short time I have spent there, I found the department of Vehicle Engineering and Autonomous Systems at Chalmers as a very nice place, especially due to the kind people. Thanks to all the researchers and PhD students from the department for nice and inspiring talks during coffee or lunch breaks. Special thanks goes to Bengt Jacobson, who, although not being directly involved, was always ready to help with vehicle dynamic specific problems, or the organisation of the project.

During my stay abroad I realised I miss some special people - my friends, thank you for being close, although physically so far. Thank you Martina for surviving my long stay away. Your words always help me realise what is important. Thank you mum and dad, for making all this possible and for the never-ending support.

CONTENTS

Abstract	i
Preface	iii
Acknowledgements	v
Contents	vii
Nomenclature	ix
1 Introduction	1
1.1 Project background	2
1.2 Problem motivating the project	2
1.3 Envisioned solution	2
1.4 Objectives	2
1.5 Deliverables	3
1.6 Limitations	3
1.7 Report structure	3
2 Literature review	4
2.1 Tyre models	4
2.2 Friction estimation approaches	9
2.3 Requirements of real-time processing	12
2.4 Recursive estimation algorithms	13
3 Methodology and tools	16
3.1 Model based development	16
3.2 Description of investigated vehicle	17
3.3 Vehicle simulation model	18
4 Estimator development	20
4.1 Identification of driving modes	20
4.2 Mild steering (Mode M3)	23
4.3 Severe steering (Mode M4)	29
4.4 Longitudinal tyre force excitation	29
5 Results of development and discussion	58
5.1 Estimation using lateral tyre excitation	58
5.2 Estimator using longitudinal tyre excitation	59
6 Conclusions and future work	60
6.1 Project conclusions	60
6.2 Future work	61
Bibliography	62
A Definitions of vehicle variables	65
A.1 Longitudinal acceleration	65
A.2 Tyre slip	65
B Magic Formula tyre model used in VTM	67
B.1 Pure lateral load	68
B.2 Pure longitudinal load	69
B.3 Combined load	70

C Results of testing	72
C.1 Intensive braking on dry road	72
D Documentation to the appended files	74
D.1 Evaluation of friction utilisation needed for accurate friction estimation	74
D.2 Implementation of the recursive friction estimation algorithm	75
D.3 Testing performance of the estimator	76
D.4 Measure of non-linearity evaluation	78
D.5 Experimental data processing	78

Nomenclature

a_X	longitudinal acceleration of the vehicle CoG (ISO8855 5.1.11)
$a_{X,IMU}$	longitudinal acceleration measured by vehicle IMU
$F_{T,usage,req}$	tire requested usage by applied driving or braking torque, see equation (4.5)
T_{drag}	engine drag torque - resistance of the engine at no load
CoG	vehicle centre of gravity
ADAS	Advanced Driver Assistance System
AEBS	Advanced Emergency Braking System
α	tyre slip angle
MoN	Measure of Nonlinearity
A_{req}	acceleration request, page 20
a_Y	vehicle lateral acceleration
B_{req}	brake request, page 20
C_d	vehicle aerodynamic resistance coefficient
C_R	dynamic rolling circumference
$\dot{\delta}_{s,w.}$	derivative of steering wheel angle - velocity of steering wheel [rad/s]
δ_{req}	steering angle request, page 20
D_{lock}	differential lock flag
EKF	Extended Kalman Filter
EPS	Electric Power Steering
ESP	Electronic Stability Program
φ	roll angle
f_r	tyre rolling resistance coefficient
F_{XT}	tyre longitudinal force
F_{YT}	tyre lateral force
J_{wz}	wheel rotational inertia
λ	road inclination angle, page 65
μ_{T-R}	maximum tyre-road friction coefficient , see equation (1.1)
μ_{util}	friction utilisation in percent of maximum achievable tyre-road friction, see equation (4.6)
M_{ZT}	tyre aligning torque
ω_W	wheel-spin angular velocity, page 65
ω_{W0}	reference wheel-spin angular velocity, page 65
p_{br}	brake pressure
r_{dyn}	dynamic rolling radius
σ_x	theoretical longitudinal slip, see equation (A.6)
S_X	longitudinal tire slip according to ISO8855, see equation (A.5)
$T_{br,ij}$	brake torque on vehicle wheel
$T_{br,req}$	requested brake torque on vehicle wheel
$T_{dr,ij}$	drive (propulsion) torque on vehicle wheel
$T_{dr,req}$	requested drive (propulsion) torque on vehicle wheel
θ	pitch angle

θ	vehicle pitch angle relative to ground plane, page 65
θ_{road}	vehicle pitch angle relative to road plane, page 65
v_X	vehicle longitudinal velocity
v_r	linear longitudinal velocity of the tyre in the wheel ground contact point
v_Y	vehicle lateral velocity
v_Z	vehicle vertical velocity

1 Introduction

Road transport keep people and goods moving. Every day more than hundreds of thousands of vehicles drive on roads all around the world. The road traffic density increases and thus also the risk of accident increases since the human driver's capabilities are limited. At the same time as the traffic density is increasing, one of the most important goals of vehicle manufacturers, road authorities and governments around the globe is to reduce the number of fatalities. To help the driver with the more and more demanding task of driving, electronic driving assistance systems have been introduced commonly called Advanced Driver Assistance Systems (ADAS). Number of such systems rise as the performance of the electronic devices rapidly grows and their price decreases. Furthermore the development of sensors allow use of information that has not been present on board the vehicle in the past.

The ADAS could be of various types, one of them that directly influence the behaviour of the vehicle by application of control forces, like Advanced Emergency Braking System (AEBS). AEBS automatically starts braking the vehicle should the collision to vehicle ahead be unavoidable. This system is going to be mandatory on all heavy vehicles produced after 1st November 2015 [1]. Similarly the Electronic Stability Program (ESP) applies brakes at individual wheels to prevent the driving of losing control of the vehicle. Any such control system of road vehicle can only affect the vehicle heading and velocity by horizontal tyre forces.

The horizontal tyre forces are however limited and if the limits are exceeded, wheel locks or slides and cannot provide any further control force. It is therefore of highest interest to know the limits, especially in critical situations, where the limits can be easily reached. The limit can be expressed as the tyre-road friction coefficient μ_{TR} . The limit for the horizontal tyre force can then be expressed as

$$F_{horizontal,max} \leq \mu_{TR} \cdot F_{vertical} \quad (1.1)$$

where $F_{horizontal,max}$ represents maximal resultant of longitudinal force F_{XT} (braking, driving) and lateral force F_{YT} (cornering), $F_{vertical}$ is then actual vertical load on the tyre. The maximum tyre-road friction is mainly affected by the road conditions. Typical tyre behaviour under different road conditions can be seen in Figure 1.1. Different tyres can then achieve different level of tyre-road friction on the same road conditions. Besides that it is affected by many other vehicle-related parameters that are changing in time.

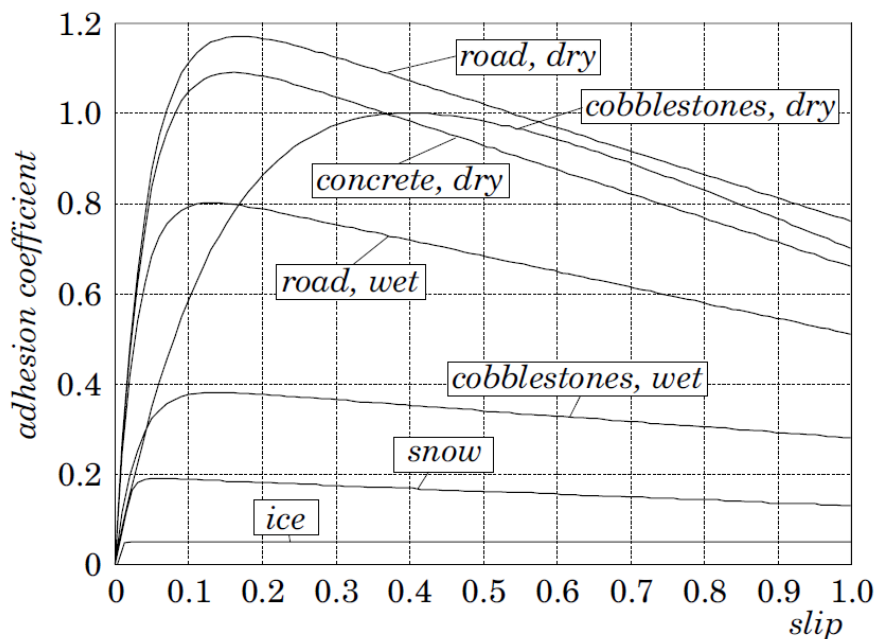


Figure 1.1: Typical friction (adhesion) coefficient of vehicle tyre for different road properties [2]. Different types of tyres can show different quantities, while the qualitative behaviour applies generally.

1.1 Project background

This thesis is conducted in collaboration Volvo Group Trucks Technology. Safety is Volvo's core value and the development of new Volvo products is driven by the vision of zero accidents [3]. Trucks produced by Volvo are nowadays equipped with number of motion control systems and the number of such systems is further increasing. The vehicle can be controlled by steering the wheels on one or multiple axles (producing lateral tyre force), by application of driving or braking torques on wheels (producing longitudinal tyre force), or both. Trucks produced by Volvo can have 4, 6, 8 or even 10 tyres on a rigid vehicle (without trailer). That gives a large solution domain of how to distribute the control forces over all tyres of the vehicle. One way to solve this is to use Control Allocation [4], another can be rule based coordination. The actual tyre-road friction can significantly affect the distribution process as the limit tyre friction can change in time and it can differ for each wheel. In that case the knowledge of tyre-road friction would allow the distribution process to limit how braking, propulsion and steering actuators are used, in order to efficiently use tyre capabilities.

1.2 Problem motivating the project

The main motivation is the road traffic safety. Information about the tyre-road friction can improve the active safety functions and thus also the road traffic safety. The already mentioned AEBS system can be used as an example. The system shall automatically brake in order to avoid or mitigate collision with the object in front. The vehicle thus has to evaluate the distance of the object in front of it and if it is decreasing under safe margin it has to warn the driver. If the driver doesn't react on the warnings and the collision is almost unavoidable the system has to apply brakes. The most common mean how to decelerate the vehicle is by using longitudinal tyre forces. In case of driving on a road with low friction, the available longitudinal tyre forces can be less than one fourth of what would be available on the road with high friction. Therefore also the longitudinal deceleration can be less than one fourth and the stopping distance would be more than four times longer. Thus the margin left for braking would not be enough and a collision will not be avoided.

1.3 Envisioned solution

To provide the information about tyre-road friction coefficient, a system that can evaluate it on board the vehicle should be developed. The system should be able to adapt to the effects of changing road conditions and/or vehicle parameters. In this case it is envisioned that the system uses the observation of the behaviour of tyres.

1.4 Objectives

Brief research before start of the project show that there are different methods for friction estimation. A literature review of known method for friction estimation should be conducted to explore these methods more in detail. One of the methods has to be selected, assessed in simulation model and implemented in the test vehicle.

Research questions that is be covered in this project are:

- In which situations can the friction be estimated?
- What methods for friction estimation are known?
- How much excitation is needed to have an accurate estimation?
- What is preventing an accurate friction estimation in a real vehicle today?
- How fast the friction can be estimated? How fast can change in friction be detected?

1.5 Deliverables

- Review of possible methods how to estimate friction
- The estimation algorithm implemented in MATLAB Simulink
- Evaluation of estimator performance in simulations
- Evaluation of the estimator performance with experimental data

1.6 Limitations

Volvo offers enormous variety of truck configurations. This project will be limited to a specific variant and possible variability will be kept in mind for possible extension in future. The truck used in this project is Volvo FMX – an 8x4 (eight wheels of which 4 are propelled) construction truck without trailer. The available input (excluded for project to derive - provided by Volvo GTT) will be vehicle longitudinal speed v_x , wheel rotational speed $\omega_{W,i}$ and normal force estimation $F_{ZT,i}$. Several driving situations are studied, as explained later. The estimation during braking is of high interest and resources will be prioritized, but not limited, to this situation.

1.7 Report structure

In Chapter 2 results of the literature review are documented. A review focuses on tyre models that are used later on (Section 2.1), methods for estimation of friction (Section 2.2), requirements of realtime processing (Section 2.3) and recursive estimation algorithms (Section 2.4).

A development method that is used throughout the report is explained in Section 3.1, followed by description of simulation model environment in Section 3.3 and description of the vehicle in Section 3.2.

In Chapter 4 the development is documented. The complex driving operation is broken down into more specific situations, which are introduced in Section 4.1 and in following sections a development for each of those situations is documented separately. Results of the development are then summarised in Chapter 5.

The report is closed in Section 6 by concluding the results and giving proposition of further development in this field.

2 Literature review

The estimation of tyre-road friction is subject to research since early 1990s. Single query in library database reveals tens of papers dealing with the problem. This knowledge-base has been studied in order to build the essential knowledge for dealing with the problem in this project. A basic introduction to the problem is provided in this chapter which serves as a reference for further development. Discovered methods for estimation of the tyre-road friction are covered in Section 2.2. Part of the study was devoted to tyre modelling, because tyre properties are envisioned to be used in the estimation algorithms. Tyre models are covered in Section 2.1. The fundamental overview of real-time computing and its requirements is presented in Section 2.3.

2.1 Tyre models

Tyre models present mathematical formulation of relations between tyre variables and parameters. The main variables are the horizontal forces the tyre acts against the road. These forces are results of certain deflection quantity of the tyre. For longitudinal force F_{XT} the deflection quantity is the difference between the velocity of the tyre and the velocity of the ground in the point of contact, which is dimensionless when normalised with either wheel or wheel hub velocity, then called the longitudinal slip. Longitudinal slip is denoted S_X if not otherwise stated. The definition of longitudinal slip can differ, for details see Section A.2.1. For lateral force F_{YT} as well as for the aligning torque M_{ZT} the deflection quantity is the slip angle α , which is the angle between the velocity vector of the tyre and the wheel plane. The vertical force between the tyre and the road is then called tyre vertical force F_{ZT} . For detailed definition of tyre forces and deflection quantities refer to [5].

Models are either empirical, physical or combination of both, called semi-empirical. Empirical models are mathematical relations derived in order to match experimental results of tyre behaviour. As such the terms of the empirical models does not have physical meaning. The most often used empirical model is called Magic Formula derived by Pacejka [6]. Physical models, on the other hand, are derived by analytical description of tyre parts (belt, treads) to represent the tyre performance characteristics by physical phenomena. In other words, complex tyre behaviour is represented by physically motivated analytical relations.

2.1.1 Magic Formula

The Magic Formula is an empirical tyre model, that describes tyre forces and aligning torque in common form

$$y(x) = D \sin [C \arctan [(1 - E)x + (E/B) \arctan (Bx)]] \quad (2.1)$$

where $y(x)$ then represent $F_{XT}(S_X)$, $F_{YT}(\alpha)$ and $M_{ZT}(\alpha)$ respectively. Coefficients B , C , D and E are then specific for each quantity and describe the tyre characteristics. Further extension of the model has been done to better comply with tyre measurements [6, 7], where the number of parameters further grow.

2.1.2 The brush model

The brush model approximates the tyre tread by a brush made of little beams (tread elements) [8, 6]. The carcass is assumed rigid and forces are generated due to deformation of brush elements in a direction parallel to the road plane. The deflection of brush elements is limited to certain maximum value, governed by the coefficient of friction μ , vertical force distribution q_z and the stiffness of the element c_{py} . The pressure, and consequently the vertical force distribution is usually assumed to be parabolic [6], but other distributions may also be used.

The description of the brush model behaviour in this section is based on [6] if not stated otherwise.

In [7] the brush model is extensively discussed together with its suitability for friction estimation using longitudinal dynamic manoeuvres. Experimental validation of the brush model has been done and proved sufficient match of the real tyre behaviour.

2.1.2.1 Pure lateral slip

For the case of pure lateral slip the brush elements deflect in direction perpendicular to the wheel plane. The deflection of element can be described following the Figure 2.1 as follows

$$v = (a - x) \tan \alpha \quad (2.2)$$

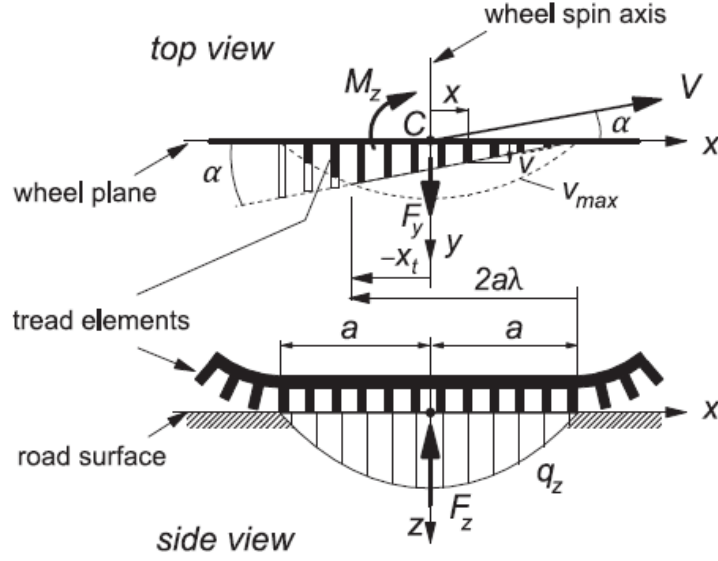


Figure 2.1: *Brush model of the tyre under pure lateral slip [6]. Note the pressure distribution q_z and definition of a and α .*

where a lateral slip $\sigma_y = \tan \alpha$ may be introduced, then

$$v = (a - x) \sigma_y \quad (2.3)$$

For simple case $\alpha \rightarrow 0$ and for ideal $\mu \rightarrow \infty$ the expression (2.2) and with the lateral stiffness of the tread elements c_{py} the lateral force can be expressed as an integral

$$F_y = c_{py} \int_{-a}^a v dx = 2c_{py} a^2 \alpha \quad (2.4)$$

and similarly for aligning torque

$$M_z = c_{py} \int_{-a}^a v x dx = -\frac{2}{3} c_{py} a^3 \alpha \quad (2.5)$$

With taking into account the finite μ and a parabolic pressure distribution, equations for lateral force and aligning moment become [6, p. 94]

$$F_{YT} = \begin{cases} 3\mu F_{ZT} \theta_Y \sigma_Y \left\{ 1 - |\theta_Y \sigma_Y| + \frac{1}{3} (\theta_Y \sigma_Y)^2 \right\} & |\alpha| < \alpha_{sl} \\ \mu F_{ZT} \text{sgn}(\alpha) & |\alpha| \geq \alpha_{sl} \end{cases} \quad (2.6)$$

$$M_{ZT} = \begin{cases} -\mu F_{ZT} a \theta_Y \sigma_Y \left\{ 1 - 3|\theta_Y \sigma_Y| + 3(\theta_Y \sigma_Y)^2 - |\theta_Y \sigma_Y|^3 \right\} & |\alpha| < \alpha_{sl} \\ 0 & |\alpha| \geq \alpha_{sl} \end{cases} \quad (2.7)$$

where F_{ZT} is vertical tyre load and the tyre properties are described by parameter θ_Y in terms

$$\theta_Y = \frac{2c_{py} a^2}{3\mu F_{ZT}} \quad (2.8)$$

where c_{py} is the tread stiffness in lateral direction and a is half of the length of tyre contact patch, see Figure 2.1. Further simplification can be applied using the cornering stiffness parameter in terms

$$C_\alpha = 2c_{py} a^2 \quad (2.9)$$

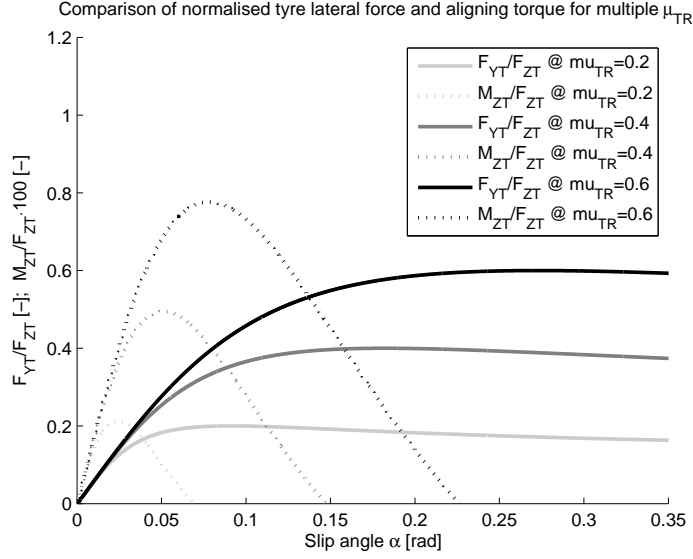


Figure 2.2: Qualitative comparison of aligning torque M_z and lateral force F_y [9]

According to the model the tyre force saturates when full sliding occurs, ie. when $|\alpha| \geq \alpha_{sl}$. The full sliding occurs at

$$\tan(\alpha_{sl}) = \frac{1}{\theta_Y} \quad (2.10)$$

The aligning moment has a peak value of

$$M_{ZT,peak} = \frac{27\mu F_{ZT}}{256} \quad (2.11)$$

which occurs for $\sigma_Y = 1/(4\theta_Y)$. The aligning torque M_{ZT} is more sensitive to change of friction than the lateral force F_{YT} for medium slip angles, see Figure 2.2. In the graph are plotted characteristics of tyre lateral force and aligning torque, both normalised by the vertical load, for different levels of tyre-road friction. The tyre-road friction is here determined by the peak of the lateral force normalised by the vertical load. The lines of the aligning torque are scaled in order to show the qualitative comparison.

2.1.2.2 Pure longitudinal slip

Under pure longitudinal slip the tread elements are deflected in longitudinal direction, see Figure 2.3, thus creating the longitudinal force. Following the figure a longitudinal deflection of element is

$$u = -(a-x) \frac{V_{sx}}{V_x - V_{sx}} = (a-x) \frac{S_X}{1 + S_X} \quad (2.12)$$

where

- V_{sx} brush elements base longitudinal slip velocity
- V_x longitudinal velocity of wheel centre
- x coordinate of brush element position from the centre of the contact patch
- a half the length of the contact patch
- S_X practical longitudinal slip as per ISO 8855 [5] (for details see Appendix A)

When defining a theoretical slip $\sigma_x = -V_{sx}/V_r = S_X/(1 + S_X)$ the (2.12) becomes

$$u = (a-x) \sigma_x \quad (2.13)$$

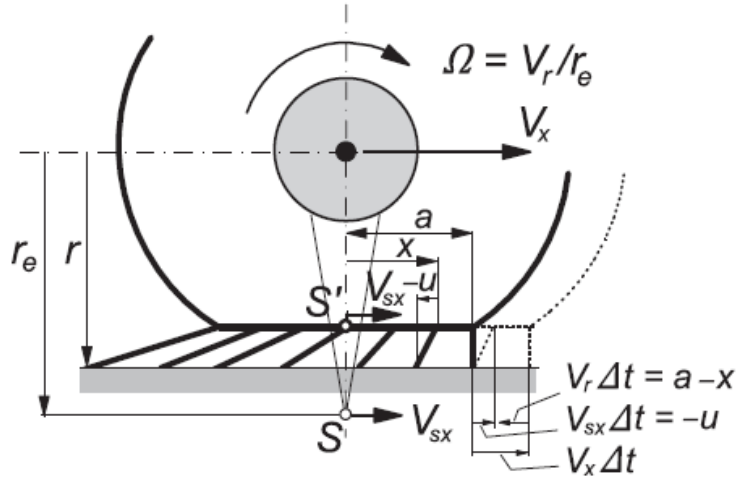


Figure 2.3: *Brush model of tyre under pure longitudinal slip [6]*

V_r is then circumferential (linear) velocity of the tyre in the point of contact with ground. The deflection in lateral direction in pure lateral slip and in longitudinal direction for pure longitudinal slip are of the same form, compare (2.3) with (2.13). Finally the same form of equation as in case of pure lateral slip applies for longitudinal slip:

$$F_{XT} = \begin{cases} 3\mu F_{ZT} \theta_X \sigma_x \left\{ 1 - |\theta_X \sigma_x| + \frac{1}{3} (\theta_X \sigma_x)^2 \right\} & |\sigma_x| < \sigma_{x,sl} \\ \mu F_{ZT} \text{sgn}(\sigma_x) & |\sigma_x| \geq \sigma_{x,sl} \end{cases} \quad (2.14)$$

where tyre is described by parameter θ_X as follows

$$\theta_X = \frac{2c_{px}a^2}{3\mu F_{ZT}} \quad (2.15)$$

In case the slip stiffness parameter C_x is used, where

$$C_x = 2c_{px}a^2 \quad (2.16)$$

then equation (2.14) reads

$$F_{XT} = \begin{cases} C_x \sigma_x - \frac{1}{3} \frac{C_x^2 \sigma_x |\sigma_x|}{\mu F_{ZT}} + \frac{1}{27} \frac{(C_x \sigma_x)^3}{(\mu F_{ZT})^2} & \sigma_x < \sigma_{x,sl} \\ \mu F_{ZT} \text{sign}(\sigma_x) & \sigma_x \geq \sigma_{x,sl} \end{cases} \quad (2.17)$$

The slip $\sigma_{x,sl}$ when tyre saturates is then

$$\sigma_{x,sl} = \frac{1}{\theta_X} = \frac{3\mu F_{ZT}}{2c_{px}a^2} = \frac{3\mu F_{ZT}}{C_x} \quad (2.18)$$

2.1.2.3 Combined slip

If the tyre is subjected to both longitudinal load and lateral load, then the combined slip situation occurs. Following [6] the force vector is given as

$$\mathbf{F} = F \frac{\boldsymbol{\sigma}}{\sigma} \quad (2.19)$$

where $\boldsymbol{\sigma}$ is the slip vector with magnitude $\sigma = |\boldsymbol{\sigma}| = \sqrt{\sigma_x^2 + \sigma_y^2}$ and components

$$\boldsymbol{\sigma} = \begin{pmatrix} \sigma_x \\ \sigma_y \end{pmatrix} \quad (2.20)$$

that relate to practical slip in terms

$$\sigma_x = \frac{S_X}{1 + S_X}; \quad \sigma_y = \frac{\tan(\alpha)}{1 + S_X} \quad (2.21)$$

Further the force magnitude $F = |\mathbf{F}|$ is given by

$$F = \begin{cases} \mu F_{ZT} [3\theta\sigma - 3(\theta\sigma)^2 + (\theta\sigma)^3] & \sigma < \sigma_{sl} \\ \mu F_{ZT} & \sigma \geq \sigma_{sl} \end{cases} \quad (2.22)$$

where full sliding occurs at $\sigma_{sl} = 1/\theta$. A value θ is given as

$$\theta = \frac{2}{3} \frac{c_p a^2}{\mu F_{ZT}} \quad (2.23)$$

where a is the half of the contact length and c_p is the tread stiffness, being assumed as isotropic for both directions, i.e. $c_p = c_{px} = c_{py}$. Lateral and longitudinal forces can thus be expressed in terms

$$F_{XT} = \frac{|\mathbf{F}|}{|\boldsymbol{\sigma}|} \sigma_x = \frac{F}{\sigma} \sigma_x = \mu F_{ZT} [3\theta - 3\theta^2\sigma + \theta^3\sigma^2] \sigma_x \quad (2.24)$$

$$F_{YT} = \frac{F}{\sigma} \sigma_y = \mu F_{ZT} [3\theta - 3\theta^2\sigma + \theta^3\sigma^2] \sigma_y \quad (2.25)$$

The self-aligning torque is then expressed using F_{YT} and pneumatic trail t , that is defined as

$$t = \begin{cases} \frac{1}{3} a \frac{1-3|\theta\sigma|+3(\theta\sigma)^2-|\theta\sigma|^3}{1-|\theta\sigma|+\frac{1}{3}(\theta\sigma)^2} & \alpha < \alpha_{sl} \\ 0 & \alpha \in \langle \alpha_{sl}; \pi/2 \rangle \end{cases} \quad (2.26)$$

The self-aligning torque is then product of pneumatic trail and the lateral force as follows

$$M_{ZT} = -t(\sigma) \cdot F_{YT} \quad (2.27)$$

2.1.2.4 Extension of brush model for carcass compliance

The extended brush model accounts for carcass lateral flexibility to provide more accurate description of aligning torque under combined slip conditions [6]. The carcass axis is in that case no longer assumed to lie in the wheel plane, but can be offset in longitudinal or the lateral direction, thus describing longitudinal, lateral compliance of the carcass respectively. The carcass line is still assumed to be parallel to wheel plane line. Moreover an initial lateral offset caused by e.g. camber angle is taken into account. Due to introduction of the two offsets, additional contribution of F_{XT} and F_{YT} on self-aligning torque is introduced, thus allowing to better follow the Magic Formula tyre behaviour. This complexity will not be further discussed here, as it presents additional parameters of tyres. More on the topic can be found in [6].

2.1.3 Brush-string model

Further extension of the brush model leads to introducing carcass compliance, modelled as a string [8]. The brush is then placed on the flexible string. The carcass compliance in form of compliant string then adds additional degrees of freedom for the model. That also brings the need for additional parameters of tyre in form of carcass stiffness, which is in reality different for lateral and longitudinal direction, hence two more parameters are needed. For the additional complexity the brush-string model is not further used in this thesis.

2.1.4 Burckhardt model

In [10] an empirical model is introduced. Unlike previously described Brush model and Magic formula model, this model defines slips in direction of wheel velocity vector (longitudinal slip s_L) and perpendicular to this direction (side slip s_S). Resultant horizontal force generated by the tyre is in direction of the resultant slip $s_{res} = \sqrt{s_L^2 + s_S^2}$. The tyre model then reads

$$F = (c_1 (1 - e^{-c_2 s_{res}}) - c_3 s_{res}) e^{-c_4 s_{res} v} (1 - c_5 F_{ZT}^2) \quad (2.28)$$

where F is the resulting tyre force. The model contains five empirical parameters. Simplified relation uses only three parameters and then the relation (2.28) becomes

$$F = (c_1 (1 - e^{-c_2 s_{res}}) - c_3 s_{res}) \quad (2.29)$$

This model assumes tyre characteristics to be equal in both directions, which limits the accuracy of this model [7]. This tyre model is not further used within this thesis.

2.1.5 Dugoff model

Dugoff tyre model was discussed in [7]. This model takes into account dependence of friction on a velocity. Then a relation for combined slip is given in the form

$$F_x = \frac{C_x \lambda}{1 - \lambda} f(\theta) \quad (2.30)$$

$$F_y = \frac{C_y \tan(\alpha)}{1 - \lambda} f(\theta) \quad (2.31)$$

$$f(\theta) = \begin{cases} \theta(2 - \theta) & \theta \leq 1 \\ 1 & \theta > 1 \end{cases} \quad (2.32)$$

where λ is here the longitudinal slip, $\lambda = -S_X$, where S_X is slip defined by ISO 8855[5], and the quantity θ is defined as

$$\theta = \frac{\mu_0 F_z \left(\left(1 - \epsilon v \sqrt{\lambda^2 + \tan^2(\alpha)} \right) (1 - \lambda) \right)}{\sqrt{2C_x^2 \lambda^2 + C_y^2 \tan^2(\alpha)}} \quad (2.33)$$

where μ_0 is the nominal friction coefficient and ϵ represents the velocity dependency of the friction [7]. Parameters of the model are

C_x	longitudinal slip stiffness
C_y	lateral slip stiffness
μ_0	nominal friction coefficient
ϵ	velocity dependency factor

Dugoff tyre model is more complex than the brush tyre model and for that reason it is not further discussed in this thesis.

2.1.6 Transient tyre models

In general, forces in tyres does not occur instantaneously given a certain slip angle/slip ratio, but due to the flexible nature of the tyre a certain time is needed before the forces build up [7, 6]. For critical manoeuvres, where safety control systems intervene, this delay affects the overall vehicle dynamics. A so called relaxation length is introduced to describe this delay [6, 8].

Another approach is used in LuGre model, which focuses on detailed description of the bristles representing tyre tread behaviour. Movement of these bristles is described using differential equations. The contact patch is thus carefully modelled, while the carcass compliance is ignored.

Short Wavelength Intermediate Frequency Tyre (SWIFT) model approximates the tyre belt as a rigid ring flexibly attached to rim. An interesting property of this model is that the pneumatic trail is modelled as a second order differential function of the lateral slip. Therefore self-aligning torque builds up slower than the lateral force [7].

Transient tyre models can provide more detailed description of the tyre behaviour, but for the cost of additional complexity. For this reason they are not discussed more within this thesis.

2.2 Friction estimation approaches

From the short extensive study of the problem it seems that many authors have been dealing with the problem, but all of them seems to end up in development of experimental case, say a proof of concept. A certain development in time is recognized especially due to the progress in available sensor equipment of the vehicles. The study hasn't revealed any case that is under serious development to an end product used in production vehicles. This may however be a result of confidentiality of such information.

Different methods can differ in terms of computational complexity, needs for *a priori* known parameters, etc. It is also of importance if the friction information is estimated for individual wheel or as an average value

for whole vehicle. This is usually related to the availability of enough information to estimate the friction coefficient individually for each of wheels.

The review revealed that estimation approaches can be divided into categories based on the fundamental idea on which the approach is working. The methods based on observation of the road condition using environmental sensors are shortly presented in Section 2.2.1. A short overview of methods using cooperation between the road users and road authorities is presented in Section 2.2.2. This thesis mainly focuses on implementation of the friction estimator based on the observation of the actual tyre behaviour using sensors already available in the vehicle. Therefore main focus is put on methods using vehicle dynamics, that are presented in Section 2.2.3.

2.2.1 Road and environment sensing

A human driver can adapt the driving style according to observations of environment ahead of the vehicle. For instance a presence of water on the road is easily detected by humans. The same idea is behind the use of sensors identifying the road conditions ahead, e.g. to detect the presence of snow, water or ice. Although the road condition does not determine the maximum tyre forces, the information can serve as useful first guess of what is upcoming. Simplest environmental sensor is the thermometer measuring the ambient temperature. If the temperature drops to around 0° C, the risk of ice on the road increases, especially if the humidity is high. Obviously, if the road is dry, the friction coefficient is still high. The risk of slippery road increases also in case when rain is detected by sensors used by automatic windscreen wipers. More decisive for presence of ice on road than the ambient temperature is the road temperature, which is in turn hard (and expensive) to measure. More advanced sensors use optical recognition of the road texture. A commercial product Road Eye analyse the backscatter of laser radiation to detect the presence of water or ice on the road [11, 9]. Laser scanning sensors, known as LIDAR, can detect the presence of precipitations ahead of the vehicle [9], but that is quite expensive solution compared to simple rain detector mounted to windscreen. Another sensor presented in [9] is based on camera mounted behind the windscreen, that analyse polarisation difference of the road surface and estimates the granularity. Under development are methods of road condition recognition using radars [9], which can classify road status based on analysis of the backscatter. Since forward facing radars are employed to vehicles for use by ADA systems, this might be interesting in the future.

2.2.2 Cooperative methods

With the emerge of communication between road vehicles and infrastructure, the idea of cooperative methods is to share the information about actual conditions among all interested parties using the road. Information obtained from within the vehicle, like the simple environmental sensing regarding the temperature of the air, can be send to the road authority and combined with static environmental sensors, e.g. the temperature of the road, humidity, etc., which can thus present broader information base for estimation of the actual road conditions. Such estimation can then be distributed back to road vehicles in form of warning, that there is a risk of low friction on the road ahead. An information about slippery spot on the road can come from a vehicle that just recognised such the slippery road because the some of the vehicle motion control systems (e.g. ABS, ESP) had to intervene. Such an information can then serve as a signal to the road authority where to focus the maintenance works. A pilot project implementing the idea in experimental practice is being held in west Sweden [12].

The cooperative methods can combine the road and environmental sensing methods with vehicle dynamics observation methods. The benefit of cooperative methods is the possibility to combine multiple sources of information and distribute them. Also among the road users that are not equipped with the all the needed sensors for either road sensing or vehicle dynamic observation. However as already mentioned in Section 2.2.1, the tyre-road friction not only depends on road conditions, but also on tyre conditions. It might be interesting to see how much the tyre-road friction coefficient can spread for variety of tyres and vehicles. So far it is expected that the spread is not very significant so that the cooperative methods can provide at least general warning for possible danger on the road ahead.

2.2.3 Vehicle dynamics observation methods

The vehicle dynamics can be used to estimate the tyre-road friction. It is especially the tyre behaviour that can provide the information about the tyre-road friction. The methods are therefore divided by the type of tyre loading - either pure longitudinal loading, pure lateral loading, or their combination. A separate section is devoted to each of tyre loading type.

2.2.3.1 Longitudinal dynamics based

It has been reported [13, 14] that the actual road condition affects the slip stiffness in the low slip region, where the tyre F_{XT} - S_X characteristic is approximately linear. This basic idea therefore needs measurement of F_{XT} and S_X in order to identify points of the slip curve. Particular methods differ in way how these fundamental variables are obtained. In one of the first papers on this topic, estimation of S_X was possible only for 2WD vehicles while driving, because there was no other way how the vehicle velocity can be determined than from wheel angular velocity sensors on non-driven (hence slip-less) wheels [14]. With new sensor possibilities the vehicle velocity can be obtained from multiple sensors using sensor fusion [2], allowing friction estimation for braking situations. The longitudinal force can be either obtained from whole vehicle model or for each wheel individually using the wheel model. Such model requires knowledge of drive/brake torques applied on each of wheels [2, 15].

To obtain the slope of linear approximation of the F_{XT} - S_X points, usually a Recursive Least-Square (RLS) method is used [2, 7]. Another option is Kalman filter that has been used in [14].

Finally from the obtained slip-slope C_{0x} the value of friction is determined. In [15] a simple linear relation $\mu = A \cdot C_{0x} + C$ is proposed, where A and C are constants obtained from experimental correlation. In [14] artificial classification rules are set as a result of many experiments. These rules say that to certain range of slope C_{0x} belongs a range of friction coefficient μ . However different tyres can have different properties leading to wrong classification of μ . In [7], parameters C_{0x} and μ are estimated together using the brush tyre model and either RLS (for low slip) or Gauss-Newton algorithm (for large slip). Similar approach is also used in [16], where combined-slip brush model is used and Linearised RLS (LRLS) method is used for simultaneous estimation of tyre parameters C_x , C_α and the friction coefficient μ using the non-linear tyre model. However, this simultaneous estimation assumes same properties for all wheels of the vehicle, which may not be valid assumption.

2.2.3.2 Lateral dynamics based

Methods based on lateral dynamics of the vehicle use the relation between the lateral force F_{YT} and the self-aligning torque M_{ZT} . Both are functions of vehicle side slip angle α and both are also affected by tyre-road friction coefficient μ_{T-R} . The important discovery discussed in Section 2.1 and depicted in Figure 2.2 is that the self-aligning torque is more sensitive to change of friction and it also achieves the significant differentiation between certain friction levels at lower levels of slip angle. The F_{YT} - M_{ZT} relation can be plotted into one graph, called the Gough plot [17], see Figure 2.4. Actual values of F_{YT} , M_{ZT} determine the actual values of α , μ [17]. However the Gough plots similar to Figure 2.4 have to be obtained for changing vertical load F_{ZT} and changing longitudinal tyre force F_{XT} if the approach has to be extended to cover combined slip situations as well. Authors of [17] proposed the use of neural networks for online learning and later using the relations leading to Gough plot. In [9] the actual values of M_{ZT} and α are compared with the reference tyre model for identification of friction, which however needs the good a priori knowledge of the tyres. A nonlinear observer is used for friction estimation in [18] where gains are subject of optimization that takes into account plant uncertainties and non-linear stability conditions. The uncertainties in [18] are in form of lower and upper bounds of tyre characteristics - which relax the need for good a priori knowledge of tyre characteristics. The brush tyre model was used in [17, 18] for its simplicity and low number of parameters.

While theory looks bright, in practice it is first needed to estimate the inputs - namely tyre forces $F_{XT, YT, ZT}$ and aligning torque M_{ZT} . The latter can be estimated on the steered axles of modern cars equipped with Electric Power Steering (EPS). The estimation is however not straightforward due to changing suspension and steering kinematics and the influence of other tyre forces. The tyre forces need to be estimated using vehicle dynamic model.

2.2.3.3 Methods integrating longitudinal and lateral dynamics

To cover more than one ideal situation a combination of multiple approaches can be used with application of appropriate approach for specific situation. Such approach was demonstrated in [18], where a switching logic was implemented. However, in that case the estimation can only be performed in the pure longitudinal slip or pure lateral slip case.

To extend the estimation to cases of combined slip, the tyre model used in the “pure” cases can be extended to account for influence of the additional slip. The idea remains the same, but the additional tyre force is taken into account in form of tyre model that reflects the influence of combined slip. Such approach was

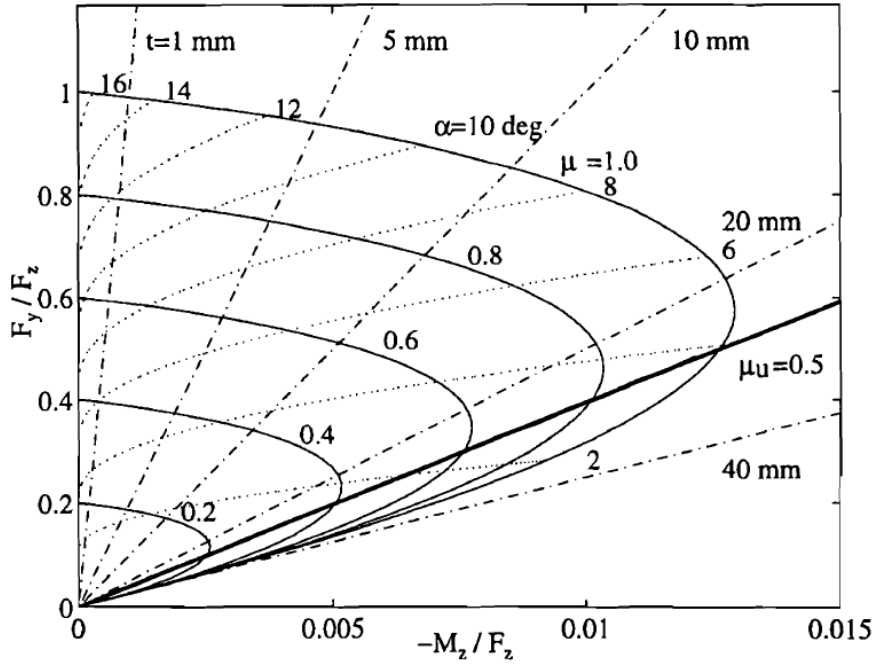


Figure 2.4: *Gough plot - normalised lateral force against normalised aligning torque [17]*

demonstrated in [16], where brush model for combined slip is fitted with RLS method to measured points, tuning three parameters C_x , C_α and μ . In [17] the F_{XT} effect on $F_{YT}-M_{ZT}$ relation is taken into account when μ is estimated from actual $F_{YT}-M_{ZT}$ values. Similar approach is used in [18], which further extend the applicability of the approach presented therein.

This added complexity of tyre model inherently decrease its accuracy as it tries to capture effect of combination of multiple non-linear behaviours. More complex tyre models can better fit the combined slip situations, but at the cost of more parameters, which in turn requires extended a priori knowledge of tyre parameters. The a priori knowledge is hard to fulfil in reality, as tyres can be freely changed and, in the end, their properties change over time.

2.2.4 Conclusion to reviewed methods

In general most of the methods for estimating friction coefficient are based on observation of the tyre behaviour using in-vehicle measurements. The methods differ in the level of excitation that is needed for good estimation. In general it is of interest to estimate friction at lowest possible excitation, because the higher the excitation, the less often it happens. Few authors have reported that it is possible to identify friction with low excitation, when the tyre operates in the linear region. However it is clear that in that case the tyre parameters have to be known very well in advance, providing calibration for the estimation. On the other hand with the tyre operating in the non-linear region several authors have shown that it is possible to estimate the friction by approximation the real tyre behaviour by simple tyre model. Tyre model simplicity can in this case be assessed by the number of parameters that the model contains.

2.3 Requirements of real-time processing

Real-time (RT) term is used in the name of the project as the intention of it is to develop an estimator that updates the information about tyre-road friction in *real-time*. Modern data-acquisition and control systems are discrete systems, which means that the values are updated in discrete time instances. The term *real-time* means in practice that the information is updated within a strictly defined period of time. In case the friction information should be important input for vehicle control systems, that are responsible for vehicle safety operation, the demand for real-time update is clear.

The update period can in general vary for different use cases and doesn't have to be as short as possible, it can also be in order of multiple seconds. Feedback control systems usually requires short time periods in order to react on the dynamics of the controlled system in a stable manner. Real-time systems are differentiated to *hard real-time*, where fulfilling the time constraint is necessary, and *soft real-time*, where it is desirable, but not mandatory [19].

To ensure the condition of *real-time* update, the whole application has to follow specific requirements. Important concept is *determinism*. Deterministic process is defined as a process that provides predictable output for given input in a time, that is well known in advance. With the use of deterministic processes one can have control over the operation of the system. While use of indeterministic processes may work well in one moment, but since the behaviour is not predictable, it may stop working in the future.

The above mentioned properties of RT systems implies two basic requirements for the implementation of the estimation algorithm:

1. the computational complexity has to be kept in mind, because even though the hardware can be powerful, the performance is still limited. The computational complexity contains the CPU time needed to process the task and the memory that is needed. Deterministic operations have a priori known CPU time and memory need;
2. the application has to be verified before it is deployed.

2.4 Recursive estimation algorithms

The requirements posed by the real-time processing leads into need for recursive processing of the measurements. In general, the task that has to be done is a parameter identification of a known model

$$\mathbf{y}_m = F[\Theta, \mathbf{u}(t)] \quad (2.34)$$

where \mathbf{y}_m are system outputs, known by measurement, $\mathbf{u}(t)$ are known system inputs and Θ are unknown system parameters. The goal is to adapt the system model behaviour by adjusting parameters Θ to match the real system behaviour as good as possible. In other words the error between the measured output of the real system and response of the model of the system to the given input has to be minimized.

Perhaps the most known approach how to achieve that is the least-squares method, which minimizes the sum of squares of the errors. Let's have a linear model in form

$$y_m = \Theta_1 \cdot F_1[u(t)] + \Theta_2 \cdot F_2[u(t)] + \dots + \Theta_N \cdot F_N[u(t)] \quad (2.35)$$

The least-square method gives a unique algebraic solution [2], that minimizes the sum of squares of errors, in form

$$\begin{bmatrix} \hat{\Theta}_1 \\ \hat{\Theta}_2 \\ \vdots \\ \hat{\Theta}_N \end{bmatrix} = [\Psi^T \quad \Psi]^{-1} \cdot \underline{\Psi}^T \begin{bmatrix} y_m(t_1) \\ y_m(t_2) \\ \vdots \\ y_m(t_M) \end{bmatrix} \quad (2.36)$$

for M system outputs, with Ψ being the observation matrix:

$$\Psi = \begin{bmatrix} F_1[u(t_1)] & F_2[u(t_1)] & \dots & F_N[u(t_1)] \\ F_1[u(t_2)] & F_2[u(t_2)] & \dots & F_N[u(t_2)] \\ \vdots & \vdots & \ddots & \vdots \\ F_1[u(t_M)] & F_2[u(t_M)] & \dots & F_N[u(t_M)] \end{bmatrix} \quad (2.37)$$

In the real-time parameter estimation the estimate should be updated in every time step. In case of least-squares method it would require to store all historical samples and consequently the computational demands would increase with every new sample. Such a calculation procedure is not deterministic and therefore it doesn't fulfil the fundamental requirement of real-time processing.

To overcome the problem with growing number of samples a recursive evaluation procedure can be used. Recursive processing in general relates results of actual iteration to result of finite number of previous iterations. In the simplest case the new iteration result is related just to the previous iteration. Thus there is no need to store all historical data and also the calculation procedure is deterministic.

2.4.1 Recursive least-squares (RLS)

The above mentioned least-squares method has a recursive version, that works as following equations describe [2].

$$\gamma(k) = \mathbf{P}(k+1) \cdot \boldsymbol{\Psi}(k+1) = \frac{\mathbf{P}(k) \cdot \boldsymbol{\Psi}(k+1)}{\boldsymbol{\Psi}^T(k+1) \mathbf{P}(k) \boldsymbol{\Psi}(k+1) + \mathbf{1}} \quad (2.38)$$

$$\hat{\boldsymbol{\Theta}}(k+1) = \hat{\boldsymbol{\Theta}}(k) + \gamma(k) \cdot \left[y(k+1) - \boldsymbol{\Psi}^T(k+1) \cdot \hat{\boldsymbol{\Theta}}(k) \right] \quad (2.39)$$

$$\mathbf{P}(k+1) = \mathbf{P}(k) - \gamma(k) \cdot \boldsymbol{\Psi}^T(k+1) \cdot \mathbf{P}(k) \quad (2.40)$$

The estimated parameters $\hat{\boldsymbol{\Theta}}(k+1)$ are updated as per equation (2.39), using the last iteration estimates $\hat{\boldsymbol{\Theta}}(k)$ and updated by the error multiplied by the gain $\gamma(k)$. The gain determines how big influence the k -th sample error will have on the estimate, thus the gain itself is updated every sample as per equation (2.38). Finally the error covariance matrix is updated in equation (2.40). For first iteration the error covariance matrix has to be initialised in form

$$\mathbf{P}(0) = \delta^{-1} \mathbf{I} \quad (2.41)$$

where \mathbf{I} is identity matrix of rank N and δ is small positive number [20].

The described steps appear in the same form every iteration, thus conforming the need for determinism required by real-time systems.

2.4.2 Kalman filter

Kalman filter is in general an estimator of unknown states of linear system, the model of which is partly known [21]. Kalman filter compares the response of the model with the measurements of real system and makes correction to the system states. The theory of Kalman filter expects influence of process noise (presenting uncertainty of the model) and measurement noise (presenting uncertainty of the measurement). Similarly as in case of RLS the procedure of Kalman filter is deterministic in every iteration, thus suitable for real-time processing. The procedure comprises of following steps:

1. predict the states of the dynamic system with the knowledge of system model, its previous states and the system input, if any
2. measure the response of the real system and compare it with predicted response of the system model with states predicted in 1, thus obtaining the error
3. update the states of the system model based on the error evaluated in step 2 using the Kalman gain

The Kalman filter presents an optimal estimator if the system is linear and both the measurement and process noises are Gaussian zero mean.

For non-linear systems an extension of Kalman filter has been introduced, called Extended Kalman filter (EKF). Basically the same procedure applies as in case of KF, but in this case a linearisation of the non-linear system is applied in every iteration. Due to the non-linear nature of the system dynamics the EKF is no more considered optimal and EKF may diverge, if the subsequent linearisation is not well approximating the non-linear system.

For EKF the system can be described using the state-space description, which reads in general form

$$\mathbf{x}_{k+1} = f_k(\mathbf{x}_k) + w_k \quad (2.42)$$

$$\mathbf{y}_k = h_k(\mathbf{x}_k) + v_k \quad (2.43)$$

Steps of the algorithm then are:

1. Linearise model of system dynamics f_k in point of the state estimate from last iteration $\hat{\mathbf{x}}(k-1|k-1)$ yielding updated Jacobi matrix \mathbf{F}_k

$$\mathbf{F}_k = \begin{bmatrix} \frac{\partial f_k}{\partial x_1} & \frac{\partial f_k}{\partial x_2} & \dots & \frac{\partial f_k}{\partial x_n} \end{bmatrix} \quad (2.44)$$

where n is number of states.

2. Apply the prediction step to system dynamics to obtain prediction of states $\hat{\mathbf{x}}(k|k-1)$ and updated error covariance matrix $\mathbf{P}(k|k-1)$,

$$\hat{\mathbf{x}}(k|k-1) = \begin{bmatrix} 1 & 0 \\ 0 & 1 \end{bmatrix} \hat{\mathbf{x}}(k-1|k-1) \quad (2.45)$$

$$\mathbf{P}(k|k-1) = \mathbf{P}(k-1|k-1) + \mathbf{Q}(k-1) \quad (2.46)$$

where \mathbf{Q} is the process noise covariance matrix.

3. Linearise the function h_k around $\hat{\mathbf{x}}(k|k-1)$ yielding updated Jacobi matrix \mathbf{H}_k , similarly to equation (2.44).
 4. Determine the Kalman gain,

$$\mathbf{K}(k) = \mathbf{P}(k|k-1) \mathbf{H}(k)^T \left[\mathbf{H}(k) \mathbf{P}(k|k-1) \mathbf{H}(k)^T + \mathbf{R}(k) \right]^{-1} \quad (2.47)$$

where \mathbf{R} is the measurement noise covariance matrix.

5. Apply the update step to the linearised measurement equation to obtain corrected state estimates $\hat{\mathbf{x}}(k|k)$ and updated error covariance matrix $\mathbf{P}(k|k)$.

$$\hat{\mathbf{x}}(k|k) = \hat{\mathbf{x}}(k|k-1) + \mathbf{K}(k) [\mathbf{y}_k - h_k(\hat{\mathbf{x}}(k|k-1))] \quad (2.48)$$

$$\mathbf{P}(k|k) = [\mathbf{I} - \mathbf{K}(k) \mathbf{H}(k)] \mathbf{P}(k|k-1) \quad (2.49)$$

Parameters of the Kalman filter are process noise covariance matrix \mathbf{Q} , measurement noise covariance matrix \mathbf{R} and initial error covariance matrix \mathbf{P}_0 .

3 Methodology and tools

In this section the methodology and tools used for development in this project will be presented. Later on where the development itself will be presented in Chapter 4, it will reference to this section for a terminology of methods and tools.

In Section 3.1 the development method work-flow is described. The vehicle that is used to investigate the problem is presented in Section 3.2. In Section 3.3 then the virtual environment used for simulation is presented.

3.1 Model based development

The friction estimation is a complex task and one can expect number of potential risks preventing implementation of the estimator in real conditions. Exploration of all the risks before the project work is started is hard and time consuming job and one can be almost sure that some risks will not be identified in advance. An agile development method hereafter called Model-Based Development (MBD) is used in this project to increase development flexibility and simplify documentation. The idea of MBD is to start with simplest model possible and keep the development steps as small as possible, so that the development can proceed quickly and steps can be quickly evaluated for viability.

The complex goal – a realtime in-vehicle friction estimation is decomposed to more specific situations, hereafter called “driving modes”. For each driving mode a specific conditions will apply and therefore a specific approach to estimate friction may be used. More on driving modes is presented later in Section 4.1. For now it is only important to know that development of friction estimation will be treated separately for each driving mode.

Work-flow of the MBD can be described by a diagram shown in Figure 3.1. In the beginning the driving mode is analysed and a brief idea of the friction estimator is set as a **prerequisite**. The idea can then be quickly **simulated** - evaluated using modelling and simulation tools. In this first simulation the ideal values that are not available in real truck can be used to prove that the prerequisite is viable. For better imagination, say that the friction estimation should be based on knowledge of longitudinal force and slip (F_{XT} and S_X) of the respective wheel. In reality, these values themselves have to be estimated in the vehicle state estimator. But to see whether the basic idea works, these values can be used in the simulation model to evaluate the viability of the prerequisite. Only if the viability is proven it is worth to continue to **implementation** of the estimator functionality where practical limitations like availability and accuracy of necessary signal may occur. E.g. following the example that has just been used, an estimation of the F_{XT} and S_X from the available measurements has to be developed. If the implementation is possible, then the friction estimation functionality is tested in real vehicle in **validation** step. That closes the development cycle by comparing the validation results with the prerequisite.

Note that in Figure 3.1 multiple cycles are depicted. The first cycle represents the most simplified and idealised case. If the idea proves to be viable in this simplified case, additional complexity may be taken into account in next cycle. For example a sensor noise, or lack of specific sensor on production vehicle. With increasing number of development cycles the functionality model moves towards the end product that will be used on final production vehicle.

As mentioned in the beginning of this section, problems that restrict the successful development will most probably occur. When MBD method is used, these problems can be quickly discovered and accurately identified and documented. Good documentation of problems is of high interest for future development.

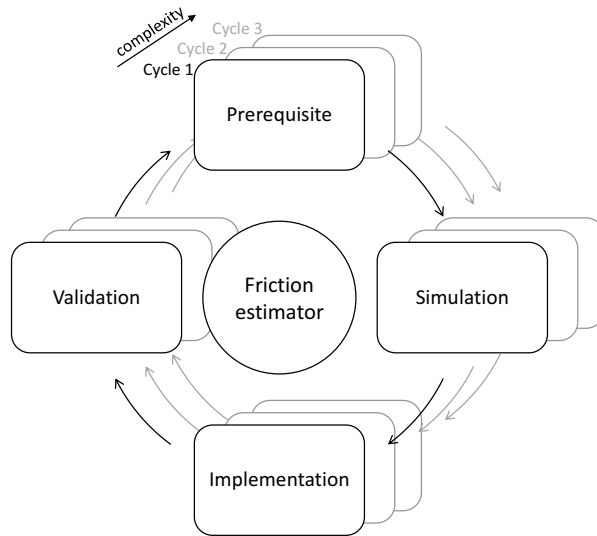


Figure 3.1: *Work-flow scheme of the Model-Based Development*

3.2 Description of investigated vehicle

The truck used for development of the friction estimator functionality is the Volvo FMX model in 8x4 configuration, see Figure 3.2. Purpose of this truck is to transport soil or other material in the tipper that is



Figure 3.2: *Volvo FMX 8x4 Tridem truck - similar vehicle is used for investigation and testing within this thesis*

attached to the chassis frame. It has 4 axles, where one of those is steered front axle, two following axles are driven, and the last axle is called tag axle, which is steered, but not driven. The tag axle can be lifted during the operation of the vehicle. Tyres used on the vehicle are described in Table 3.1. Tyre and wheel rotation inertia are summarised in Table 3.2. Weight of the vehicle and individual axle loads with no load in the tipper are summarized in Table 3.3.

Table 3.1: Tyres used on the testing vehicle

Position	Dimensions	Manufacturer and type
Front axle	385/65 R22.5	Michelin X Multi XF2
Drive axles	315/80 R22.5	Michelin X Works XDY M+S
Tag axle	385/65 R22.5	Michelin X Works XZY3

Table 3.2: Physical properties of tyres and rims on testing vehicle

Axle	J_{Wz} [kg·m ²]
Front	17.3
Driven 1	35.8
Driven 2	35.8
Tag	17.3

Table 3.3: Testing vehicle weight and individual axle loads

Axle	Load [kg]
Front	5120
1st driven	5720
2nd driven	6380
Tag	0 (lifted)
Total	17220

3.3 Vehicle simulation model

To study the behaviour of the vehicle a model of the vehicle is used and simulated using the MATLAB Simulink environment. The model is build using blocks from common library for vehicle dynamics modelling that is used within Volvo GTT. Vehicle is modelled as multi-body object using the SimMechanics toolbox of Simulink. Main components are the chassis frame, the driver’s cabin and the axles. Due to use of parametrised blocks from common modelling library different vehicles produced by Volvo GTT are modelled in consistent and scalable way.

Of highest interest in this project is the behaviour of tyre as the estimation algorithm is expected to use the observation of tyre behaviour. The tyre model is thus assumed to represent the real behaviour of physical tyre.

3.3.1 Driver’s cabin

The cabin is flexibly attached to the chassis where the suspension allows 3 DOF¹, namely bounce, pitch and roll. Parameters of the cabin (mass, inertia, etc.) and of its suspension (stiffness, damping, etc.) are provided by Volvo GTT and are assumed to match the physical vehicle.

3.3.2 Chassis

Volvo trucks are having ladder frames, that are compliant in torsion. This torsional compliance is captured by the model. In other modes the chassis is assumed to be stiff. The chassis model accounts also for payload. In this case the payload is assumed to be fixed which means it’s CoG and inertias are constant. Parameters of the chassis are provided by Volvo GTT and are assumed to match the physical vehicle. The amount of payload can be adjusted (with the impact to related chassis parameters) to allow for simulation different loading conditions. The chassis has 6 DOF with respect to inertial coordinate system.

3.3.3 Axles

All four axles of the vehicle are rigid, therefore modelled as single body. All axles are flexibly connected to the chassis allowing for 2 DOF, namely bounce and roll. The front axle model incorporates the steering system with certain compliance. On the driven axles double tyres are used on both sides of the vehicle. The tag axle model incorporates stiff steering system and has single tyres. Parameters of the respective axle are provided by Volvo GTT and are assumed to match the physical vehicle.

¹Degrees of freedom

3.3.3.1 Tyres

Tyres are modelled using the non-linear Magic Formula model PAC2002 that has been introduced in [22]. The basic structure of Magic Formula model is shortly described in Section 2.1.1. This tyre model is said to be accurate for steady state conditions and for transients with upper limit at 15 Hz [23]. The parameters used here were obtained by fitting experimental measurements of different tyres, than those that are actually on the testing vehicle. Parameters for the tyres that the test vehicle is using were not available during the thesis project. Behaviour of the tyre model used in this thesis is discussed in Appendix B.

3.3.4 Model validation

The simulation model is used in the project to analyse behaviour of the vehicle and especially its tyres in order to make conclusions about possible application of friction estimation system. The model will also serve for testing the functionality and performance of the estimation algorithm. It is therefore of interest to have model that will well describe the real behaviour of observed system in the region of interest.

The model of tyres that is used in the simulation model is based on experimental testing of different tyres than the testing vehicle is equipped with. It can therefore be assumed that qualitatively the model follows physical behaviour of the tyres. It has to be noted that the quantitative behaviour of tyres used on the testing vehicle can significantly differ from the tyre model used. Moreover, the quantitative behaviour of the tyre differs with the road conditions and thus a lot of experimental testing would be needed to assure quantitative validity of the tyre model. It is therefore assumed, that the Magic Formula tyre model well represents the behaviour of the real tyre on roads with different tyre-road friction levels. This certainly is a limitation of applicability of conclusions made by this thesis. On the other hand the estimator should be developed such that no a priori knowledge of tyres is needed, therefore it is the qualitative validity that matters the most.

4 Estimator development

In this section the development of estimator function is described, following method described in Section 3.1. As first the complex driving situation is broken into specific driving modes in Section 4.1. In following sections development of estimator function for each mode is treated separately. Summary is then provided in Chapter 5.

4.1 Identification of driving modes

As outlined in Section 3.1 driving can be treated as a state machine, where states are here called *driving modes*. With differentiation of driving to specific modes, an estimator better suited for the specific conditions can be selected, rather than trying to create a general estimator that would be able to deal with all driving situations at once. Driving modes can be described by conditions of certain vehicle variables. For instance when considering the mode hard braking, the transition condition could be $a_X \leq -0.5g$.

For transient conditions it might be beneficial to use control requests rather than the resulting effect on vehicle state. For example during braking the acceleration measured on the vehicle chassis is a result of already existing tyre forces. Furthermore the inertia of the vehicle system introduce delay between the time when tyre forces are applied and the time the acceleration of the chassis is measured. The control request can originate either from driver's controls (steering wheel, pedals) or from the vehicle motion control system. By using the requested values for the driving modes conditions a certain time might be gained. The following *request* variables can be introduced:

B_{req}	braking request (e.g. from position of brake pedal)
$T_{br,req}$	requested braking torque in percentage of maximum braking torque
A_{req}	acceleration request (e.g. from position of accelerator pedal)
$T_{dr,req}$	requested driving torque in percentage of maximum driving torque
δ_{req}	steering request (e.g. from position of the steering wheel)

In case of steering request, observation of steering angle rate ($\dot{\delta}$) can be also used for prediction of future steering request.

In following sections the particular driving modes are discussed with a summary given in Table 4.1.

Coasting occurs when the vehicle is freely rolling in straight direction with non-zero longitudinal velocity ($v_x \neq 0$). The free rolling condition can be expressed in terms of zero applied braking torque $T_{br} = 0\text{Nm}$ and zero applied driving torque $T_{dr} = 0\text{Nm}$. If the motion management framework is used, the condition can be introduced in the *requested* form: $T_{br,req} = 0\%$, $T_{dr,req} = 0\%$, which will assure that no braking, driving force will be applied. When the vehicle is coasting, the engine is usually still connected to driving wheels, introducing engine drag torque T_{drag} , that introduces some braking torque on the driven wheels. This braking torque shall be taken into account for estimation of the longitudinal forces on the driven wheels.

During coasting there is no, or very little longitudinal load on tyres, therefore tyres are lacking the excitation that is necessary for tyre-road parameters estimation using observation of the tyre response. In that case the environmental sensing could be used to evaluate road conditions as presented in Section 2.2.1. It is important to note that the actual tyre-road friction is still dependant on tyre characteristics, therefore environmental sensing can only provide rather broad range of estimated friction. The coasting mode is not further investigated in this thesis.

Static steering occurs when the vehicle is standstill and the wheels of the steered axle are being steered. The standstill condition means that the vehicle longitudinal velocity is equal to zero - $v_x = 0$. Although the steering angle is non-zero, the tyres may be relaxed as the vehicle stopped with non-zero steering angle and therefore no aligning torque will be present. That is why the condition is applied to the rate of steering angle - $\dot{\delta}_{s.w.} \neq 0$, to assure that the tyre turn-slip is used for evaluating the friction. The aligning torque might then serve as an indicator of the tyre-road friction, where the aligning torque might be estimated from the electronic power steering system.

The static steering mode is not further investigated in this thesis. To investigate this mode in spirit of MBD, explained in Section 3.1, the realistic model of the tyre under static steering conditions, should be used.

Table 4.1: Summary of driving modes (for notations see nomenclature list and text)

#	Mode name	Start condition	End condition	Brief description	Possible test case
M1	Coasting	$T_{dr,req} \doteq 0$; $T_{br,req} \doteq 0$	$T_{dr,req} \neq 0$; $T_{br,req} \neq 0$	Free rolling of vehicle with no applied driving or braking torque - no excitation.	coasting \rightarrow identify C_d, f_r ?
M2	Static steering	$v_x = 0$; $\dot{\delta}_{req} \neq 0$	$v_x \neq 0$; $\dot{\delta}_{req} = 0$	Steering while the vehicle is stand still.	static steering on different μ
M3	Mild steering	$ \delta_{req} \in (0, ??)$; $ S_X \doteq 0$	$F_{T,usage,req} > 20\%$	Cornering at pure lateral slip, low excitation.	fishhook test / skid-pad test / lane change
M4	Severe steering	$ \delta_{req} > ??$; $ \dot{\delta}_{req} > ??$; $ S_X \doteq 0$	$F_{T,usage,req} > 20\%$	Cornering at pure lateral slip, higher excitation.	evasive manoeuvre test
M5	Off-road driving	$D_{lock} = ON$	$D_{lock} = OFF$	Driving with diff-lock activated.	acceleration on uneven terrain
M6	Normal driving	$T_{dr,req} > 0$	$T_{dr,req} > 10\%$	Straight driving at very low excitation.	highway driving at constant speed
M7	Mild acceleration	$T_{dr,req} \in (10; 50)\%$	$ \delta > 0$	Driving at pure longitudinal slip, low excitation.	driving on diff. μ , μ change detection? Split μ
M8	Strong acceleration	$T_{dr,req} > 50\%$	$ \delta > 0$	Driving at pure longitudinal slip, high excitation.	driving on diff. μ , μ change detection? Split μ
M9	Mild braking	$T_{br,req} \in (5; 50)\%$	$ \delta > 0$	Braking at pure longitudinal slip, low excitation.	braking at μ change, split- μ
M10	Strong braking	$T_{br,req} > 50\%$ or ABS ON	$ \delta > 0$	Braking at pure longitudinal slip, high excitation.	braking at μ change, split- μ
M11	Emergency braking	AEBS = ON	AEBS = OFF	Vehicle entering the AEBS procedure.	short brake pulse(s) $\rightarrow \dot{\mu}$?
M12	Combined slip	$T_{br,req} > 0$; $ \delta_{req} > 0$		Driving at combined slip.	evasive manoeuvre - lane change & braking
M13	Tyre initialisation	Tyre changed = True	Initialisation done	When tyre change has been detected, until the tyre initialisation is done.	
M14	Unclassified			When no other pre-identified driving mode applies, estimator holds values.	

Mild steering represent situation when slip angle α and tyre lateral force F_{YT} are at low levels, which present low excitation for the tyre. The level of excitation is determined by magnitude of α .

Low level of lateral tyre force mean low level of lateral vehicle acceleration, so the condition can be expressed using lateral acceleration, that is higher than a threshold for mode M3 and lower than threshold for mode M4

$$a_{Y,threshold,M3} < a_Y < a_{Y,threshold,M4} \quad (4.1)$$

where the thresholds are subject to further definition. This can be taken as a condition for the case when the situation persist for certain time. However, when the lateral acceleration already occurs in measurement, there is already the certain F_{YT} and α present and some time is lost. It may therefore be better to express the level of excitation in some predicted form, that would extend the availability of the estimation algorithm.

In case of steady state cornering, the lateral acceleration is related to vehicle velocity v_X and radius of the curve R

$$a_Y = \frac{v_X^2}{R} \quad (4.2)$$

and if Ackerman steering is considered, then the steering angle is related to curvature radius [8]

$$\delta = \frac{L}{R} \quad (4.3)$$

where L represents vehicle wheelbase. For first approximation these two equation can be used together to express expected level of lateral acceleration based on velocity and steering angle

$$a_{Y,expected} = \frac{v_X^2}{L} \delta \quad (4.4)$$

This driving mode assumes negligible effect of longitudinal forces, so that the pure lateral slip tyre model can be used. To assure this assumption is valid an end condition is introduced. Tyre usage term is introduced here in its *requested* form, relating the requested wheel torques to the vertical load per particular wheel as follows

$$F_{T,usage,req} = \frac{\max \{T_{dr,req}, T_{br,req}\}}{F_{ZT}} \quad (4.5)$$

The condition can then be expressed in terms of tyre usage, that the driving mode ends when tyre force request exceeds certain threshold.

Severe steering can occur when a evasive manoeuvre is introduced by driver. Such an evasive manoeuvre will bring high levels of lateral acceleration. It may be expected that in such case some form of stability control may occur. If friction can be estimated during the early phase of evasive manoeuvre, the control system can then better use tyre limits to keep the vehicle stable. The condition for the driving mode can again be expressed in terms of expected lateral acceleration as in previous case. As in case of mild steering mode this mode assumes no big effect of longitudinal tyre forces. To assure this assumption is valid the end condition is introduced using the requested tyre force usage $F_{T,usage,req} > 20\%$.

Off-road driving is specific because a very uneven terrain can be expected. In such cases lifting of wheel from ground can occur. To prevent the loss of traction the differential lock is applied in such cases. The activation of differential lock can thus be used as indicator for driving on uneven terrain. Specific considerations will need to be taken into account in development of algorithm, e.g. lumping of wheels rotation inertia to an axle rotating inertia as a result of differential lock.

The off-road driving mode is not further investigated in this thesis.

Normal driving represents the case when vehicle is driving in straight direction and maintaining speed with no, or very low longitudinal acceleration. To overcome the resistances certain driving torque has to be applied on driven wheels, thus introducing tyre longitudinal slip. The tyre certainly operates in its linear region.

Mild acceleration In this mode the longitudinal tyre response is expected to be used for estimation of friction. Mild acceleration presents low excited level of tyre longitudinal slip S_X and tyre still operates in its linear region. The condition for entering this state can be expressed in terms of magnitude of requested driving torque $T_{dr,req}$. Mild acceleration gives low levels of tyre excitation and the tyre is hence still operating in the linear region.

Strong acceleration During strong acceleration again the longitudinal tyre response is expected to be used for friction estimation. In this case the excitation of tyre is high so that tyre operates outside the linear region. Again the condition can be expressed in terms of $T_{dr,req}$.

Mild braking presents the case with negative longitudinal acceleration. Brake torque request $T_{br,req}$ can be used as condition for entering this mode. Low magnitude resulting in tyre operating in its linear range is expected. No lateral tyre force is expected, so lateral acceleration above certain threshold indicates end of this driving mode.

Strong braking is extension of previous mode, when the brake torque request $T_{br,req}$ is high, thus tyre operates outside its linear region. Again no lateral tyre force is allowed.

Pulse braking Review presented in Section 2.2 revealed that for accurate friction estimation high values of torques applied on wheel are required, such that the tyre operates outside its linear region. Such excitation can be introduced from the motion control system in form of brake pulse(s), so that this mode presents the extension of driving mode M10.

The pulse braking mode is not further investigated in this thesis.

Combined slip occurs when tyres are loaded both in longitudinal and lateral direction. Combined slip tyre models are expected to be used to estimate the tyre-road friction. The driving mode occurs when lateral acceleration is not negligible and the driving or braking torques are requested.

The combined slip mode is not further investigated in this thesis.

Tyre initialisation presents a mode after the tyre change has been detected. In case that storing the tyre parameters would be beneficial, this driving mode can serve to identify them for later use. For example during tyre initialisation the driver might be asked to perform certain manoeuvres so that the vehicle motion control system learn the parameters of tyres.

Tyre initialisation mode is not further investigated in this thesis.

Unclassified presents a situation when no other presented driving modes can be distinguished. That means estimation of friction using observation of tyre behaviour is not possible and other type of estimation shall be used, e.g. environmental sensing, if available.

4.2 Mild steering (Mode M3)

4.2.1 Prerequisite

The prerequisite for estimation of friction in this driving mode is that the approximation of the simple brush tyre model to the actual tyre response can be used to estimate the tyre-road friction. That can be formulated as:

The simple brush model for pure lateral loading of tyre can be used for estimation of friction.

The approximation is done using non-linear curve fitting algorithm `lsqcurvefit` from MATLAB, that finds the optimal parameters of the brush model in least-squares sense. The brush model has three parameters as described in equation (2.6) on page 5: c_{py} , a , μ . In Figure 4.1a can be seen the result of approximation of the brush tyre model to the simulation model tyre behaviour (introduced in Section 3.3.3.1). The parameter of the brush tyre model μ is equal to the actual tyre-road friction coefficient μ_{TR} and the prerequisite is thus confirmed. In this case however whole the tyre characteristic from zero slip angle to point of maximum of lateral tyre force is used for the approximation. It is however of interest to estimate the friction before the peak of tyre force is reached. The term friction utilisation is introduced here, μ_{util} which is a fraction of normalised tyre force ($f_{YT} = F_{YT}/F_{ZT}$) in current point of operation of the tyre to the tyre-road friction coefficient as follows

$$\mu_{util} = \frac{f_{YT}}{\mu_{TR}} \quad (4.6)$$

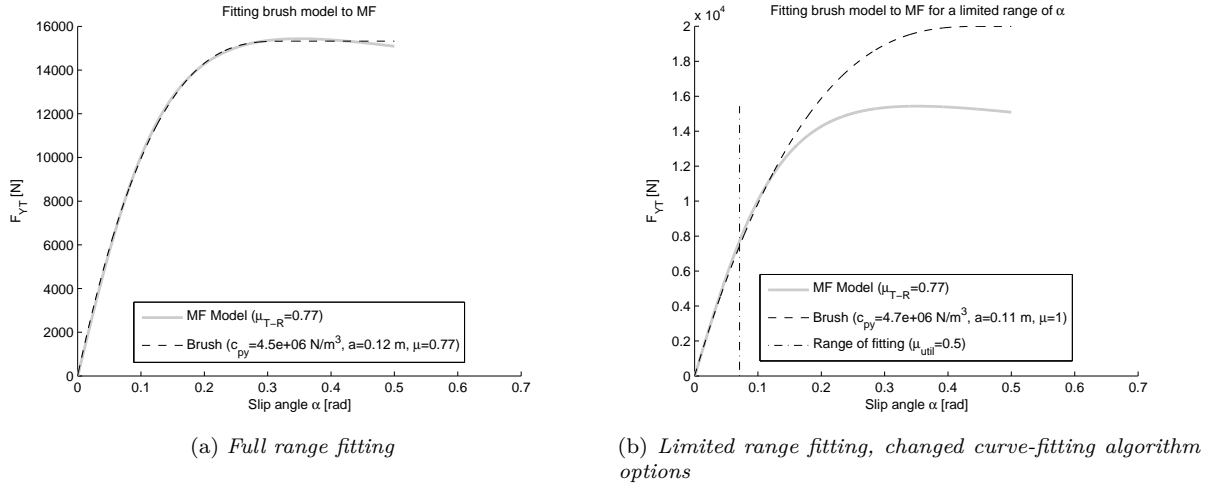


Figure 4.1: Results of brush model fitting for $\mu_{T-R} = 0.77$

In Figure 4.1b the approximation of the brush model is shown for limited friction utilisation to $\mu_{util} = 0.5$ (or 50%). In this case the parameter μ of the brush model is not equal to μ_{TR} . That means a certain utilisation of friction is needed for accurate estimation.

4.2.2 Simulation

To find out what amount of friction utilisation is needed to correctly estimate μ_{TR} using the approximation of the brush model the following procedure is used:

1. Get response of tyre (using the MF tyre model as described in Section 3.3.3.1) to the slip angle sweep - tyre characteristics $F_{YT,MF} - \alpha$, $M_{ZT,MF} - \alpha$. Assume constant vertical load for initial simplicity.
2. Approximate the tyre characteristics by brush model yielding brush model parameters c_{py} , a , μ , for limited friction utilisation $\mu_{util} = 0.1, 0.2, \dots, 1$, so that only corresponding part of the tyre characteristic from zero slip angle to the point of allowed friction utilisation is used for approximation.
3. Evaluate the sum of square residuals between Magic Formula values $F_{YT,MF}$ and brush model values $F_{YT,brush} = f(c_{py}, a, \mu_{est})$, where c_{py} , a are obtained by approximation in step 2, for different values of friction estimates $\mu_{est} = 0.1, 0.2, \dots, 1$

$$J = \sum_{i=1}^N (F_{YT,MF} - F_{YT,brush}(c_{py}, a, \mu_{est}))^2 \quad (4.7)$$

where N represents the number of samples within the limited range of friction utilization. Repeat evaluation of J for all levels of friction utilisation set in step 2.

4. Repeat previous steps for different values of true tyre-road friction μ_{TR} set in the simulation model.

The μ_{TR} is introduced here in order to denote the actual tyre-road friction coefficient (cf. equation (1.1)) achieved by the tyre model under given conditions. The friction level in the simulation model set using parameter, that is hereafter denoted μ_{VTM} . The reason is that for the same tyre model and same μ_{VTM} parameter the actual maximum friction coefficient depends on tyre vertical load.

The evaluation procedure yields graphs that show what is the most probable estimate of friction μ_{est} for given friction utilisation μ_{util} - the most probable one shows the minimal sum of square residuals. Example of such graph for $\mu_{TR} = 0.5$ is shown in Figure 4.2, where it can be observed that the accurate estimate, i.e. $\mu = \mu_{TR} = 0.5$ shows the minimal sum of square residuals J for friction utilisation $\mu_{util} > 0.8$. In other words, friction utilisation higher than 80% is needed for accurate estimation of tyre-road friction using the brush tyre model. For lower levels of friction utilisation the brush tyre model approximation overestimates the tyre-road friction.

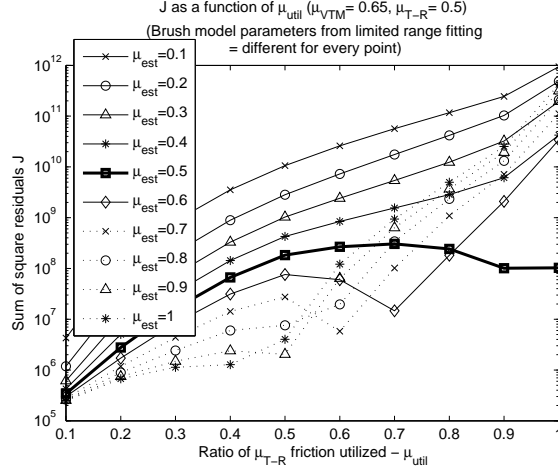


Figure 4.2: Sums of square residuals for $\mu_{TR} = 0.5$ (note the logarithmic scale of Y axis)

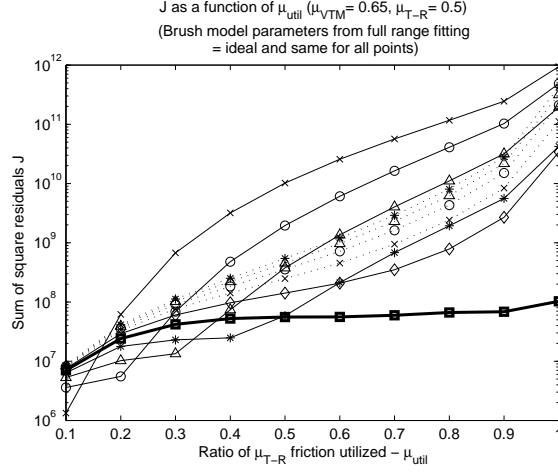
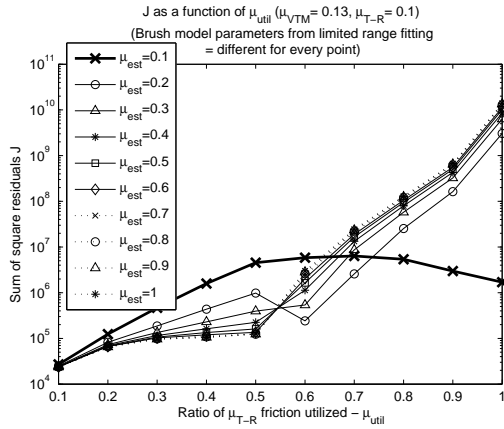


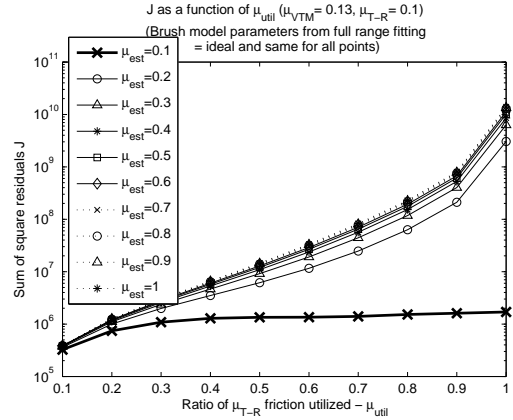
Figure 4.3: Sums of square residuals for $\mu_{TR} = 0.5$ using “ideal” brush model parameters c_{py} , a (note the logarithmic scale of Y axis)

Let’s also consider the case that the the tyre lateral stiffness coefficient $C_\alpha = 2c_{py}a^2$ is known, for example from previous situations when tyre operates only in linear range. That means that parameters c_{py} , a are accurately known and only the friction parameter μ has to be determined. To see how much friction utilisation is needed in that case, the sums of square residuals J are evaluated as described above (cf. equation (4.7)), but in this case the c_{py} and a parameters are used those that are obtained from approximation of the brush model at 100% friction utilisation ($\mu_{util} = 1$). These “ideal” parameters are then used in brush model to evaluate J for all levels of μ_{util} , which represents the situation that only the friction parameter μ_{est} needs to be estimated online. This yield the same type of graph, e.g. for $\mu_{TR} = 0.5$ the graph is shown in Figure 4.3 , where we can observe that the friction utilisation needed for accurate estimation needs to be $\mu_{util} > 0.5$. That is 30% less friction utilisation needed compared to the case when all parameters of the brush model have to be estimated at once.

The evaluation has been performed for $\mu_{TR} = [0.1 \ 0.3 \ 0.5 \ 0.7]$ and the remaining graphs for $\mu_{TR} = [0.1 \ 0.3 \ 0.7]$ can be seen in Figures 4.4, 4.5 and 4.6. It can be concluded that when “ideal” tyre parameters are used the correct friction estimate can in general be identified for friction utilization higher than 50%. That would require accurate a priori knowledge of brush model tyre parameters c_{py} and a . If these also have to be estimated online, the friction utilization has to be higher to obtain the correct friction estimate, in general higher than 80%. The friction estimate with accuracy of ± 0.1 can be identified for friction utilisation around 70%.

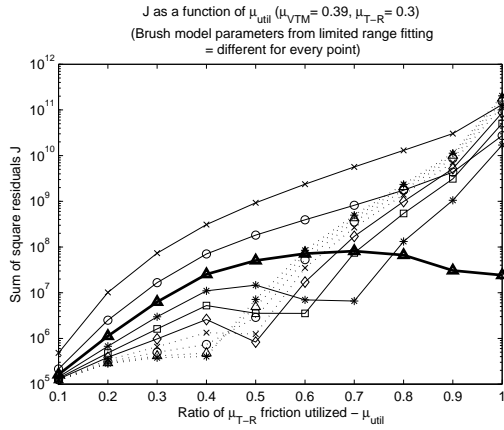


(a) Using realistic brush model parameters

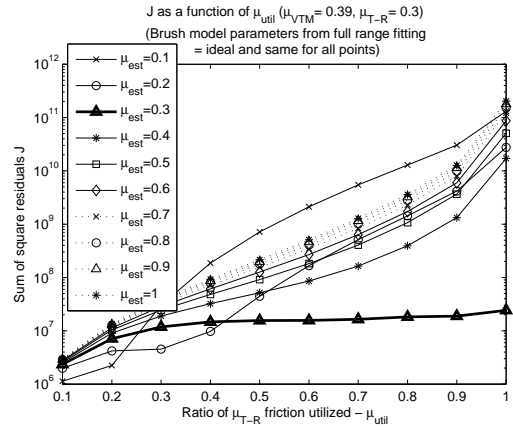


(b) Using ideal brush model parameters

Figure 4.4: Sums of square residuals for $\mu_{T-R} = 0.1$ (note the logarithmic scale of Y axis)

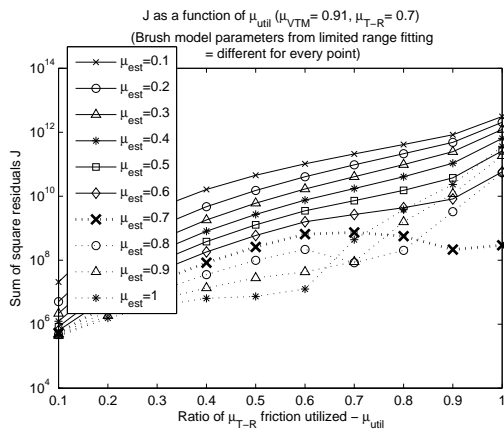


(a) Using realistic brush model parameters

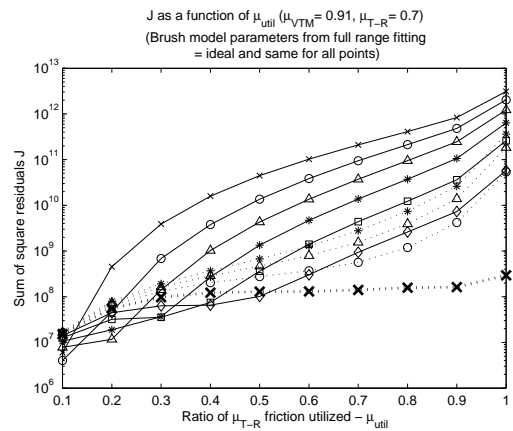


(b) Using ideal brush model parameters

Figure 4.5: Sums of square residuals for $\mu_{T-R} = 0.3$ (note the logarithmic scale of Y axis)

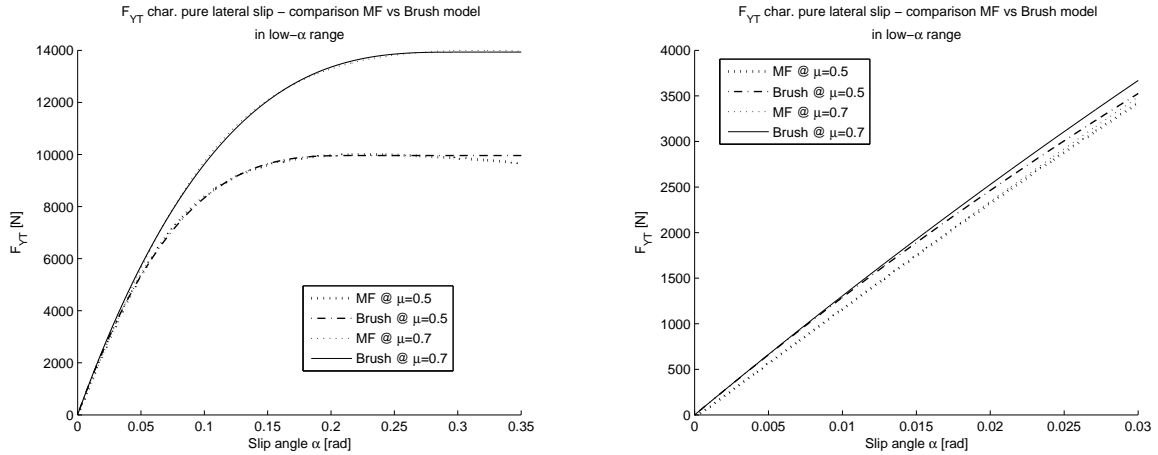


(a) Using realistic brush model parameters



(b) Using ideal brush model parameters

Figure 4.6: Sums of square residuals for $\mu_{T-R} = 0.7$ (note the logarithmic scale of Y axis)



(a) The brush model is fitted for whole region from zero slip angle to peak of the lateral force.

(b) Detail of the low slip angles region. Notice the non-adherence of brush model with the Magic Formula model.

Figure 4.7: Comparison of Magic Formula with brush model for $\mu_{TR} = [0.5 \ 0.7]$.

Of interest is that for lower friction utilisation the estimates of higher than the correct friction provides the lowest J - so that the friction is overestimated. The reason for this behaviour is the fact that Magic Formula model is more linear than brush model for low slip angle values¹, see Figure 4.7. When only samples corresponding to low values of slip angles are available for curve fitting, the brush model friction parameter is overestimated to better follow the linear curve of Magic Formula in low slip angles region.

Sum of square residuals - aligning torque

The same procedure was also applied for the aligning torque. The brush model for aligning torque was presented in (2.7) on page 5. Resulting graphs of sums of square residuals for tyre-road friction levels

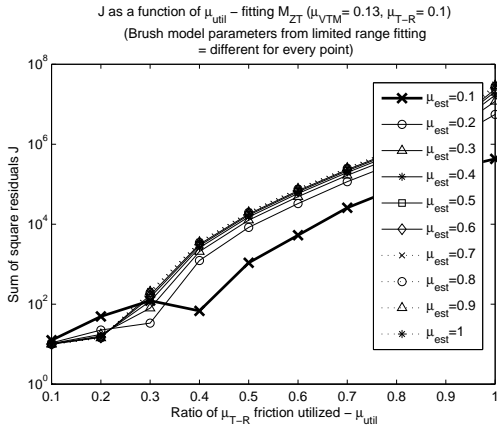
$$\mu_{TR} = [0.1 \ 0.3 \ 0.5 \ 0.7]$$

are shown in Figures 4.8, 4.9, 4.10 and 4.11. With ideal tyre parameters the correct friction estimate can be identified for friction utilisation higher than 50%, however for increasing μ_{TR} it is less clear and finally for $\mu_{TR} = 0.7$ both $\mu_{est} = 0.7$ and $\mu_{est} = 0.8$ provide the lowest J . If the tyre parameters are not well known a priori the right friction estimate is well distinguished for low μ_{TR} , but with increasing μ_{TR} it can be less distinguished. Therefore the higher the μ_{TR} the higher friction utilisation has to be reached in order to identify correct estimate of friction. While for $\mu_{TR} = 0.1$ more than 40% utilisation is enough for accurate estimation, for $\mu_{TR} = 0.3$ it is 60%, for $\mu_{TR} = 0.5$ 70% and for $\mu_{TR} = 0.7$ not a single estimate is clear even for 100% utilisation, but more than 70% is enough for ± 0.1 accuracy. It is however important to state that these findings hold for the one tyre that has been investigated. This is not a general conclusion that all tyres behave in the same manner.

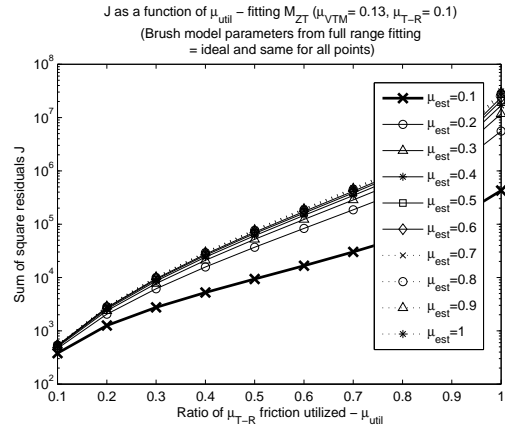
Similarly to lateral force characteristics in this case the Magic Formula is more linear than brush model in low slip angle region which leads to overestimation of the friction parameter to better fit this part of brush model curve to Magic Formula response.

In both cases (lateral force and aligning torque) the absolute accuracy ± 0.1 may not be the best comparison, since at $\mu_{TR} = 0.1$ the ± 0.1 accuracy means possible relative error 100%. Therefore it would be interesting to inspect the behaviour of the required friction utilisation, but instead of $\mu_{est} = 0.1, 0.2, \dots, 1$ use $\mu_{est} = (\pm 0.01, 0.02, 0.05, 0.1, 0.2) \cdot \mu_{TR}$. This has not been done within the time devoted to the project and remains as an idea for future work.

¹There is no difference whether 3, or only 2 brush model parameters are used.

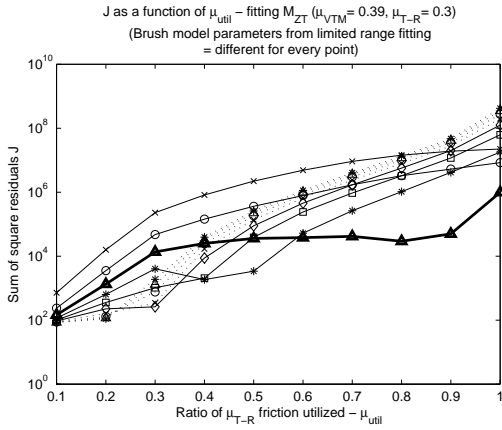


(a) Using realistic brush model parameters

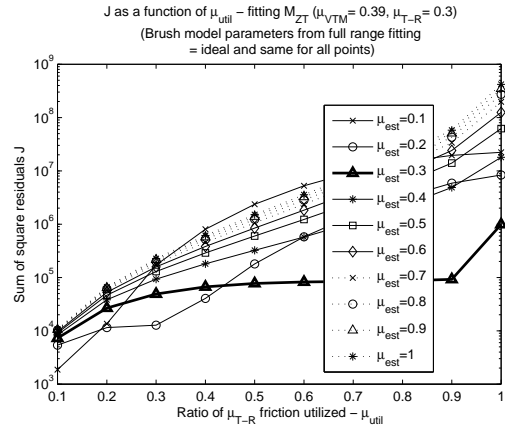


(b) Using ideal brush model parameters

Figure 4.8: Aligning torque fitting and corresponding sums of square residuals for $\mu_{T-R} = 0.1$

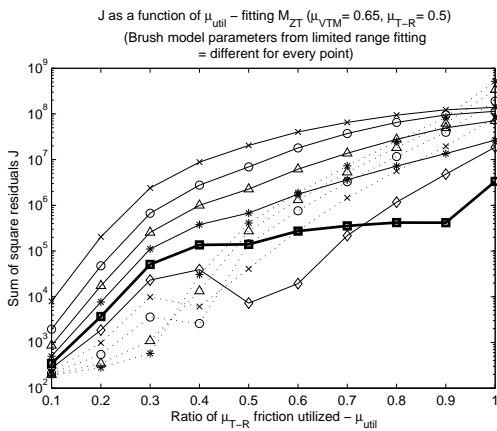


(a) Using realistic brush model parameters

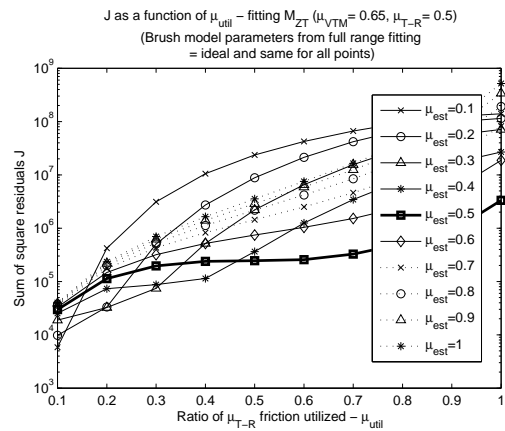


(b) Using ideal brush model parameters

Figure 4.9: Aligning torque fitting and corresponding sums of square residuals for $\mu_{T-R} = 0.3$



(a) Using realistic brush model parameters



(b) Using ideal brush model parameters

Figure 4.10: Aligning torque fitting and corresponding sums of square residuals for $\mu_{T-R} = 0.5$

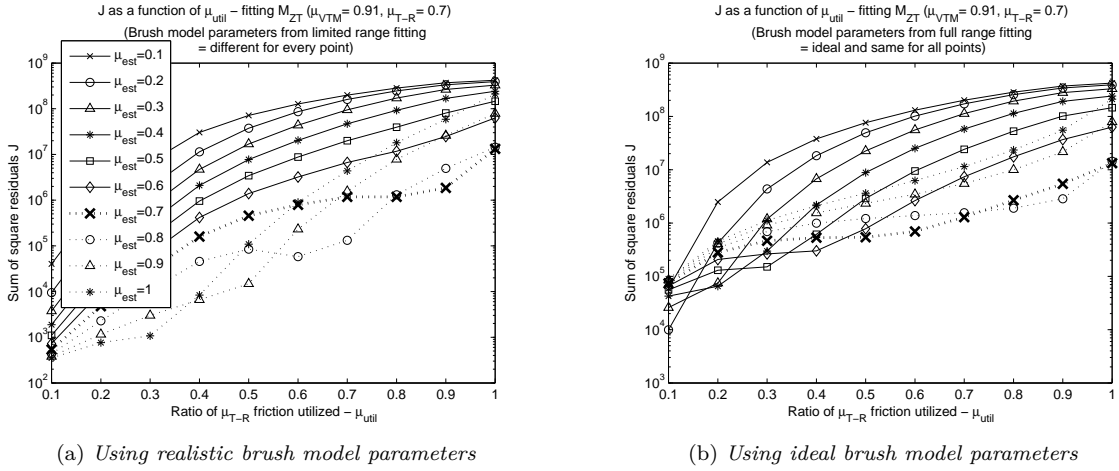


Figure 4.11: Aligning torque fitting and corresponding sums of square residuals for $\mu_{T-R} = 0.7$

4.3 Severe steering (Mode M4)

Severe steering mode can be understood as an extension of the mild steering. It was concluded that significant friction utilisation is needed to reliably estimate the friction coefficient. The level of friction utilisation is in steady state proportional to the lateral acceleration of the vehicle. Heavy vehicles are very likely to roll over for high lateral accelerations. A so called static roll-over threshold for trucks is usually in range $SRT = 0.25 - 0.35 G$. Therefore the lateral acceleration higher than SRT cannot be physically reached. This limits the estimation of friction using the lateral tyre behaviour to $\mu_{T-R} \leq 0.36 - 0.5$.

Also note that the obtained results are provided the ideal inputs and accurate and noise-free signals of F_{YT} and M_{ZT} . These are however not directly measured in the vehicle. The F_{YT} has to be estimated from the vehicle dynamics. Aligning torque M_{ZT} may be estimated from the torque applied by the electric power steering (EPS) and the knowledge of the steering system model. Obviously M_{ZT} can only be estimated on steered axles equipped with EPS. For these reasons no further effort is made in this case.

4.4 Longitudinal tyre force excitation

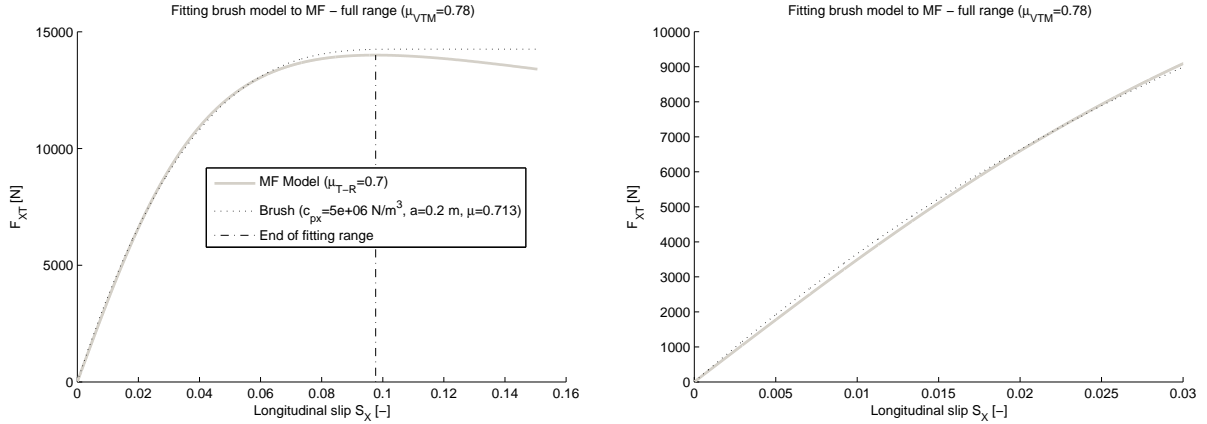
In this section the behaviour of the tyre response under pure longitudinal tyre force excitation is inspected, thus taking the driving modes M6-M10 together, see Table 4.1.

4.4.1 Prerequisite

Similarly as in evaluation of the Mild steering mode in Section 4.2, the prerequisite is that brush model approximation can be used to accurately estimate tyre-road friction. A similar procedure is applied in this case, only changing the lateral tyre response for longitudinal tyre response and lateral brush model for longitudinal brush model. The brush model has three parameters as described in (2.14) on page 7: c_{px} , a , μ . Results of the approximation (again using a function `lsqcurvefit` from MATLAB) is shown in Figure 4.12a. From the figure it can be seen that although whole the region is known for curve fitting, the optimal brush model fit a bit overestimates the friction potential. The reason for this is the linearity of the Magic Formula tyre model in low slip region. The curve fitting algorithm therefore overestimates the μ tyre parameter in order to achieve linearity of the brush model F_{XT} characteristic in the low- S_X region. It can be seen from Figure 4.12b that even if all the slip data are used, the brush model longitudinal slip stiffness (slope of the curve) is overestimated.

4.4.2 Simulation

As in Section 4.2 to find out what amount of friction utilisation is needed to correctly estimate μ_{TR} using the approximation of the brush model the following procedure is used:



(a) Whole σ_X region. Note that although the curve fitting was applied to full slip range (up to the peak of force), the optimal brush model fit overestimates the friction parameter.

(b) Detail of the low- S_X region where it can be clearly seen the different curvature of brush model (blue) compared to Magic Formula model (red), that ultimately leads to overestimation of friction.

Figure 4.12: Fitting brush model for pure longitudinal slip to Magic Formula response

1. Get response of tyre (using the MF tyre model as described in Section 3.3.3.1) to slip angle sweep - characteristics $F_{XT,MF} - S_X$. Assume constant vertical load for simplicity. Assume this response as the *real* tyre characteristics.
2. Approximate the *real* characteristics by brush model yielding brush model parameters c_{px} , a , μ , for limited friction utilisation $\mu_{util} = 0.1, 0.2, \dots, 1$, so that only corresponding part of the $F_{XT} - S_X$ characteristic from zero slip to the point of allowed friction utilisation is used for approximation.
3. Evaluate the sum of square residuals between Magic Formula values $F_{XT,MF}$ and brush model values $F_{XT,brush} = f(c_{px}, a, \mu_{est})$, where c_{px} , a are obtained in step 2, for different values of friction estimates $\mu_{est} = 0.1, 0.2, \dots, 1$

$$J = \sum_{i=1}^N (F_{XT,MF} - F_{XT,brush}(c_{px}, a, \mu_{est}))^2 \quad (4.8)$$

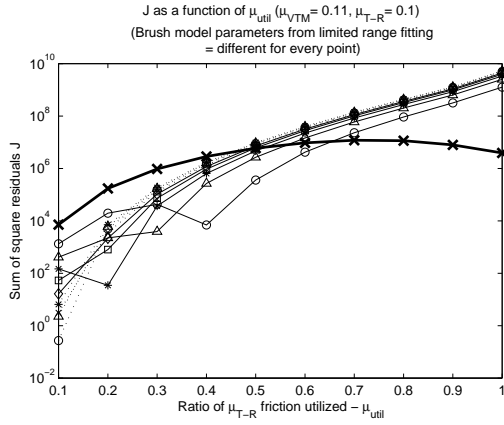
where N represents the number of samples within the limited range of friction utilization. Repeat evaluation of J for all levels of friction utilisation set in step 2.

4. Repeat previous steps for different values of true tyre-road friction μ_{TR} set in the simulation model.

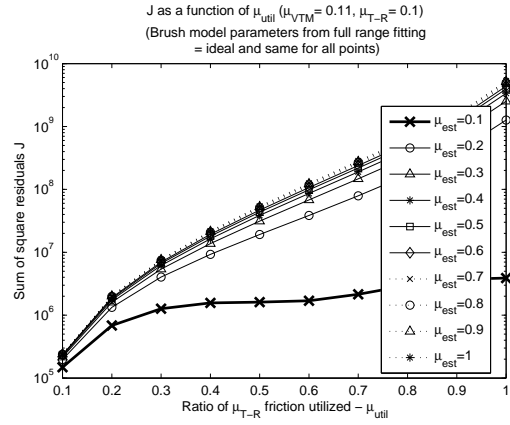
The resulting graphs with plotted J as a function of utilised friction μ_{util} for $\mu_{TR} = [0.1 \ 0.3 \ 0.5 \ 0.7]$ are shown in Figures 4.13, 4.14, 4.15 and 4.16 respectively. It can be concluded that relatively high friction utilisation is again needed to correctly estimate the friction coefficient. It was observed that in this case the friction utilisation needed for accurate friction estimation increases with increasing friction coefficient μ_{TR} , but it is not sure whether this holds in general for all tyres. In case both parameters c_{px} , a have to be estimated together with the friction parameter μ , the friction utilisation needs to be over 90% for $\mu_{TR} = 0.7$, while for $\mu_{TR} = 0.3$ more than 80% is enough. In general to estimate friction with ± 0.1 accuracy the utilisation has to be at least 80% for the tyres used here.

In case the c_{px} , a parameters of the brush model are well known, the required utilisation is lower. These “ideal” brush model parameters c_{px}, a are in this case obtained by approximation of the brush model with 100% friction utilisation. Using these ideal parameters of the brush model only friction parameter μ needs to be estimated and then the friction utilisation higher than 50% is sufficient.

The absolute accuracy ± 0.1 may not be the best comparison, since at $\mu_{TR} = 0.1$ the ± 0.1 accuracy means possible relative error 100%. Therefore it would be interesting to inspect the behaviour of the required friction utilisation, but instead of $\mu_{est} = 0.1, 0.2, \dots, 1$ use $\mu_{est} = (\pm 0.01, 0.02, 0.05, 0.1, 0.2) \cdot \mu_{TR}$. This has not been done within the time devoted to the project and remains as an idea for future work.

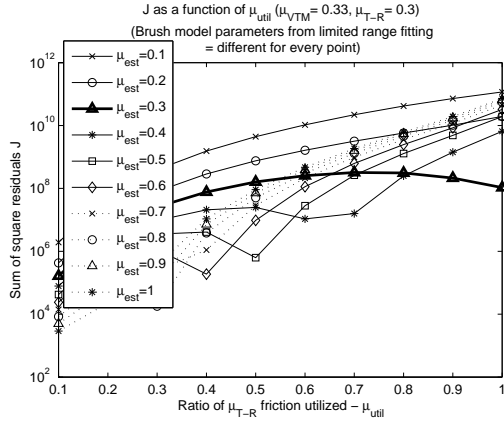


(a) Using realistic tyre model parameters

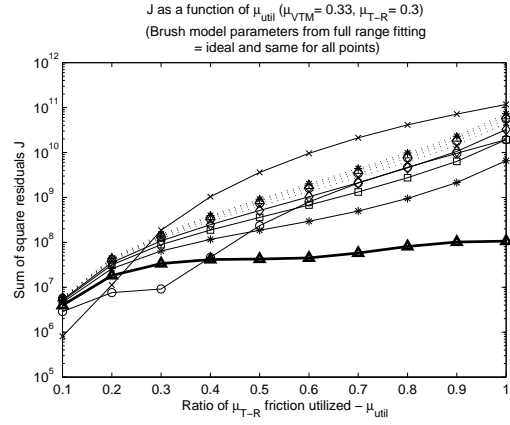


(b) Using ideal tyre model parameters

Figure 4.13: Sums of square residuals for longitudinal slip fitting at $\mu_{T-R} = 0.1$

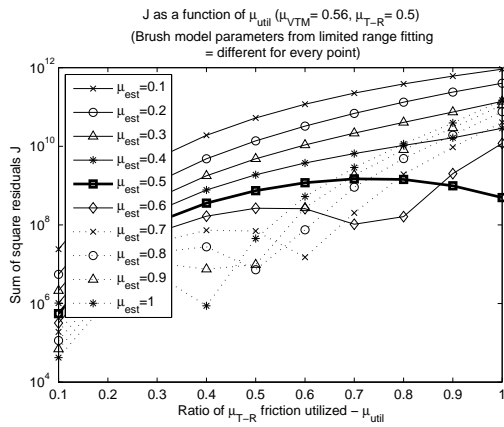


(a) Using realistic tyre model parameters

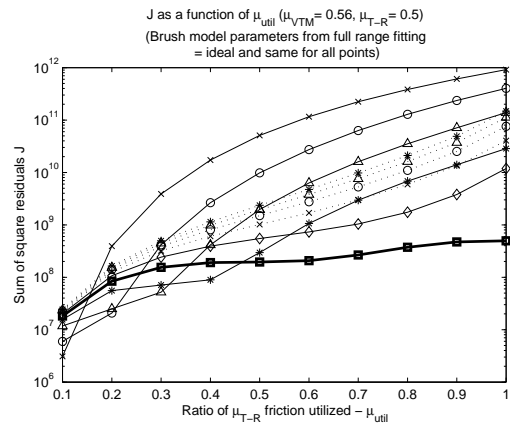


(b) Using ideal tyre model parameters

Figure 4.14: Sums of square residuals for longitudinal slip fitting at $\mu_{T-R} = 0.3$



(a) Using realistic tyre model parameters



(b) Using ideal tyre model parameters

Figure 4.15: Sums of square residuals for longitudinal slip fitting at $\mu_{T-R} = 0.5$

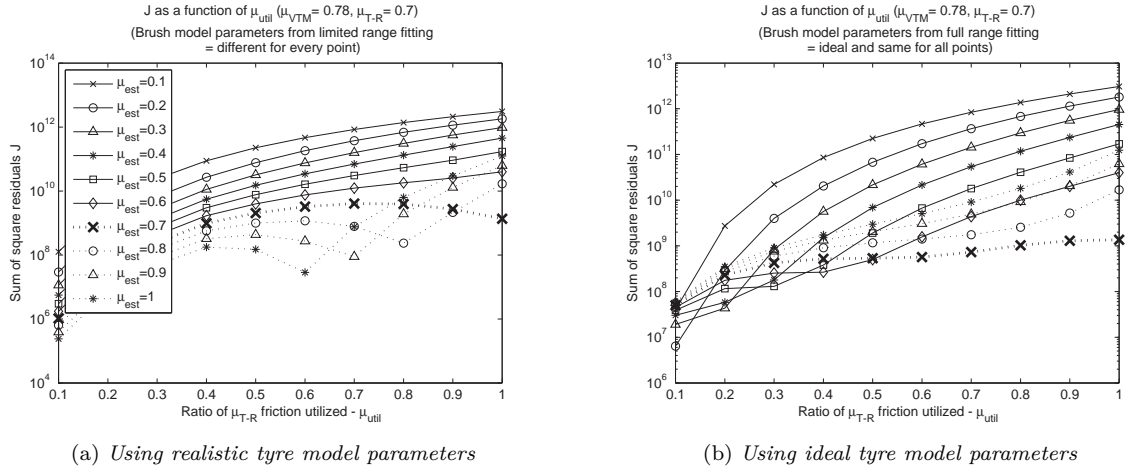


Figure 4.16: Sums of square residuals for longitudinal slip fitting at $\mu_{T-R} = 0.7$

4.4.3 Implementation

The longitudinal case presents more viable opportunity to estimate the friction than the lateral case due to availability of high tyre excitation. Therefore the possibility to estimate friction using the recursive estimation algorithm from the measurements is further explored.

First the recursive algorithm is needed that can process the arriving measurements as shown in block diagram in Figure 4.17. As the recursive algorithm the Extended Kalman Filter has been selected as a first option, because it is deterministic, it can handle non-linear models, it is relatively simple and it allows tuning.

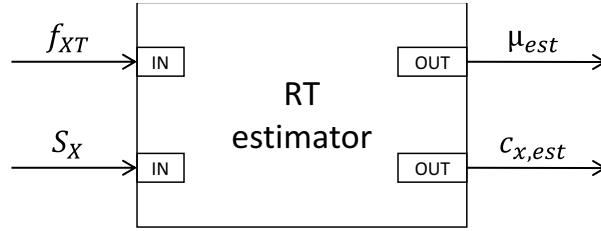


Figure 4.17: Block diagram of the estimator functionality

4.4.3.1 Extended Kalman Filter for tyre model parameters estimation

An Extended Kalman filter introduced in Section 2.4.2 is used for estimation of the unknown parameters of the brush tyre model. The system model for EKF then has state vector² $\mathbf{x}_k = [c_x \ 1/\mu]^T$. The estimated parameters are related to the actual road conditions which can vary stochastically and therefore no model of the dynamics of estimates exist. A random walk model is therefore used to represent the system dynamics in form

$$\mathbf{x}_{k+1} = \begin{bmatrix} 1 & 0 \\ 0 & 1 \end{bmatrix} \mathbf{x}_k + w_k \quad (4.9)$$

Obviously, the model of the system f_k is linear in this case. The term w_k presents the process noise that is affecting the states. The changing road and tyre conditions present the process noise in this case.

The measurements are the tyre longitudinal force normalised by the vertical load f_{XT} , therefore $y_k = (f_{XT})_k$, for certain tyre slip S_X . The simple brush model given by equation (2.17) then represents the model of the measurement equation h_k of the state space model description. The brush model is here further modified to its normalised form. If the brush model given by equation (2.17) is normalised by the vertical load F_{ZT} and the normalised slip stiffness is used in form

$$c_x = \frac{C_x}{F_{ZT}} \quad (4.10)$$

²Friction coefficient is used in inverted form for later convenience of partial derivatives.

the equation (2.17) reads

$$f_{XT} = \begin{cases} c_x \sigma_x - \frac{c_x^2 \sigma_x |\sigma_x|}{3\mu} + \frac{c_x^3 \sigma_x^3}{27\mu^2} & \sigma_x < \sigma_{x,sl} \\ \mu \cdot \text{sign}(\sigma_x) & \sigma_x \geq \sigma_{x,sl} \end{cases} \quad (4.11)$$

where the saturation slip is then, using equation (2.18) and equation (4.10)

$$\sigma_{x,sl} = \frac{3\mu F_{ZT}}{C_x} = \frac{3\mu}{c_x} \quad (4.12)$$

equation (4.11) then represents the non-linear function h_k . The Extended Kalman filter linearise the non-linear function h_k in the point of last known estimate. The Jacobi matrix of function h_k reads

$$\mathbf{H}_k = \left(\begin{array}{cc} \frac{\partial h_k}{\partial c_{x,k}} & \frac{\partial h_k}{\partial (1/\mu_k)} \end{array} \right) \quad (4.13)$$

where

$$\left. \frac{\partial h_k}{\partial (c_{x,k})} \right|_{\substack{\mu_0 \\ c_{x0}}} = \sigma_X - \frac{2\sigma_X |\sigma_X|}{3} c_{x0} \frac{1}{\mu_0} + \frac{3\sigma_X^3}{27} c_{x0}^2 \frac{1}{\mu_0^2} \quad (4.14)$$

$$\left. \frac{\partial h_k}{\partial (1/\mu_k)} \right|_{\substack{\mu_0 \\ c_{x0}}} = 0 - \frac{\sigma_X |\sigma_X|}{3} c_{x0-1}^2 + \frac{2\sigma_X^3}{27} c_{x0}^3 \frac{1}{\mu_0} \quad (4.15)$$

The point of linearisation is described by variables c_{x0} , μ_0 , which are obtained by the prediction cycle of the EKF algorithm such that

$$\begin{bmatrix} c_{x0} \\ 1/\mu_0 \end{bmatrix} = \mathbf{x}_{k+1} \quad (4.16)$$

The EKF parameters \mathbf{Q} , \mathbf{R} and \mathbf{P}_0 are to be tuned. The measurement noise covariance \mathbf{R} can be evaluated by analysing the measurement process and its uncertainties. There is however no information about the process noise - in other words the estimated states does not have any dynamics.

Functionality of the EKF as the recursive estimator has been implemented in MATLAB code. The estimator algorithm comprises from EKF as a recursive estimation algorithm and additional data processing:

1. initialisation of EKF parameters
2. limitation of estimates to reasonable values to prevent divergence

The additional processing is shown in the block diagram of the implementation under the respective number, see Figure 4.18.

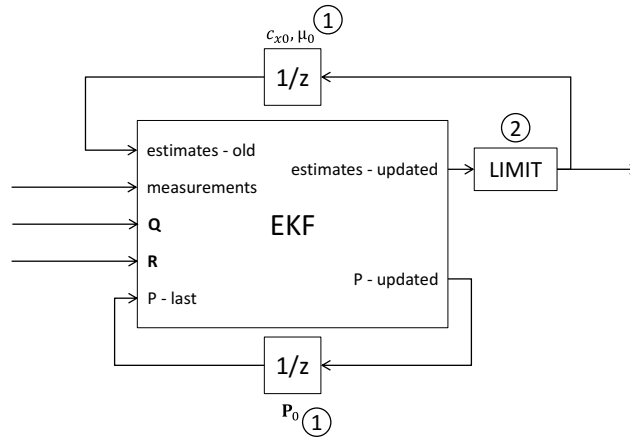


Figure 4.18: Block diagram of implementation of the EKF as a recursive estimator of tyre model parameters. 1 presents the initialisation of the EKF parameters, 2 then the limitation of the estimates to reasonable values.

Initialisation of EKF parameters involves setting of initial guess of the estimates and setting of covariance matrices \mathbf{P}_0 , \mathbf{Q} , \mathbf{R} . The initial guess is set to $\hat{c}_{x0} = 25$ and $\hat{\mu}_0 = 0.5$. To set the values in comparable way for both estimated states a normalisation is introduced, so that

$$\mathbf{Q} = \begin{bmatrix} Q_{11} \cdot x_{1,nom} & 0 \\ 0 & Q_{22} \cdot x_{2,nom} \end{bmatrix} \quad (4.17)$$

$$\mathbf{P}_0 = \begin{bmatrix} P_{11} \cdot x_{1,nom} & 0 \\ 0 & P_{22} \cdot x_{2,nom} \end{bmatrix} \quad (4.18)$$

where $x_{1,nom}$, $x_{2,nom}$ is the nominal value of state $x_1 = c_x$, $x_2 = 1/\mu$ respectively. The nominal values are here put equal to the initial guesses, so that $x_{1,nom} = \hat{c}_{x0}$ and $x_{2,nom} = \hat{\mu}_0$. Without the normalisation the same value of variance for both states would have different impact as the states are of different order. The values Q_{11} , Q_{22} , P_{11} and P_{22} are tuned manually to achieve good results.

Limitation of estimates is set to saturate the estimates when the EKF outputs them out of reasonable range. The ranges are set as

$$0.05 < \mu_{est} < 1.1 \quad (4.19)$$

and

$$5 < c_{x,est} < 50 \quad (4.20)$$

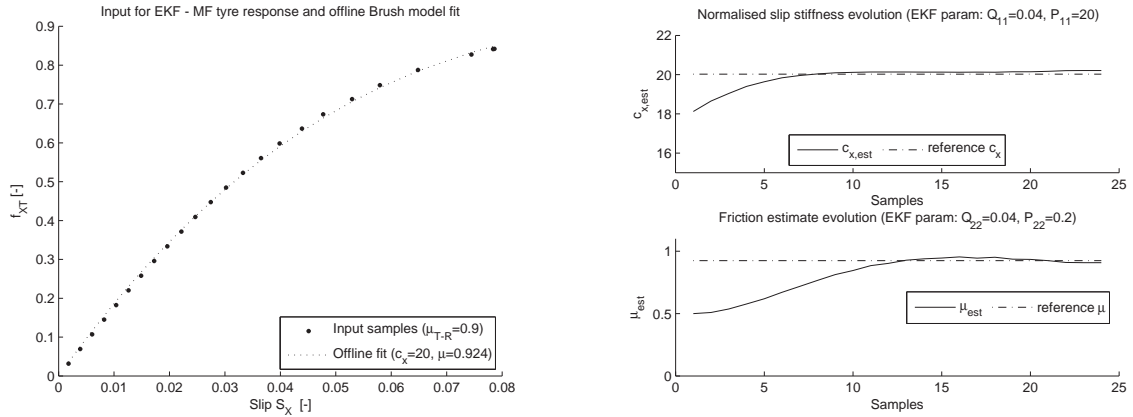
The reasonable range for the normalised slip stiffness estimate was set to provide space around typical values for truck tyres. The estimates resulting from one iteration of EKF are then limited to the specified reasonable range and fed back to another iteration of the EKF, as seen from Figure 4.18..

4.4.3.2 Estimator test on ideal input

For evaluation of functionality the estimator is applied on force-slip samples obtained from simulation of the Magic Formula tyre model under braking. These samples can be seen together with offline fit of the brush model in Figure 4.19a.

Reference values of estimates are determined by approximation of the brush tyre model to all available samples, hereafter called and in graphs denoted as *offline fit* of the brush model, as shown in Figure 4.19a. This is the best overall fit that can be achieved by the brush tyre model. It can however be seen that the friction parameter estimated by this method is higher than the actual peak friction (noted μ_{T-R} in the graph) exhibited by the MF tyre model under given conditions.

In Figure 4.19b are then plotted the results of the online estimator, where the parameters of the EKF are shown in the annotation of the graph. In this case measurement noise covariance is $\mathbf{R} = 0$ as no noise is present. The test shown here is proving the functionality of the estimation algorithm on ideal input data - without noise and with limited number of points that are rather well distributed. Besides the measurement noise, the real signal can also provide unequal distribution of measurement points and also the number of points will be different based on actual driving scenario. This affects the performance of EKF with fixed settings of parameters. For instance the initial error covariance of friction estimate was set low in order to not trust the input samples when updating μ until samples from non-linear tyre range are available. If this is not done and the EKF is allowed to estimate friction in linear region, then it can easily diverge as seen in Figure 4.20.



(a) Input to EKF - response of tyre to increasing torque load under constant vertical load. Dots represent measurements as the input to EKF estimator. Dotted line is the brush model with parameters obtained by non-linear least-squares approximation of all the shown samples.

(b) Evolution of estimation of states - estimator converges to reference values.

Figure 4.19: Functionality of parameter estimator based on EKF for $\mu_{TR} = 0.9$

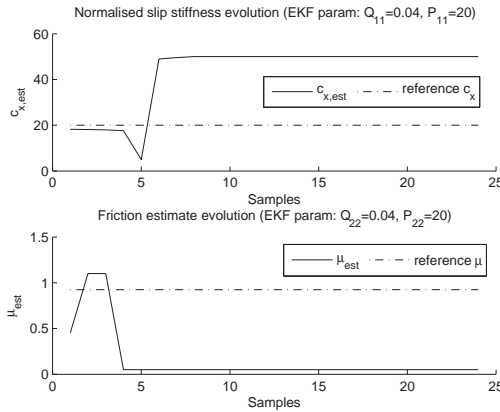


Figure 4.20: Divergence of the EKF estimator

4.4.3.3 Estimator test on vehicle model

To test the estimator functionality in more realistic driving conditions it has been implemented in the full vehicle model. The estimator includes a simple logic to update the estimates only when the brake situation occurs. The estimator starts updating when the force and slip are below³ threshold:

$$f_{XT} \leq -0.05 \quad (4.21)$$

and

$$S_X \leq -0.005 \quad (4.22)$$

and updates as long as the vehicle velocity is above threshold:

$$v_X \geq 2 \text{ m/s} \quad (4.23)$$

These limits have been set to avoid enabling the estimator by very low excitation, that may be caused by small disturbances, or by measurement noise once real input signals are used. The values of thresholds may need to be adjusted once dealing with real signal.

³below because both force and slip are negative during braking

In this case the inputs for the estimator ($f_{XT} - S_X$) are taken directly from the tyre model and the estimator process them with sampling period 0.01 s (the same as shall be available in vehicle). The EKF procedure as described in Section 4.4.3.1 is implemented in the embedded MATLAB function block. EKF parameters are initialised in MATLAB Workspace in same manner as described in 4.4.3.2.

Performance on high friction For the first test the vehicle is driving at constant velocity $v_{X0} = 65$ km/h and then applies braking torque on all wheels up to standstill. Friction of the surface is set to $\mu_{VTM} = 1$, for which the Magic Formula tyre model used on the front axle reach tyre-road friction $\mu_{TR} = 0.9$. The drive scenario can be seen from Figure 4.21. In Figure 4.23 is then shown the normalised longitudinal force of the front left tyre which is here used for testing of the estimator. One may notice that the force curve is little wavy. This is caused by the oscillating vertical load on the tyre due to longitudinal load transfer and vehicle suspension. The behaviour of the suspension in the vehicle model is therefore the reason why in this case the brake torque changes rather slow, see Figure 4.21b. The brake actuator dynamic is modelled as a first order system and therefore the time constant τ determines the rise time of the brake torque. Reasonable value of the brake actuator time constant for hard braking is in range $\tau \in (0.1; 0.2)$ s. When the brake torque dynamics is modelled using this short time constant on a high friction, a significant peak in the vertical load appears, see Figure 4.22a, which consequently distorts the obtained tyre characteristic, see Figure 4.22b. Such a significant distortion then confuses the estimator and it is assumed that such a significant and abrupt change of vertical load is not realistic. For this reason the brake actuator time constant is in this case $\tau = 0.5$ s.

From results shown in Figure 4.24 the estimator converges well to the reference values as more and more samples are read. In Figure 4.24a is shown the input force-slip characteristic of the tyre together with the offline fit of the brush model and the brush model parametrised by the recursive (*online*) estimator, hereafter called and in graphs denoted as *online fit* of the brush model. The last values provided by the online estimator are used for parametrising the brush model. The reference values have again been obtained from offline curve fitting of the input samples with a brush model. Notice however, that the peak friction for this tyre model is at $\mu_{TR} \doteq 0.9$, while the offline brush model fit returns value $\mu \doteq 0.84$. It has been shown earlier that for lower friction utilisation the brush model should overestimate the friction. The reason why in this case it underestimates could be the little waviness of the tyre response. From the comparison of input samples and resulting brush model it can also be seen that although the estimator does not converge to the reference value of the slip stiffness, it fits the samples rather well. The slip stiffness is decreasing with increasing vertical load, as shown in Section B.2 in Figure B.5. The parameters of the EKF have been changed compared to previous test on the ideal input. Especially notice the introduction of non-zero measurement noise covariance R , that allows to decrease trust to the input samples as they are themselves subject to change due to the slip stiffness dependency on the vertical load.

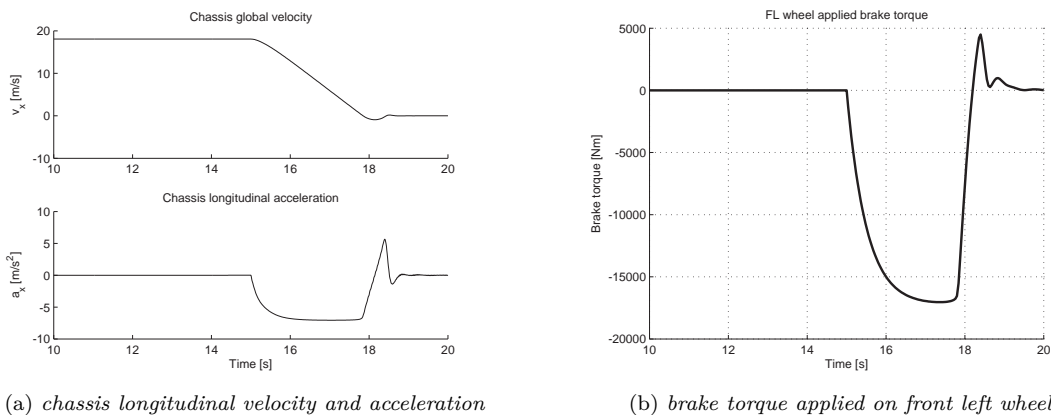
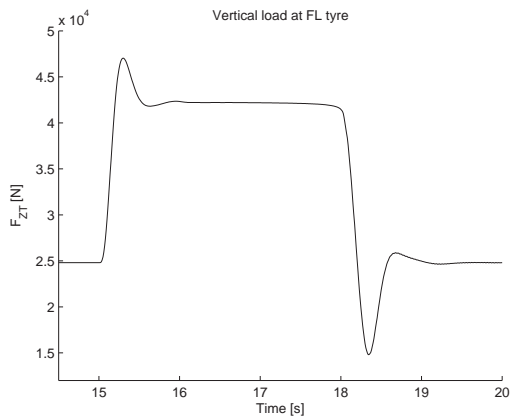
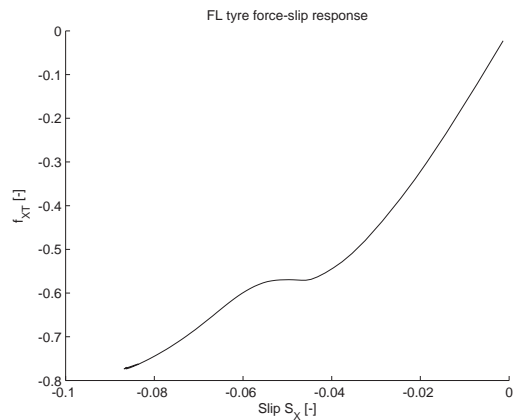


Figure 4.21: Drive scenario for test of the estimator implementation. Time constant of the brake actuator is here $\tau = 0.5$ s. Note that the signals start at the time 10 s to ensure the vehicle model is in steady state before the brakes are applied at 15 s.

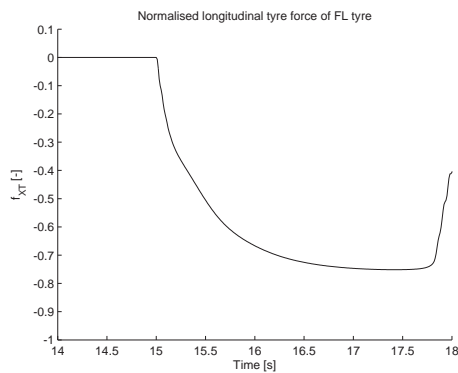


(a) front left tyre vertical load

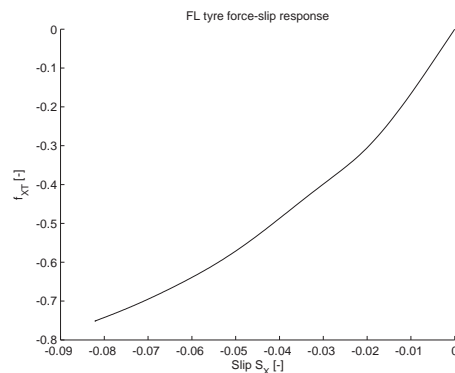


(b) front left tyre force-slip characteristic, distorted by the significant peak in the vertical load

Figure 4.22: Response of the vehicle model for fast increase of the brake torque. Time constant of the brake actuator here is $\tau = 0.15$ s.

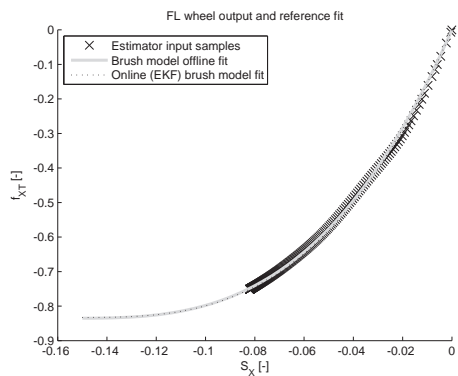


(a) against time

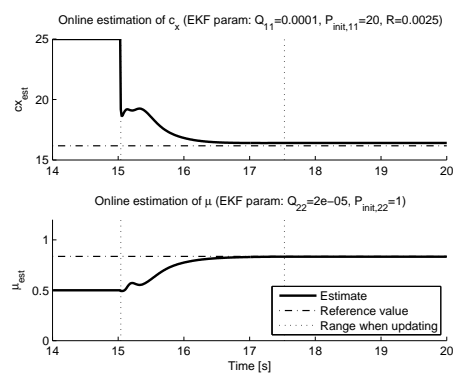


(b) against slip

Figure 4.23: Normalised longitudinal tyre force. Note that here the sign convention is kept - negative force and negative slip for braking. It can be seen that the saturation was not reached. The force decays just before 18 s as the vehicle stops.



(a) input data and comparison of offline brush model fit and brush model parametrised by the resulting parameters of the online estimator



(b) output of the estimator over time

Figure 4.24: Results of the online estimator test in complete vehicle model.

Performance on low friction Of particular interest is the estimator’s performance on roads with low tyre-road friction μ_{TR} . To test estimator’s performance the simulation of braking on low friction is performed. Again the vehicle is driving at constant velocity $v_{X0} = 65$ km/h and then applies brake torque on all wheels. Friction of the surface is set to $\mu_{VTM} = 0.2$, for which the Magic Formula tyre model on the inspected front axle reach $\mu_{TR} \doteq 0.18$. In Figure 4.25 can be seen the normalised longitudinal tyre force of the front left wheel. Note that in this case the brake actuation is faster than in previous case of high friction, because the load transfer is not affecting the tyre characteristic significantly on low friction. The peak of the tyre force is here reached within 0.04s from initialisation of braking. That means only four samples are available before reaching the peak.

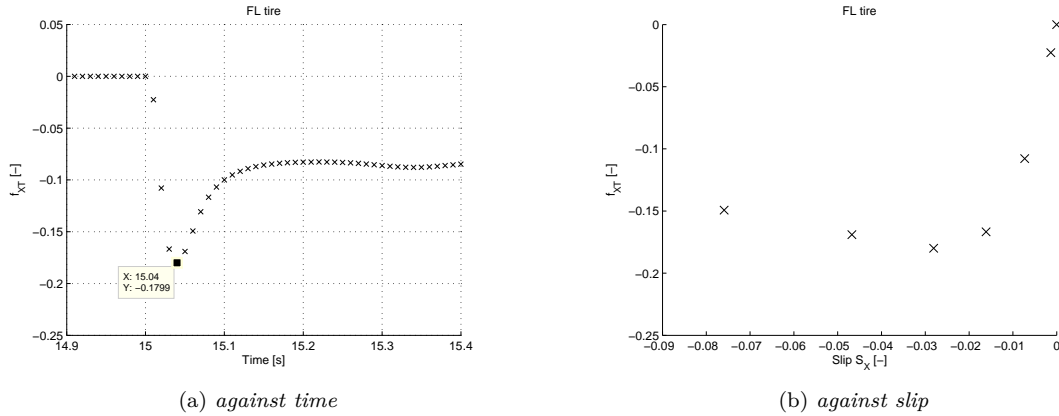


Figure 4.25: Normalised longitudinal tyre force at low friction. Note that here the sign convention is kept - negative force and negative slip for braking. It can be seen that the saturation was reached very quickly and only few samples are available before reaching the peak of the tyre force.

Results of the online estimator can be seen in Figure 4.26. With good tuning of the EKF parameters the estimator can converge close to the reference value and thus quite accurately estimate tyre-road friction in short time - at 15.03 the estimated friction is $\doteq 0.193$. To reach this value estimator used only two samples, because the estimator still follows the conditions for updating given by equation (4.21) and equation (4.22). The estimate of friction $\mu \doteq 0.193$ is thus obtained in time 0.04 s from the start of braking. The very good performance is caused by tuning the EKF - the parameters are now different from those in test on high friction. In this case the parameters were tuned such that the first available samples are trusted more than in previous case. Whereas in previous case on high friction the first samples were in the linear region of the tyre, now the samples are in non-linear region very soon.

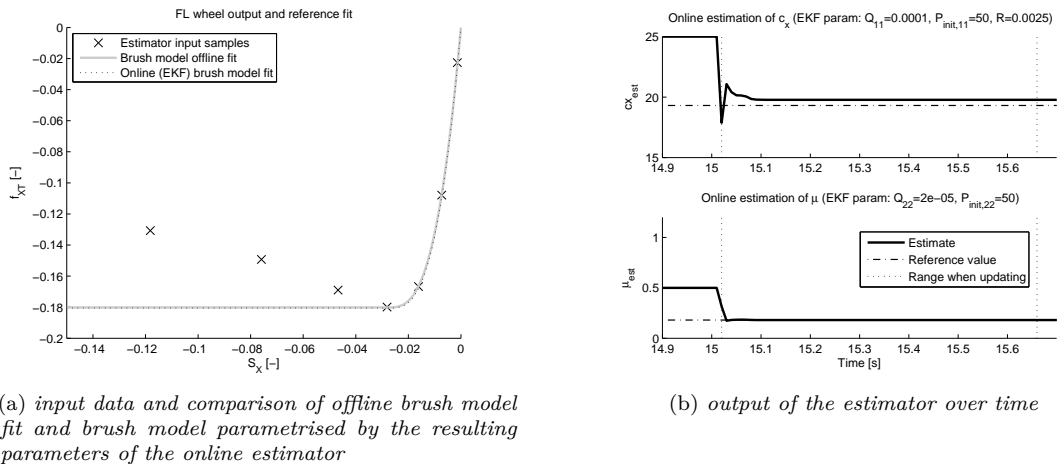
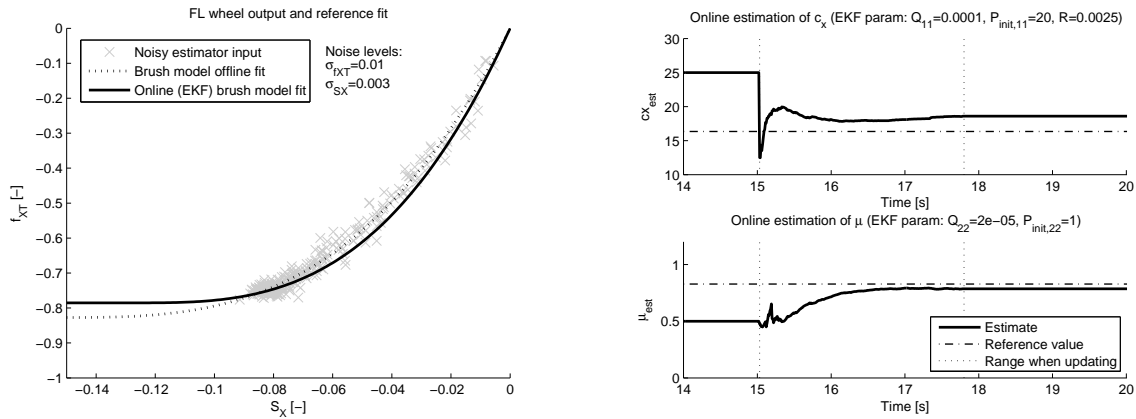


Figure 4.26: Results of the online estimator test in complete vehicle model.

4.4.3.4 Estimator test on vehicle model with added noise

The previous case is made more realistic by adding noise to the signals from the vehicle model. The resulting noisy signals then form the input signals for the estimator. In reality both the signal of normalised force f_{XT} and the signal of corresponding slip S_X are affected by noise. Here a normally distributed, zero mean random noise is added to the noise-free signals obtained from simulation model in the same way as described in Section 4.4.3.3. The noise power is characterised by its variance $\sigma_{f_{XT}}^2$, $\sigma_{S_X}^2$ respectively. In case of zero-mean Gaussian random noise $\sigma_{f_{XT}}$ represents the standard deviation of the normalised longitudinal force readings and accordingly σ_{S_X} the standard deviation of the slip signal.

Performance on high friction For the noise levels $\sigma_{f_{XT}} = 0.01$ and $\sigma_{S_X} = 0.003$ the comparison of noise-free and noisy inputs for the estimator is shown in Figure 4.27a, together with the results of the estimator. In Figure 4.27b it can be seen that the estimates converge close to the reference values, but the performance starts to deteriorate. In this case the EKF parameters are the same as in the test on high friction with noise-free inputs shown in Figure 4.24. Tuning of the EKF parameters can improve the performance, as can be seen in Figure 4.27c, where the measurement noise covariance parameter R of EKF has been increased. According to the theory of EKF the value of R should correspond to the variance of the measurement noise, which reader can see is not true in this case, as $R = 0.01$ and $\sigma_{f_{XT}}^2 = 0.0001$. A measurement a noise is however also present on the signal of slip, that is not minimized by the EKF process.

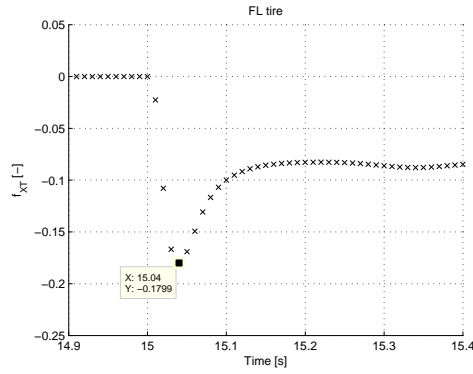


(a) input data and comparison of offline brush model fit and brush model parametrised by the resulting parameters of the online estimator

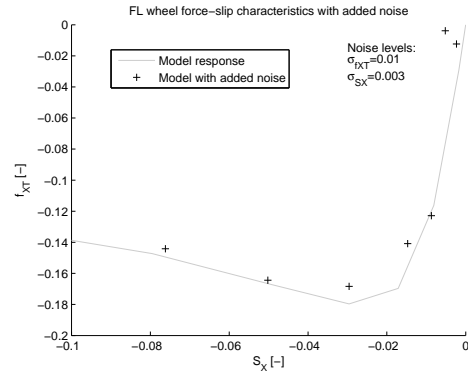
(b) output of the estimator over time - note that the settings of parameters of EKF is same as shown in Figure 4.24

(c) output of the estimator with increased measurement noise variance

Figure 4.27: Results of the online estimator test in complete vehicle model at high surface friction with added noise on input signals to the estimator.

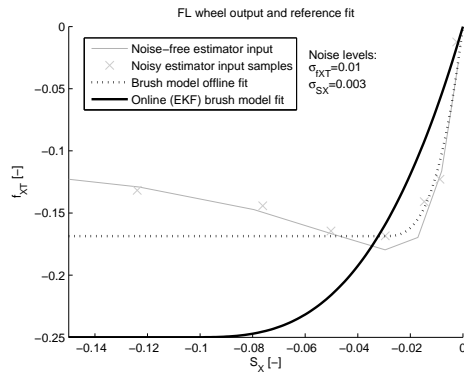


(a) tyre force in time - the peak is reached within 0.04 s from initiation of braking at 15 s

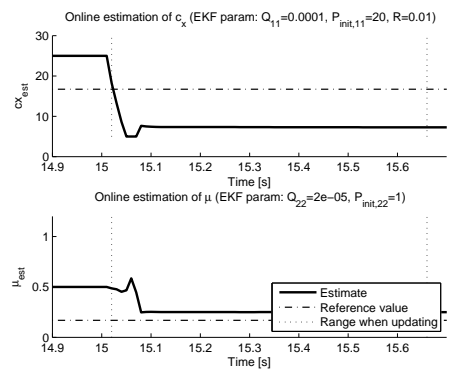


(b) force-slip graph and comparison of noise-free and noisy signals

Figure 4.28: Tyre response during braking on $\mu_{TR} \doteq 0.09$



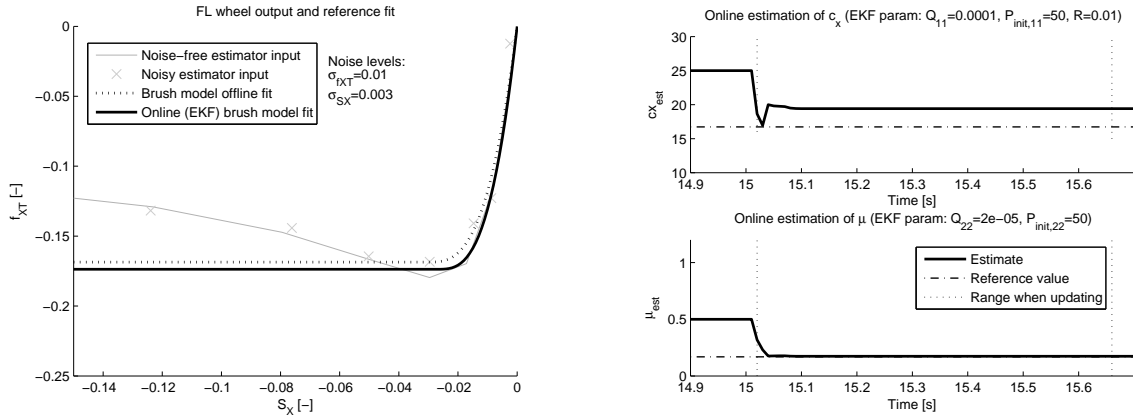
(a) input data and comparison of offline brush model fit and brush model parametrised by the resulting parameters of the online estimator; note the scale of Y axis



(b) output of the estimator over time

Figure 4.29: Results of the online estimator test in complete vehicle model at low surface friction with added noise on input signals to the estimator and parameters of EKF as in Figure 4.27c.

Performance on low friction Again the vehicle is driving at constant velocity $v_{X0} = 65$ km/h and then applies braking torque on all wheels. Friction of the surface is set to $\mu_{VTM} = 0.2$, for which the Magic Formula tyre model on the inspected front left tyre reach $\mu_{TR} \doteq 0.18$, see Figure 4.28a. In this case the brake actuator time constant is $\tau = 0.15$ s and the brake torque builds up quickly so that it takes 0.04 s or 4 samples to reach the peak of tyre force. The noise-free tyre response together with the added noise can be seen in Figure 4.28b. Results of the estimator are then shown in Figure 4.29b. With the same parameters of EKF as in previous test on high friction the estimate of friction doesn't converge to the actual tyre-road friction although the peak of tyre force has already been reached as seen also from comparison of force-slip characteristics in Figure 4.29a. The reason is low initial error covariance P_{22} of the friction estimate and also its relative value to initial error covariance P_{11} of slip stiffness estimate. In order to quickly adapt to the few samples before the peak is reached both initial error covariances are increased and the result can be seen in Figure 4.30b. With these parameters the estimator quickly updates the estimate of friction close to the actual $\mu_{TR} \doteq 0.18$. Also the estimate of slip stiffness seems to be better fitting the input data, see Figure 4.30a. Again it can be seen that the tuning of the EKF parameters plays significant role in the performance of the estimator.



(a) input data and comparison of offline brush model fit and brush model parametrised by the resulting parameters of the online estimator; note the scale of Y axis

(b) output of the estimator over time

Figure 4.30: Results of the online estimator test in complete vehicle model at low surface friction with added noise on input signals to the estimator and updated parameters of EKF.

4.4.4 Experiments

In order to evaluate the functionality and performance of the estimator in real conditions the experimental testing has been done by driving the investigated vehicle on a test track. This section describes how the signals required for the functionality of the estimator are acquired and processed. The required signals for friction estimator are normalised longitudinal tyre force f_{xT} and longitudinal slip S_x . For the decisive logic whether to estimate or not then also the longitudinal vehicle velocity v_x is used.

Neither of the signals is directly measured, all are determined from multiple measurements. The schematic diagram in Figure 4.31 shows the flow of information. In the left of the figure are shown the measured signals, which are processed as passing to the right of the diagram. The block *State Estimator* is provided by Volvo GTT, thus the output signals from the block are readily available. The complete list of signals measured on the investigated vehicle together with their source and sampling frequency is summarised in Table 4.2. All the signals are logged using data acquisition system dSpace MicroAutobox II.

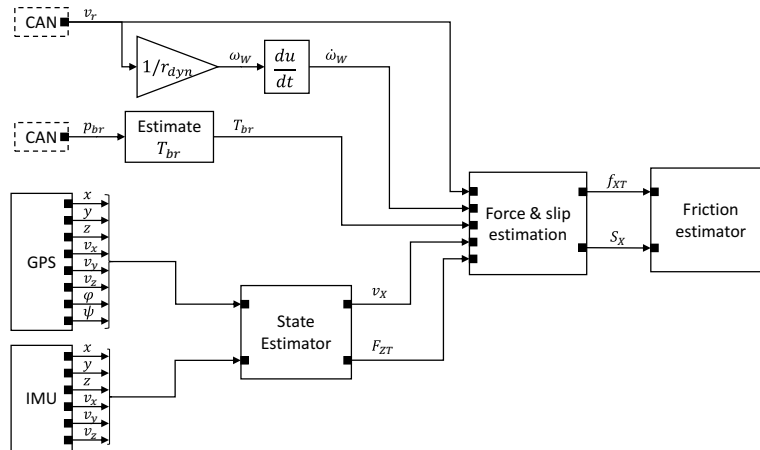


Figure 4.31: Schematic diagram of getting input signals for estimator

Linear wheel velocity is evaluated by the brake system ECU from the measurement of rotational speed of wheel ω_w [rad/s], that is measured by counting the number of teeth of the pulse-wheel that passed within a specific time interval. The ECU is provided by the supplier and exact description of signal processing is not

Table 4.2: List of signals measured on the investigated vehicle and needed for the friction estimator

Signal name	Symbol	Unit	Source	Sampling frequency [Hz]
Linear velocity of individual wheels	v_r	km/h	CAN	50
Brake pressure	p_{br}	kPa	CAN	50
Vehicle positions	x, y, z	m	GPS	10
Vehicle velocities	v_X, v_Y, v_Z	m/s	GPS	10
Vehicle attitude angles	φ, ψ	rad	GPS	10
Vehicle linear accelerations	$\ddot{x}, \ddot{y}, \ddot{z}$	m/s ²	IMU	250
Vehicle angular accelerations	$\ddot{\varphi}, \ddot{\theta}, \ddot{\psi}$	rad/s ²	IMU	250

known. It is assumed that the ECU determines the linear velocity using dynamic rolling radius r_{dyn} [m], that can be read from the ECU parameter file. The ECU then publish the linear wheel velocity of the respective wheel to the CAN network. It is assumed that this linear velocity is the velocity in the ground contact point, noted v_r . As far as is known the dynamic rolling radius in the ECU does not change to reflect short-term influences like the change of vertical load. Long-term influences like the tyre wear or inflation pressure are said to be reflected by adaptation process that is not publicly known in details.

Brake pressure is evaluated by the brake system ECU from measurement of the relative pressure at the brake control valve. At the front axle there is only one sensor for both left and right side of the axle. During normal operation the brake pressure shall be equal in both left and right brake cylinders of the front axle. In a steady state the measured pressure at the control valve should be equal to them as well. Since both left and right brake cylinders have individual control of the brake pressure in the brake cylinder downstream of the pressure sensor, during intervention of safety systems the pressure measured at the common control valve does not represent pressure in either of the individual brake cylinders. It can be simply said that the measured pressure gives maximal pressure of both individual brake cylinders. Each of rear axles then have separate pressure sensor for each of left and right side brake cylinders. In all cases the pressure sensors are located in the pneumatic system upstream the brake cylinders and therefore pneumatic system dynamics introduce a difference between actual pressure in the brake cylinder and the pressure measured by sensors.

GPS system equipped with two antennas placed on top of the driver's cab in lateral disposition, provide in three axis information about vehicle linear position (x, y, z) and linear velocity (v_X, v_Y, v_Z). Thanks to two antennas placed in lateral disposition, also angular position in roll (φ) and pitch (θ) are provided by the system. The system is assumed to provide reference values of vehicle position and velocity. The data are communicated to the data logger via serial communication line.

IMU - Inertial Measurement Unit provides information about vehicle acceleration in 6 axis - 3 linear ($\ddot{x}, \ddot{y}, \ddot{z}$) and 3 angular ($\ddot{\varphi}, \ddot{\theta}, \ddot{\psi}$). The unit is mounted to the cross member of the vehicle chassis approximately in the vehicle longitudinal plane of symmetry. The signals are communicated with the data logger via direct CAN connection.

4.4.4.1 Estimation of normalised longitudinal tyre force

The normalised longitudinal tyre force f_{XT} can be estimated from the torques applied on particular wheel. The equation of motion of a single wheel reads

$$J_{wz}\dot{\omega}_W = -F_{XT}r_{dyn} + T_{dr} - T_{br} - f_r F_{ZT}r_{dyn} \quad (4.24)$$

where J_{wz} is rotational inertia of the wheel, $\dot{\omega}_W$ is angular acceleration of the wheel, r_{dyn} is dynamic rolling radius, T_{dr}, T_{br} are drive, brake torque respectively, f_r is tyre rolling resistance coefficient. After rearranging the equation the tyre normalised longitudinal force reads

$$f_{XT} = \frac{F_{XT}}{F_{ZT}} = \frac{-T_{br} - J_{Wz}\dot{\omega}_W + T_{dr} - f_r F_{ZT}r_{dyn}}{F_{ZT} \cdot r_{dyn}} = \frac{-T_{br} - J_{Wz}\dot{\omega}_W + T_{dr}}{F_{ZT} \cdot r_{dyn}} - f_r \quad (4.25)$$

Wheel angular acceleration can be determined from wheel angular velocity that is measured on the vehicle by differentiation two consecutive samples

$$\dot{\omega}_W = \frac{\omega_W(t_2) - \omega_W(t_1)}{t_2 - t_1} \quad (4.26)$$

Wheel rotational inertia J_{W_y} is a physical property of tyre and rim combination. For the case of vehicle used here (cf. Section 3.2) they are described in Table 3.2.

Tyre rolling resistance coefficient f_r is depending on other tyre and road properties, thus can vary during operation of the truck. For a rigid road it can be in order 0.01 – 0.05, while it can reach over 0.3 for muddy soil [8]. Another source states that truck tyres on concrete or asphalt is usually in range 0.006 – 0.01[24]. A reference value selected here is $f_r = 0.01$.

Dynamic rolling radius r_{dyn} is defined as a radius of circle that has the circumference equal to distance travelled by one rotation of the wheel

$$r_{dyn} = \frac{C_R}{2\pi} \quad (4.27)$$

where C_R is the dynamic rolling circumference [5]. Dynamic rolling radius varies with the operating conditions, for instance the tyre wear or the tyre radial deflection due to varying load affect it. The value C_R is calibrated when a truck is being manufactured and the vehicle internally adapt this value every time the vehicle is started. Therefore it can be expected that low-frequency effects (like tyre wear) are covered, but high frequency effects (like radial deflection) are not covered. Table 4.3 illustrate the values obtained from ECU of the investigated vehicle.

Table 4.3: Dynamic rolling circumference and radius parameters from testing conducted 2015-04-08.

Axle	Side	C_R [m]	r_{dyn} [m]
Front	L	3.2755	0.5213
	R	3.2793	0.5219
Driven 1	L	3.3118	0.5271
	R	3.2998	0.5252
Driven 2	L	3.3048	0.5260
	R	3.3043	0.5259
Tag	L	3.279	0.5219
	R	3.3223	0.5288

Brake torque applied on wheel can be determined from brake pressure p_{br} that is measured in the brake system for each of wheels. In simple form the brake torque is proportional to pressure applied

$$T_{br} = p_{br} \cdot k_{br} \quad (4.28)$$

where $k_{br} \doteq 2114 \text{ Nm/bar}$ or, using the unit conversion factor $1 \text{ bar} = 101.325 \text{ kPa}$, $k_{br} = 2114/101.325 \doteq 21 \text{ Nm/kPa}$ is the brake factor for the particular wheel. However there are several things to consider. The brake factor can vary in short term as a result of changing temperature of the brake hardware, presence of dust, water or mud on the brake disc, etc., and in long term as a result of wear of the brake hardware [25]. For non-steady state situations it is of importance the location of the pressure measurement sensor. In case that the pressure sensor is not located directly in the brake cylinder, the length of pneumatic piping and possible restrictions (joints, orifices) introduce a dynamics between the actual pressure in the brake cylinder and the pressure measured by the pressure sensor. The influence of dynamics of the pneumatic system can be taken into account by modelling of the pneumatic system and application of the observer [26]. In the investigated vehicle the pressure measurement sensors are located at the Electronic Brake System (EBS) control valve, that is located at vehicle chassis, ie. remotely from the brake cylinder. An internal Volvo technical report shown that the pressure reading at EBS valve differs from the actual pressure in the brake cylinder. The report states that the pneumatic system acts as a low-pass filter with no further details.

Drive torque T_{dr} was not needed during this project since only braking situations are used for estimation of friction. It can be estimated from the torque of the engine [2], which can be provided by the engine ECU.

4.4.4.2 Estimation of longitudinal slip

The tyre slip is determined from difference of the tyre (wheel) velocity and the vehicle velocity in wheel ground contact point. Longitudinal tyre slip is defined in *practical* form as

$$S_X = -\frac{v_X - v_r}{v_X} \quad (4.29)$$

where v_X is the longitudinal velocity of the vehicle in wheel ground contact point and v_r represents the velocity of the tyre in the contact point in the direction of the wheel plane which is measured on each of wheels. In the case of vehicle driving straight with no steer angle ($\delta = 0$ rad) and no lateral acceleration the vehicle velocity and v_X are equal. The vehicle velocity is provided by the vehicle State Estimator, as shown in Figure 4.31.

4.4.4.3 Uncertainty evaluation

In order to express confidence of the results obtained from the measurement the uncertainty of the measured values is analysed. Of interest is the value of normalised tyre force f_{XT} at given tyre slip S_X . Both the values are obtained by means of indirect measurements and affected by noise, thus uncertainties of both f_{XT} and S_X are of interest. The uncertainty is evaluated following the recommendations of Joint Committee for Guides in Metrology [27].

Uncertainty of force The force is determined from the equation equation (4.25). In case of braking the drive torque is not present and T_{dr} can be omitted. The brake torque is replaced by equation (4.28). After these modifications equation (4.25) reads

$$f_{XT} = \frac{-p_{br} \cdot k_{br} - J_{Wy} \dot{\omega}_W}{F_{ZT} \cdot r_{dyn}} - f_r \quad (4.30)$$

where all terms are direct input quantities. These are constant parameters (k_{br} , J_{Wy} , r_{dyn} , f_r) and variables that change in time (p_{br} , $\dot{\omega}_W$, F_{ZT}). Uncertainty of each of input quantities contributes to the total uncertainty of f_{XT} . One of the situations from the testing where the investigated vehicle was braking at the dry road is considered here. For convenience only the situation at one tyre is investigated here, where chosen one is the front left tyre of the vehicle.

The input variables are changing in time, so mean values from a time interval where all the variables are in more or less steady state are taken. Then $\bar{p}_{br} \doteq 970$ kPa, $\bar{F}_{ZT} \doteq 55$ kN and $\bar{\omega}_W \doteq 13$ rad/s². Uncertainty of these variables is in this case evaluated using the Type A method [27] as a standard deviation in the observed time interval. In this case the respective uncertainties are $u(\bar{p}_{br}) \doteq 30.118$ kPa, $u(\bar{F}_{ZT}) = 5.111$ kN and $u(\bar{\omega}_W) = 9.727$ rad/s².

The constant parameters are, to some extent, also uncertain. In this case their uncertainty is evaluated using the Type B method [27]. For the rolling resistance coefficient the reported values spread from 0.006 to 0.05 for rigid road (asphalt, concrete) [8, 24]. Let's assume that the rolling resistance coefficient can lie within equal probability in this range, then $u(f_r) = (0.05 - 0.006)/2\sqrt{3} \doteq 0.013$. If it is assumed that the brake factor can change in range ± 200 Nm/bar $\doteq 2$ Nm/kPa with equal probability, then $u(k_{br}) = 2/\sqrt{3} \doteq 1.155$ Nm/kPa.

The dynamic rolling resistance shall be adapted to tyre wear by the vehicle ECU. In this case for the front left tyre the vehicle ECU stores value $r_{dyn} = 521.3$ mm. The dynamic rolling radius changes with the changing vertical load. A simple model of this relation is a linear spring with the stiffness corresponding to tyre radial stiffness. The radial stiffness changes with tyre inflation pressure, which changes with temperature. The relation is thus complex and it is not investigated in detail here. Since there is a relation between input quantities F_{ZT} and r_{dyn} , their covariance should also be taken into account for proper evaluation of uncertainty, but due to lack of time this fact is omitted here and it is assumed that they are independent. For simplicity it is thus assumed that the radius can be in range ± 0.02 m with equal probability, then $u(r_{dyn}) = 0.02/\sqrt{3} \doteq 0.012$ m.

The wheel inertia J_{Wy} is a physical property of tyre and rim combination, mostly dependent on tyre and rim dimensions and density. The free radius of tyre and its mass will decrease with tyre wear. Furthermore the value of inertia is not experimentally validated, so it is assumed that it can be in range ± 1 kg · m² with equal probability. The uncertainty is then $u(J_{Wy}) = 1/\sqrt{3} \doteq 0.58$ kg · m².

With the given input quantities the tyre force is

$$f_{XT} = \frac{-970 \cdot 21 - 17.3 \cdot 13}{55000 \cdot 0.5213} - 0.01 \doteq -0.713 \quad (4.31)$$

The combined standard uncertainty $u(f_{XT})$ is then

$$u(f_{XT}) = \sqrt{\sum_{i=1}^N \left(\frac{\partial f}{\partial x_i} \right)^2 u^2(x_i)} \quad (4.32)$$

where f represent the equation (4.30) and x_i are the input quantities p_{br} , k_{br} , etc., with $u(x_i)$ being the respective uncertainties of input quantities. Thus in this case $N = 7$. The resulting combined standard uncertainty is

$$u(f_{XT}) \doteq 0.082 \quad (4.33)$$

which means that in this particular case the estimated force is $f_{XT} = 0.713 \pm 0.082$.

Uncertainty of slip The longitudinal tyre slip is determined as per equation (4.29) using longitudinal velocity of the vehicle v_X and the linear wheel speed v_r .

The longitudinal velocity of the vehicle is given by the vehicle state estimator. The vehicle velocity is estimated from multiple inputs which are not exactly known and which can also differ during operation of the vehicle (e.g. due to loss of GPS signal). The uncertainty is thus determined from visual inspection of the estimated vehicle velocity signal from time period of driving at more or less constant velocity. The noise is assumed to be Gaussian with peaks in range ± 0.1 m/s. If it is then assumed that the range is covered by six standard deviations, uncertainty evaluated using Type A method [27] is $u(v_X) = 0.1/3 \doteq 0.03$ m/s.

The velocity of tyre v_r is obtained from vehicle ECU. One source of uncertainty presents the limited accuracy of the direct physical measurement of the rotational speed of the wheel ω_W , which is not known in detail. Further on a dynamic change of r_{dyn} that is used to calculate the respective v_r is another source of uncertainty. For simplicity it is assumed that this measurement is little more uncertain than the vehicle velocity [7], $u(v_r) = 0.035$ m/s.

Let's consider the same situation as used for evaluation of uncertainty of the tyre force - approximately steady state braking on a dry road. In this case the nominal values of input quantities are from the same time instant, $v_X = 16.74$ m/s and $v_r = 15.72$ m/s and the slip is therefore

$$S_X = -\frac{v_X - v_r}{v_X} = -\frac{16.74 - 15.72}{16.74} \doteq 0.0609 \quad (4.34)$$

The combined standard uncertainty of the slip $u(S_X)$ is then determined using relation

$$u(S_X) = \sqrt{\left(\frac{\partial S_X}{\partial v_X} \right)^2 u^2(v_X) + \left(\frac{\partial S_X}{\partial v_r} \right)^2 u^2(v_r)} \quad (4.35)$$

and numerically

$$u(S_X) \doteq 0.0027 \quad (4.36)$$

Therefore in this particular case the estimated slip is $S_X = 0.0609 \pm 0.0027$.

4.4.4.4 Sensitivity analysis

Sensitivity analysis can provide an insight to how particular measurements and parameters contribute to uncertainty of the desired inputs for the estimator.

Sensitivity of estimated force The base for sensitivity analysis is again the equation for normalised tyre force equation (4.30). To evaluate the effect of particular input quantity x_i the partial derivative to this input quantity is evaluated for the nominal values of input quantities. This partial derivative then provides a sensitivity factor of how a change of particular input quantity change the output. The change of particular input quantity Δx_i then causes a change of the estimated force as follows

$$\Delta f_{XT} = \frac{\partial f_{XT}}{\partial x_i} \cdot \Delta x_i \quad (4.37)$$

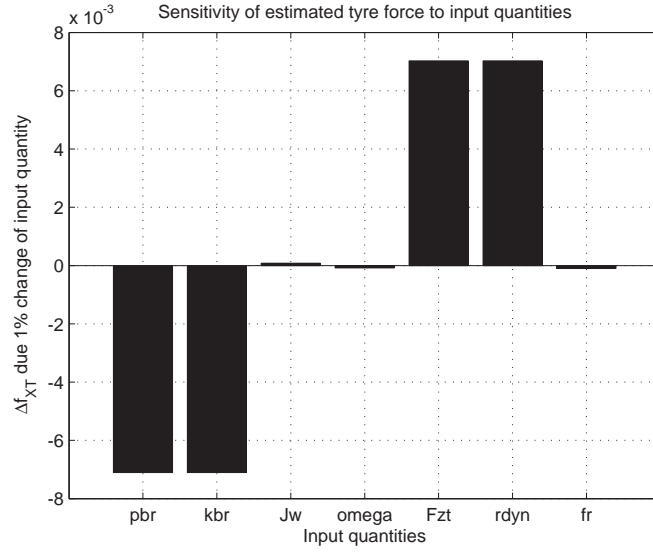


Figure 4.32: *Sensitivity of estimated force to 1% change of the input quantities*

For nominal values $\bar{p}_{br} \doteq 970$ kPa, $k_{br} = 21$ Nm/kPa, $J_W = 17.3$ kg · m², $\bar{\omega}_W \doteq 13$ rad/s², $\bar{F}_{ZT} \doteq 55$ kN, $r_{dyn} = 521.3$ mm and $f_r = 0.01$ the change Δf_{XT} for 1% change of each input quantity is evaluated, to show how much the same relative change of each of input quantities affects the final estimate. The results are shown in Figure 4.32. From the graph it can be seen that the force estimation is most sensitive to changes in brake pressure and brake factor, both with negative sign. Similar magnitude of sensitivity, but with positive sign is shown for change in vertical load F_{ZT} and rolling radius r_{dyn} . The change of inertia J_W , angular acceleration $\dot{\omega}_W$ and rolling resistance has much lower effect. That points out to which signals and parameters the attention shall be paid. The same relative error in brake pressure readings and brake factor have significantly higher effect on inaccuracy of the estimated force than the inaccurate inertia of the wheel. Needless to say that the sensitivity factor also changes with the nominal values.

Sensitivity of slip The same approach as for sensitivity of force is used for slip. In equation (4.29) for determining the slip two input quantities v_X and v_r are used. For their nominal values $v_X = 16.74$ m/s and $v_r = 15.72$ m/s, the sensitivity to each of inputs is evaluated as

$$\Delta S_X = \frac{\partial S_X}{\partial v_X} \cdot \Delta v_X \quad (4.38)$$

where again 1% change of input quantities is used, therefore $\Delta v_X = 0.01 \cdot v_X$. Analogically for v_r . From the results shown in 4.33 it can be seen that the estimate of slip is almost equally sensitive to both input quantities with positive sign. Since the relation for slip equation (4.29) is linear, the relative sensitivity to both input quantities is the same, ie. even for different nominal values slip is equally sensitive to change in both quantities. That means that inaccuracy of both input quantities have equal impact on the inaccuracy of the slip, therefore for improving the accuracy of slip both input quantities are equally important.

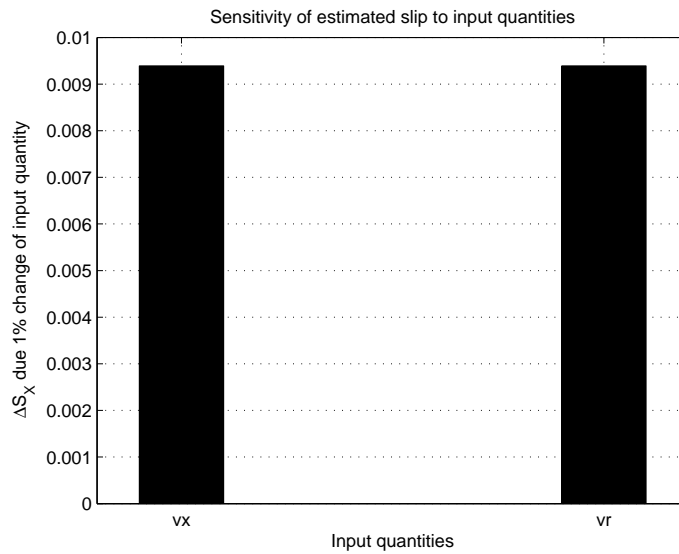


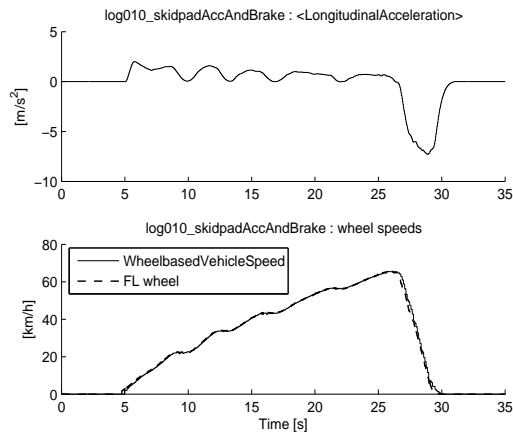
Figure 4.33: *Sensitivity of estimated slip to 1% change of input quantities*

4.4.5 Validation

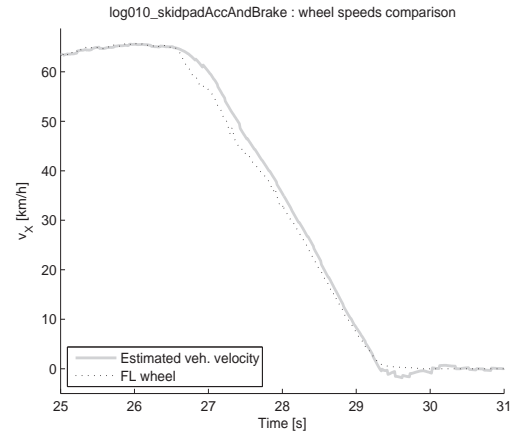
In this step the estimator functionality is evaluated on the data measured within the vehicle during testing. The tests comprised of hard braking of the test vehicle from a constant speed up to standstill. Processing of the signals measured in vehicle is described in Sections 4.4.4.1 and Section 4.4.4.2. Results of one of the conducted tests are shown in Figure 4.34. For clarity only signals related to front left (FL) tyre are shown. In the resulting force-slip characteristic shown in Figure 4.34d the characteristic curve of the tyre longitudinal force for the increasing (in absolute value) slip is expected. However two main distortions can be observed:

1. rather big spread of samples due to measurement noise
2. several points along the vertical axis

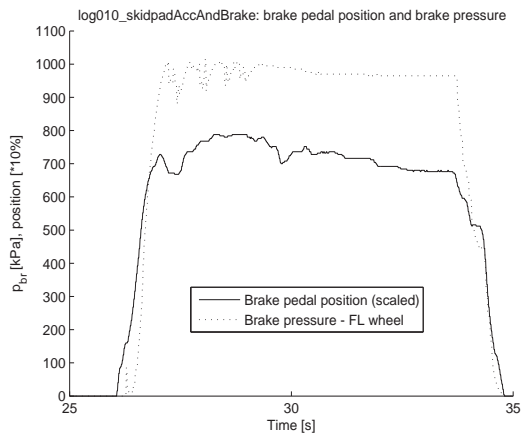
Similar behaviour can be observed on all wheels and in all test cases that have been conducted in the same test day. All the relevant test data can be found in Appendix C.1. The source of the noise shall be further inspected. Cause of the latter distortion is that the estimated force decreases earlier than the slip starts to decrease, see Figure 4.35a. The normalised longitudinal force f_{XT} is estimated using the measurements of brake pressure and the slip S_X is obtained from estimated vehicle velocity and the wheel velocity in the contact wheel ground contact point. In Figure 4.35b is then plotted the comparison of wheel angular acceleration and the measured brake pressure where the possible cause for the distortion can be seen - the brake pressure rises earlier than the wheel actually starts decelerating.



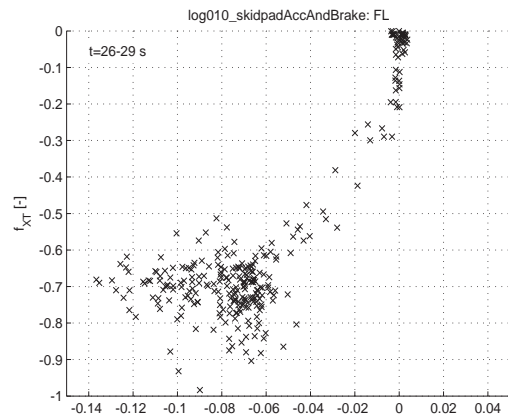
(a) chassis longitudinal acceleration and velocity - signals from vehicle CAN



(b) estimated vehicle velocity and FL wheel velocity comparison - detail on the time when braking

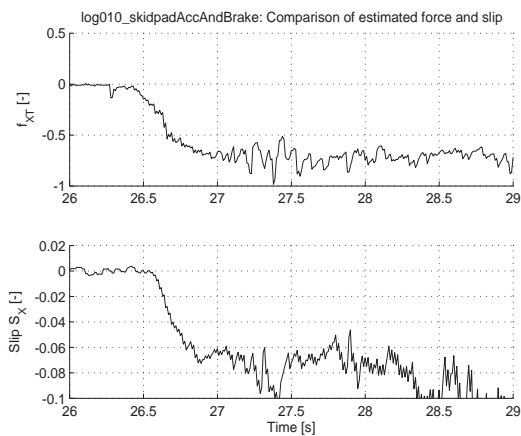


(c) brake pedal position and brake pressure in FL wheel circuit - detail on time when braking

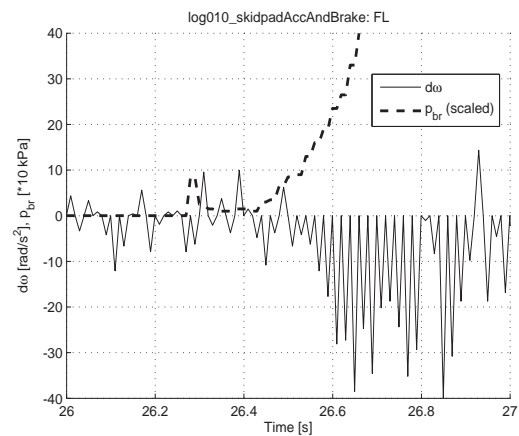


(d) force-slip response of FL tyre - from the time when braking

Figure 4.34: Test results - braking on high friction



(a) comparison of force and slip over time - detail on the time of initiation of braking

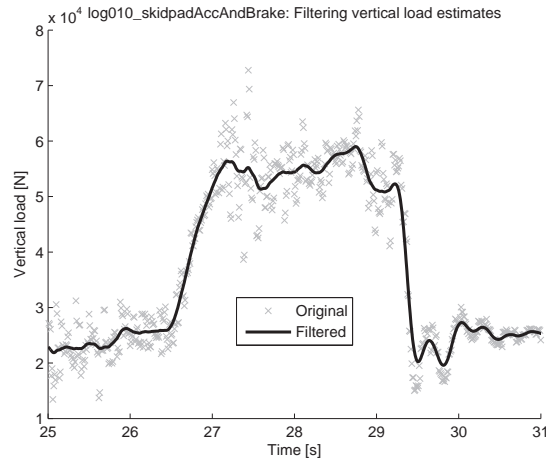


(b) comparison of measured brake pressure and wheel angular acceleration - detail on the time of initiation of braking

Figure 4.35: Inspection of the initial force-slip samples

Signal processing

A signal processing has been applied to improve the quality of input data for the estimator. First the signal of the wheel speeds has been found to be sampled at 100 Hz, while the values seem to update at 50 Hz frequency. This is also the reason why the wheel angular acceleration signal (resulting from differentiation of wheel speed signal) is equal to zero every second sample, as shown in Figure 4.35b . Offline processing allow us to downsample the original signal to 50 Hz and the interpolate it to reach 100 Hz sampling rate as all the other signals already have⁴. Further the main contributor to noise was found to be the estimation of vertical load as can be seen in Figure 4.36 It is not probable that the vertical load oscillates in range 4 – 7 kN within 0.06 s. The filtered signal presented in Figure 4.36 was achieved by application of zero-phase FIR filter with equal weighting of 15 samples. The resulting force-slip graph is shown in Figure 4.37. The improvement can be seen compared to Figure 4.34d, however the practical implementation still needs to be discussed and justified.



y

Figure 4.36: *Estimation of the vertical load on front left tyre obtained from vehicle state estimator and illustration of filtering applied.*

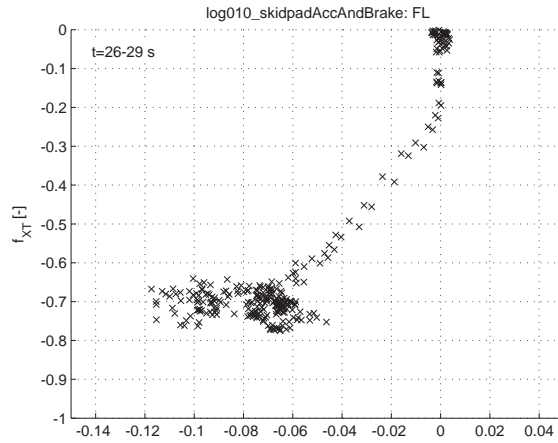


Figure 4.37: *force-slip response of FL tyre - from the time when braking*

As outlined in Section 4.4.4.1 the location of the brake pressure sensor can affect the measurement data. If the pressure sensor is not located directly in the brake cylinder, there is some dynamic of the pneumatic system involved that introduce a difference between actual pressure inside the brake cylinder and the pressure that is measured by the remotely located pressure sensor. In case of the investigated vehicle the brake pressure

⁴For further application it must be sort out whether the signal is available at 100 Hz sample rate or at 50 Hz, which affect the online processing.

sensor is located remotely, at the control valve body and in such case it has been confirmed that actual brake pressure in brake cylinder differs from brake pressure sensor readings during transient changes of the brake pressure. However further research of this phenomena has not been found.

Without detailed investigation and modelling of the pneumatic system dynamic behaviour 2 pragmatic attempts to improve the quality of the brake pressure measurement are done. Since no reference measurements of the brake pressure in the brake cylinder are available for this case, the potential improvement is judged from visual inspection of the force-slip graph.

Filtering of the brake pressure A simple first order low pass filter is applied on the brake pressure measurements. First the time constant of the low-pass filter is set to $\tau = 0.05$ s. The result of the brake pressure filtering is shown in 4.38a. In the resulting force-slip graph in Figure 4.38b can be seen that there are less samples with approximately zero slip S_X and non-zero force f_{XT} that are forming the nearly vertical part of the graph, which is not natural for the tyre behaviour. However a new distortion of the graph occur around $S_X \doteq -0.6$ and $f_{XT} \doteq -0.6$. For increased time constant of the low-pass filter $\tau = 0.1$ s the vertical part further decreases but at the same time the new distortion further increases, see Figure 4.39b. A simple low-pass filter doesn't seem to solve the issue.

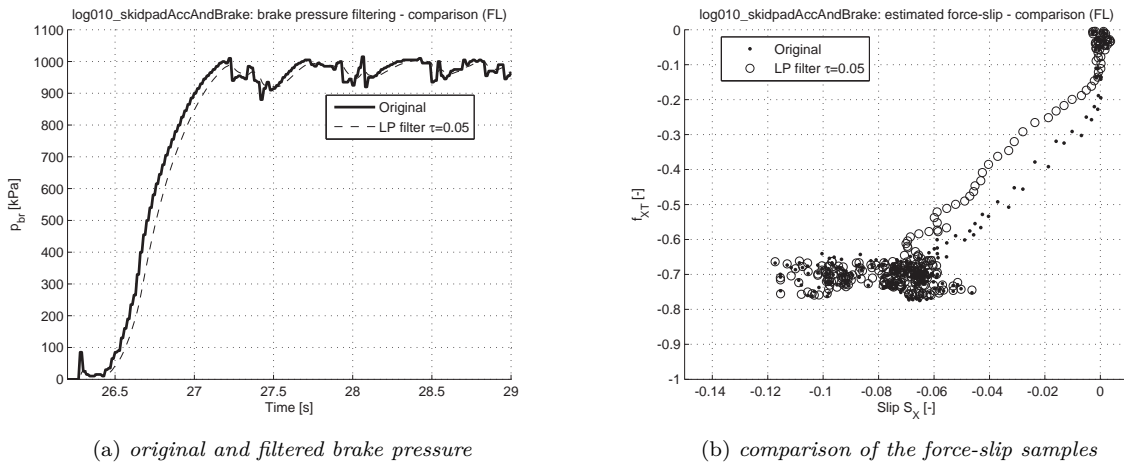


Figure 4.38: Brake pressure processing - application of low-pass filter with time constant $\tau = 0.05$ s

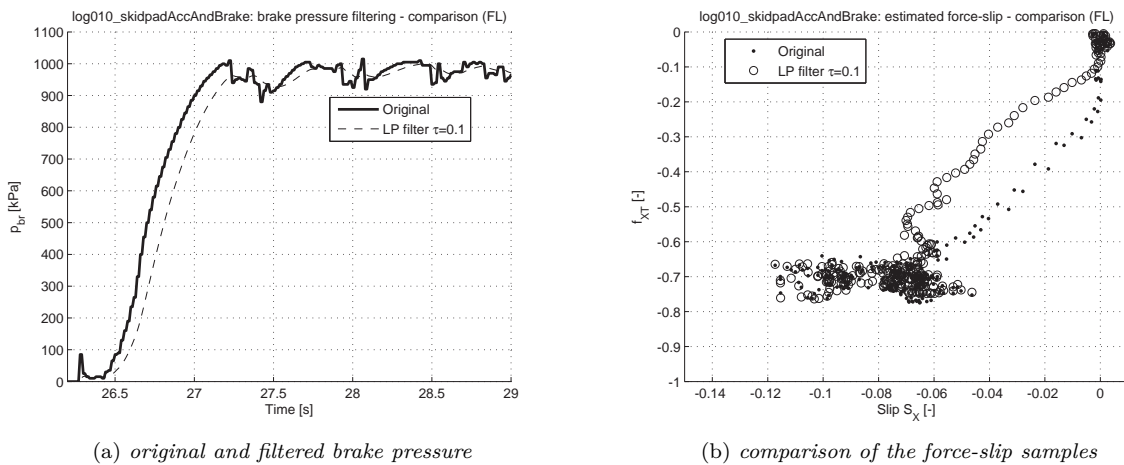
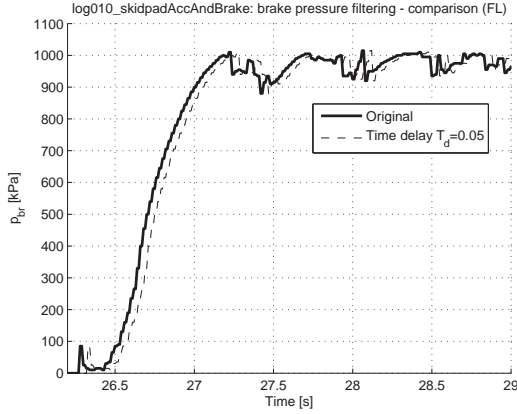
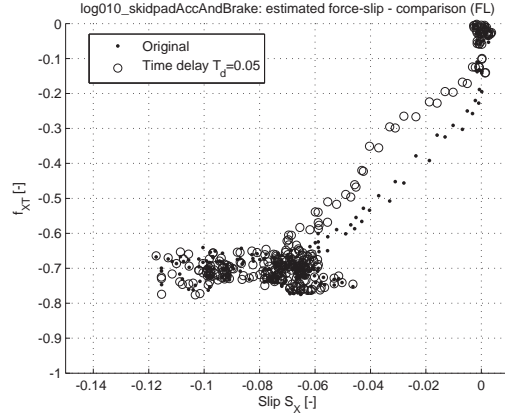


Figure 4.39: Brake pressure processing - application of low-pass filter with time constant $\tau = 0.1$ s

Adding a pure time delay Another option is to add a pure time delay to the signal of the brake pressure. For delay $T_d = 0.05$ s the comparison of original and delayed brake pressure is shown in Figure 4.40a and the resulting force-slip graph in Figure 4.40b. The effect of initial vertical samples (zero slip and nonzero force) is decreased, however there still remains quite unnatural cloud of samples. For delay $T_d = 0.1$ s the effect is even bigger as seen in Figure 4.41b.

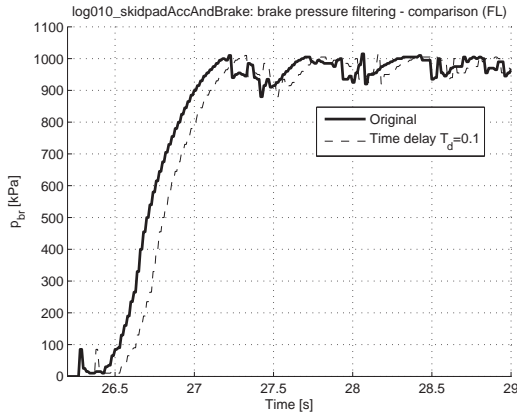


(a) original and filtered brake pressure

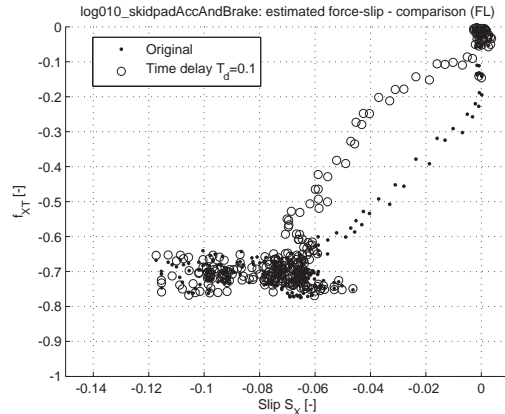


(b) comparison of the force-slip samples

Figure 4.40: Brake pressure processing - application of pure time delay $T_d = 0.05$ s



(a) original and filtered brake pressure



(b) comparison of the force-slip samples

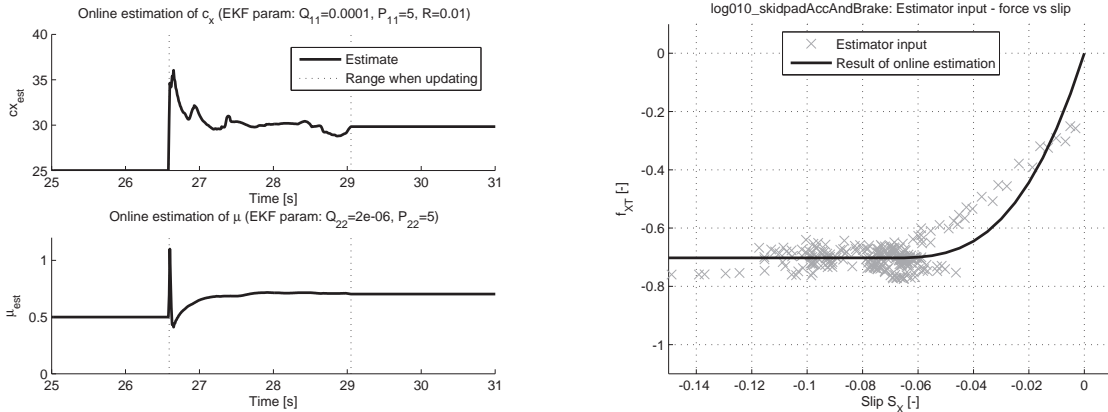
Figure 4.41: Brake pressure processing - application of pure time delay $T_d = 0.1$ s

Neither low-pass filter nor pure time delay solves the issue and creates better looking force-slip graphs. The pneumatic system dynamic can be more complex, ie. a combination of low-pass filter with pure time delay, or there may be other effects introducing the distortion than the brake pressure measurements, e.g. the general measurement noise, or wheel radius change during the braking manoeuvre. It is also possible that the brake factor is not linear, or that it changes during the braking phase significantly. More investigation has not been done by the time of completion of the thesis.

4.4.5.1 Estimator validation on high friction

The estimator implementation can now be tested on the data obtained from testing vehicle. The force-slip samples as shown in Figure 4.37 are the inputs to the online estimator in their respective time order. The estimator functionality is simulated and the results are shown in Figure 4.42. In Figure 4.42b we can see for which samples the estimator updates as a result of switching logic presented in equation (4.21), equation (4.22)

and equation (4.23). Note that the initial part with samples almost vertical is thus skipped. In Figure 4.42a is shown that the estimator updates the estimates and in case of estimated friction it finally converges to value $\mu_{est} \doteq 0.7$. That seems to be reasonable result of online estimator with respect to the inputs shown in Figure 4.42b. It is however not clear, what should the actual tyre-road friction (a reference value) in this case be. An option to find a reference value could be to actually reach the peak of actual tyre characteristic. An indicator of reaching the peak could be a locking of the wheel and an intervention of ABS. The ABS intervention did not happen in this case. It might be also possible that the actual tyre characteristic really looks like it is shown in Figure 4.42b, where there is no distinct peak, but rather a constant saturation of the tyre force. The EKF parameters were tuned to provide these results and they are shown in annotation of Figure 4.42a.



(a) Evolution of the estimates over time

(b) Comparison of estimator inputs and the brush model parameterised by the final estimates of the online estimator

Figure 4.42: Estimator test on real data - braking of the vehicle on dry road

4.4.5.2 Estimator validation on low friction

To evaluate the estimator performance to detect low friction, which is of higher interest, a testing vehicle has been braked on wet basalt. Wet basalt provides very low friction, around⁵ 0.2. This testing has been conducted in June 18, 2015.

Again only one wheel is investigated for convenience. In this case a front left wheel can't be used due to corrupted data. Instead a left wheel on 2nd axle is selected (denoted as DR1L). In Figure 4.43 is shown the comparison of wheel speed measurement of the DR1L wheel with the estimated vehicle velocity. The characteristic dips in wheel speed readings due to wheel locking can be observed. The ABS intervened to prevent total wheel sliding. As seen in the resulting force-slip graph shown in Figure 4.44b the normalised longitudinal tyre force f_{XT} stays approximately in range from -0.1 to -0.2 . That corresponds to low friction of the surface.

The quantitative accuracy of the force f_{XT} is of further discussion, since the estimation of the vertical load is given as a total load on second, third and fourth wheel together on the left (or similarly also right) side of vehicle. A simplified assumption is made here that each of these wheels is loaded with one third of the total estimated vertical load for all three. This assumption couldn't be validated by the time of finishing of this thesis.

The resulting force and slip estimates provide the input for the estimator. The estimator functionality is simulated to process the input samples in their respective time order. The results of the simulation of estimator are shown in Figure 4.45. It can be seen that the estimate of friction quickly updates to $\mu_{est} \doteq 0.26$ within the time of 0.2 s from the start of braking and then slowly decreases down to $\mu_{est} \doteq 0.23$. In Figure 4.45b it can then be seen that most of the samples have normalised force below (in absolute value) 0.2, which indicates that higher normalised longitudinal force can not be achieved with actual combination of tyre and road. In other words the tyre-road friction seems to be $\mu_{TR} \leq 0.2$. That means the estimator in this case overestimates the tyre-road friction, because $\mu_{est} > \mu_{TR}$.

⁵The actual value of tyre-road friction also depends on tyres.

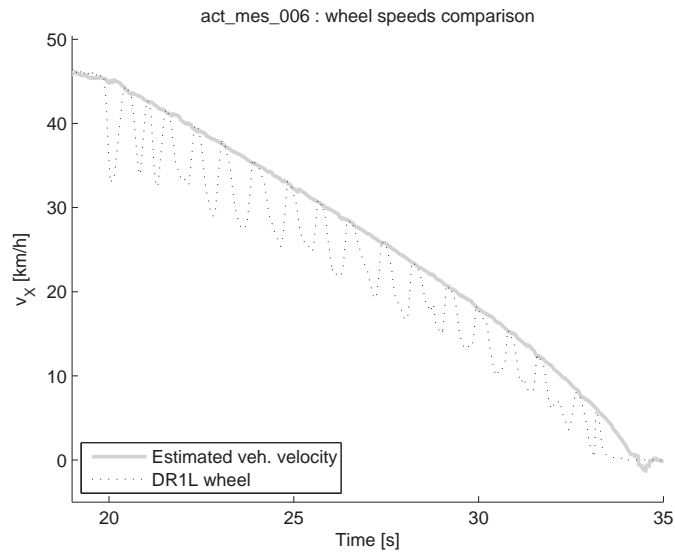
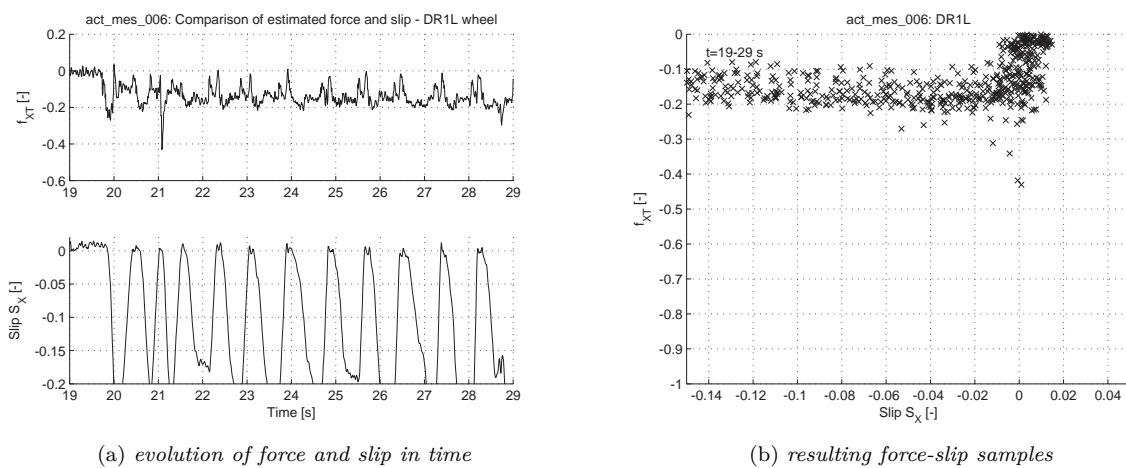


Figure 4.43: *Braking on wet basalt - comparison of estimated vehicle velocity and wheel speed readings of DR1L wheel*



(a) *evolution of force and slip in time*

(b) *resulting force-slip samples*

Figure 4.44: *Braking on wet basalt - estimated force and slip for DR1L wheel*

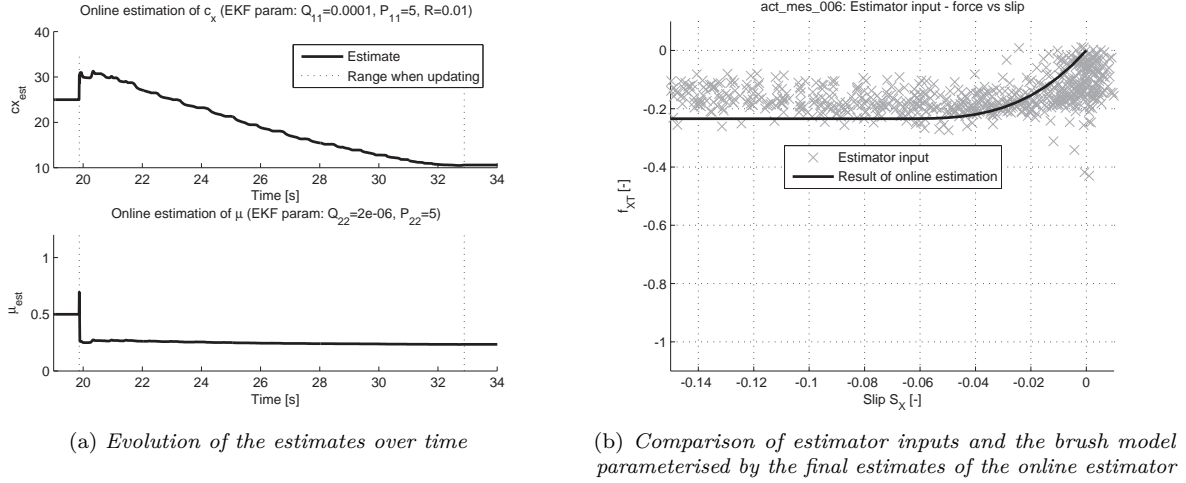


Figure 4.45: *Estimator test on real data - braking of the vehicle on wet basalt*

From Figure 4.45a it can also be seen that the estimate of normalised slip stiffness c_x increases in the beginning and then gradually decreases. In the input data shown in Figure 4.45b it is however hard to say, which slip stiffness is reasonable, as the force-slip samples does not clearly resemble the typical tyre response curve.

The performances of the estimator shown in Section 4.4.5.1 and Section 4.4.5.2 are results of tuning of EKF parameters to achieve good performance in both cases. Faster indication of low friction can be achieved by change of EKF parameters, but these can make the estimator diverging on the high friction case. The tuning strongly depends on number of samples in linear and non-linear region of the typical tyre characteristic.

4.4.6 Adaptive tuning of EKF using measure of non-linearity

It has been shown that performance of estimator based on EKF depends on number of samples and their distribution along the tyre characteristic. For that reason the the idea to relate the tuning of the EKF to the input data is introduced here. As it has been shown before the friction cannot be accurately estimated within the linear region of tyre characteristic. Therefore it is of interest to *suspend* the estimation of friction until the sufficient excitation occurs so that the non-linear tyre region is entered. In Section 4.4.3.2 this has been achieved by putting the initial error variance P_{22} of the friction estimate μ_{est} low. Any sort of static threshold applied on longitudinal slip S_X or the tyre force f_{XT} cannot be applied, since the beginning of the non-linear region is dependant on the particular tyre and road conditions. Instead an approach that will be able to distinguish the increasing non-linearity regardless the magnitude of slip or force is desired. An idea introduced here and inspired by [28] is to approximate a linear tyre model to the input force-slip samples. It is expected that the error between the between the linear tyre model and actual measurements should then rapidly increase with increasing non-linearity of the tyre response. Such quantisation is called Measure of Nonlinearity (MoN)[29].

For linear approximation a linear tyre model is used

$$f_{XT} = c_X \sigma_X \quad (4.39)$$

where c_X is parameter to be estimated and f_{XT} , σ_X are output, input of the system respectively, provided by measurements. A Recursive Least Square method introduced in Section 2.4.1 is applied. In this case $\Theta = c_X$ is the parameter to be estimated and input $u(t) = S_X$. In this case there is $N = 1$ parameters and $M = 1$ process outputs, hence the general form becomes

$$\hat{\Theta} = \frac{y_p}{u(t)} \quad (4.40)$$

In Figure 4.46a are shown two resulting linear approximations of the force-slip samples using the RLS algorithm, one using samples only in the linear region, the other then uses few more samples of the tyre characteristic, where these samples are already in the non-linear range of tyre characteristic. It can be seen

that for the first approximation it follows the input force-slip samples well, in case of the second the rising error between linear approximation and the input samples is obvious.

To evaluate the non-linearity a difference between linear approximation and the actual measurements in form of sum of square residuals is determined as

$$J = \sum_{i=1}^N (f_{XT,lin}(i) - f_{XT,meas}(i))^2 \quad (4.41)$$

where $f_{XT,lin}(i)$ is the normalised longitudinal tyre forced determined by linear tyre model from equation (4.39) using actual estimate of slip stiffness estimate $c_x(i)$ and actual slip measurement $S_X(i)$

$$f_{XT,lin}(i) = c_x(i) S_X(i) \quad (4.42)$$

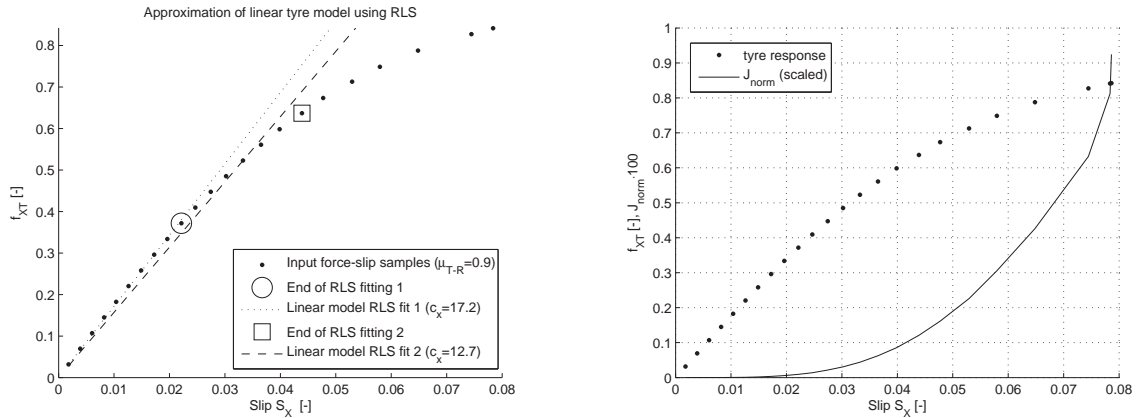
and $f_{XT,meas}(i)$ is the actual measurement of the normalised longitudinal force. For recursive evaluation the equation (4.41) reads

$$J(i) = J(i-1) + (f_{XT,lin}(i) - f_{XT,meas}(i))^2 \quad (4.43)$$

The magnitude of the error would in this case be related to the absolute values of the normalised force and thus in turn on the actual level of tyre-road friction. This influence can be avoided by introduction of a normalisation in terms

$$J_{norm}(i) = J_{norm}(i-1) + (f_{XT,lin}(i)/f_{XT,meas}(i) - 1)^2 \quad (4.44)$$

which is called *relative* MoN. Furthermore the magnitude of the error can differ with the total number of samples that have been taken into the sum. The J_{norm} is therefore normalised by the number of samples i . Resulting graph of J_{norm} against the slip is plot together with the tyre response in Figure 4.46b. The procedure has been applied on tyre response for different levels of friction level μ_{TR} . Results in Figure 4.47 show that the MoN in form of J_{norm}/i gives comparable magnitude for different levels of tyre-road friction and also for different number of samples. The qualitative behaviour follows the expectations that the MoN significantly increases when the tyre characteristics is getting more and more non-linear.



(a) Comparison of two linear tyre model approximations using RLS. Notice that while the first estimate follows the input force-slip samples very well up to the point of End of RLS fitting, few samples later the linear tyre model doesn't fit the input force-slip samples very well.

(b) Measure of non-linearity together with the tyre response. Note that J_{norm} is scaled in the figure for convenience.

Figure 4.46: Using RLS algorithm for linear tyre range approximation

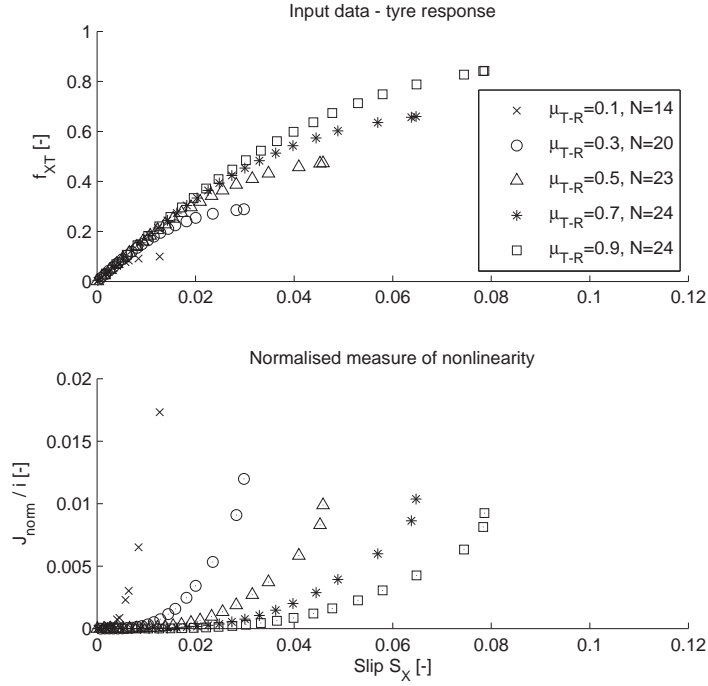
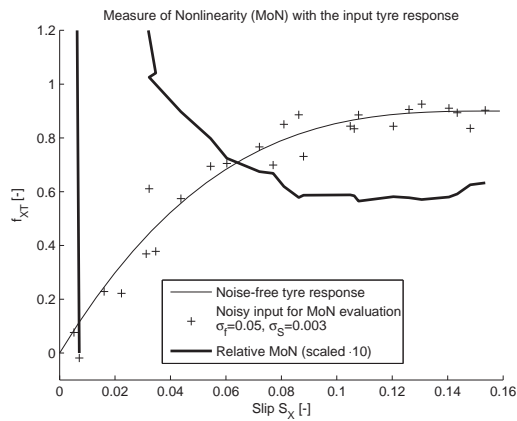
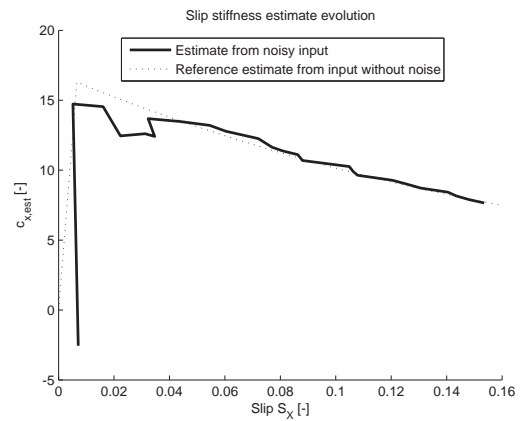


Figure 4.47: Measure of non-linearity for different levels of friction. Note that the number of input samples is not equal for different levels of friction. Also note that the magnitude of the measure of non-linearity is on approximately the same level for different levels of friction.

To assess the MoN on the more realistic input a noise is added to the signals of force f_{XT} and slip S_X . For the sake of simplicity the response of the complex Magic Formula tyre model from the VTM simulation environment is here replaced by the simple brush model. The brush model is sufficient for providing the typical tyre characteristic - the force-slip input samples that are needed as the input for MoN. The noise is zero-mean Gaussian white and its level of noise is (like in Section 4.4.3.4) represented by respective standard deviations $\sigma_{f_{XT}}$, σ_{S_X} , later shown in the graphs. Evaluation of MoN on a noisy input shown in Figure 4.48a reveals first problem. The MoN increases over the bounds within first very few samples, thus significantly degrading whole concept. From the graph of the evolution of the estimate of the slip stiffness shown in Figure 4.48b it can be seen that initially the slip stiffness is estimated negative, and with increasing number of samples (here correspond to increasing slip), the estimate gets to more reasonable values. A limitation of the slip stiffness estimate to reasonable values is therefore introduced with the same limits as introduced by equation (4.20) in Section 4.4.3.1 for the friction estimator. With these limits the $c_{x,est}$ stays in reasonable values and better follows the reference as seen from Figure 4.49b. As a result the magnitude of the peak of MoN is significantly reduced as seen from Figure 4.49a, however the peak is still persisting. In Figure 4.49a there is also plotted the MoN without the normalisation applied, which shows the expected qualitative behaviour. The peak seems to be caused by the normalisation. From equation (4.44) it can be seen that when the measured normalised force $f_{XT,meas}$ is close to zero and $f_{XT,lin}$ is not, the term $f_{XT,lin}/f_{XT,meas}$ goes to infinity. Further evaluation of the problem has not been done within the time frame of the thesis.

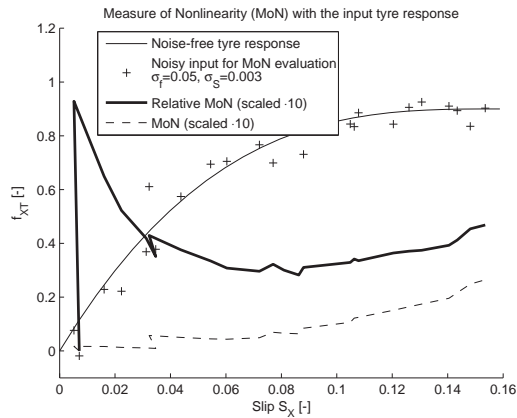


(a) Comparison of MoN and the input samples

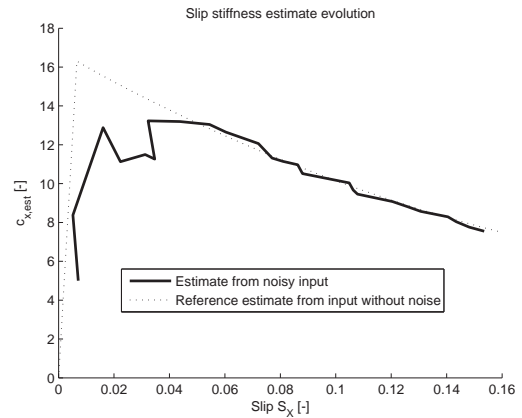


(b) Evolution of the estimated slip stiffness

Figure 4.48: Measure of Nonlinearity on noisy tyre response at $\mu_{TR} = 0.9$



(a) Comparison of MoN and the input samples



(b) Evolution of the estimated slip stiffness

Figure 4.49: Measure of Nonlinearity on noisy tyre response at $\mu_{TR} = 0.9$ with implemented limitation of slip stiffness estimate to reasonable values

5 Results of development and discussion

This chapter summarises the results that have been reached by the development, which is described in Chapter 4. In Section 4.1 the driving modes have been introduced and the rest of the Chapter 4 is devoted to description of the development done in the investigated driving modes. A summary of the development is provided here in Table 5.1. In short the driving modes in which the tyres are loaded in pure lateral direction (modes M3 & M4) and in pure longitudinal direction (modes M7-M10) have been investigated. Results of the former are discussed in Section 5.1 and results of the latter in Section 5.2. Special cases have not been treated more in depth and are thus not discussed here. The performance targets have not been set in details in advance.

Table 5.1: Summary of achieved results for particular driving modes

#	Mode name	Development maturity	Target performance	Actual performance
M1	Coasting	not evaluated	not set	-
M2	Static steering	not evaluated	not set	-
M3	Mild steering	Simulation of the prerequisite done, cf. Section 4.2	not set	Only low-friction theoretically possible
M4	Severe steering		not set	
M5	Off-road driving	not evaluated	not set	-
M6	Normal driving	not evaluated	not set	-
M7	Mild acceleration	Implementation done, preparing for validation, cf. Section 4.4	not set	Friction estimation possible under high excitation. Validation needed.
M8	Strong acceleration		not set	
M9	Mild braking		not set	
M10	Strong braking		± 0.1 error of friction estimation	
M11	Emergency braking	not evaluated	not set	-
M12	Combined slip	not evaluated	not set	-
M13	Tyre initialisation	not evaluated	not set	-
M14	Unclassified	-	-	-

5.1 Estimation using lateral tyre excitation

Evaluation of the prerequisite for the modes M3&M4 in simulation model shown that tyre-road friction can be estimated using observation of the tyre behaviour under pure lateral loading. The simple brush tyre model has been used to observe the behaviour of real tyre. However certain amount of excitation, which is here expressed as friction utilisation, is needed for accurate friction estimation. For estimation using lateral force the friction utilisation needs to be generally higher than for the estimation using aligning torque. It has been found that the lower is the friction utilisation, the more this approach overestimates the estimate of tyre-road friction.

The friction utilisation multiplied by the actual tyre-road friction corresponds to the lateral acceleration of the vehicle. The achievable lateral acceleration in trucks is limited due to their tendency to roll-over. The achievable lateral acceleration in turn limits the tyre-road friction, for which lateral tyre excitation can be used for accurate friction estimation.

In case of using the lateral force the friction utilisation should be over 70% for friction estimation with ± 0.1 accuracy. In case of using the aligning torque the required friction utilisation was found to be different for different tyre road friction. For tyre-road friction 0.5, 50% utilisation is enough for estimation accuracy ± 0.1 , and for tyre-road friction 0.1 only 30% utilisation is needed for estimation with ± 0.1 accuracy. With 50% utilisation of 0.5 tyre-road friction the lateral acceleration is approximately $0.5 \cdot 0.5 = 0.25 g$, which could be achievable for rigid truck. The estimation of friction using aligning torque thus present promising opportunity to identify low friction of the tyre-road combination.

The evaluation method to show the amount of friction utilisation needed for accurate estimation of tyre-road friction may not be generally applicable for different tyres. It may be possible that the brush model approximate some tyres better than others. Furthermore for practical implementation of the estimation using the aligning torque first the aligning torque has to be estimated. The estimation may be possible using the model of the steering system and measurement of the steer torque at the steering wheel. Such measurement is presently available on trucks equipped with electric power steering. The estimation of aligning torque has not been

performed within this thesis and thus present opportunity for future development.

5.2 Estimator using longitudinal tyre excitation

The early simulations of the tyre response under longitudinal loading have shown that, like in the case of lateral loading, high excitation is needed to provide reasonable estimate of friction using the brush tyre model. In longitudinal direction this high excitation may be achievable during operation of the vehicle and thus the development proceeded to the implementation.

The recursive estimator algorithm based on EKF has been implemented. Its testing on response of a tyre model proven that the recursive estimator can determine reasonable estimate of maximum friction coefficient before this maximum is reached by the tyre, as shown in Section 4.4.3.2. It also shown rather high sensitivity of performance to the tuning of the parameters of the EKF. The expected estimator functionality has also been proved in more realistic conditions as a part of complete vehicle model both on high and low friction. Then a noise has been added to the ideal inputs of the estimator and it has been observed that the performance deteriorates with the noise. The noise impact is the bigger the less samples are available for the estimator. There is a conflict between tuning the estimator for fast updating and the tuning to handle the noise. Fast estimator can diverge and thus provide unreliable results due to noise. Slow estimator can better handle the noise, but may converge too slow to bring any advantage, or the information may be provided too late.

A validation of the estimator functionality has been done by using the real data. Two testing sessions have been conducted with the investigated vehicle, once braking on dry asphalt (high friction) and once braking on wet basalt (low friction). The processing of the logged data shown some distortions, so that the obtained force-slip samples as the input for the estimator does not resemble the typical tyre response curve very well. These logged data have then been used for test of the estimator. In both investigated cases the estimator shown capability to update the estimate of friction based on the real input data. However, the capability of estimation of the tyre-road friction before the maximum tyre force is reached could not been proven. The reason is perhaps the significant distortion of the real input data from the expected behaviour described by the simulation model of tyre. In both investigated cases the value of estimated friction resembles approximately the maximum achieved tyre force.

Of particular interest was how fast can the estimator indicate surface with low friction. From the results of the test of the estimator on the data obtained from braking on the low friction surface it can be seen that within the time 0.2 s from the start of increase of the brake pressure the estimator decrease the estimate of friction from initial value $\mu_{est,0} = 0.5$ to $\mu_{est} = 0.26$, while the tyre-road friction is approximately $\mu_{TR} = 0.2$.

It is important to stress that the performance of the estimator is highly dependant on the setting of parameters of EKF. In all the tests of the estimator - from the test on ideal input to the test on real data - the parameters have been tuned manually. Especially important for the performance is the number of samples that are available and their distribution along the typical tyre response curve. It has been shown in early phase that even with the ideal, noise-free input the friction cannot be estimated before the non-linear region is reached, see Section 4.4.2. How fast the non-linear region is reached (i.e. within how many samples) depends on the intensity of braking (magnitude and rate of change of the brake torque) as well as on the actual tyre-road friction. While the maximum tyre force on dry asphalt was reached in time 0.6 s from the start of increase of the brake pressure, the maximum tyre force on wet basalt was reached within 0.2 s. If the estimator expects lower number of samples to reach the non-linear region (by mean of the parameter \mathbf{P}_0 and its components), then the EKF can diverge and can possibly not converge back, as shown in Section 4.4.3.2. Similar behaviour of the estimator has been observed in the test on the data from braking on dry asphalt, where the estimator first overestimates the friction and then gradually converges to more reasonable value. The tuning of the EKF shown in both the simulations of the estimator on the data from braking at dry asphalt and wet basalt has been selected as a balance between safe convergence on the dry asphalt and quick identification of low tyre-road friction on wet basalt. These two validation tests are however insufficient to make general conclusions about the generic tuning of EKF.

From the available test data it can be seen that the measurement noise presents a threat to the accuracy and reliability of the estimator.

6 Conclusions and future work

In this chapter the conclusions are given in Section 6.1. Recommendations for future development in the field of friction estimation for use in trucks are then summarised in Section 6.2. .

6.1 Project conclusions

This thesis project has explored the field of friction estimation, which is being under scope of engineers and scientists since 1990s, see Section 2.2. The biggest motivation for putting effort in this field is that reliable real-time information about friction allow modern vehicle motion control systems more efficient operation, that can in turn decrease the number of accidents on the roads. Especially important is the estimation of low friction.

This thesis is mainly focused on friction estimation methods that are based on observation of the tyre response to lateral or longitudinal loading. Due to possible variance of tyre properties in time, the requirement that no a priori knowledge of the accurate tyre properties can be used was followed. The review of tyre models and friction estimation methods resulted in use of the simple physically motivated tyre model (the brush model) to match the real tyre behaviour and thus estimate the tyre-road friction. The model-based development approach has been used to evaluate viability of friction estimation using simulation model of real tyre behaviour in different driving modes, once at pure lateral load and once at pure longitudinal load of the tyre. The amount of excitation (friction utilisation) needed for accurate friction estimation has been determined. With observation of the aligning torque characteristics the needed friction utilisation can be as low as 30% for ± 0.1 accuracy of the estimation of tyre-road friction 0.1, which is corresponding to ice. With observation of the lateral force characteristics the needed utilisation should in general be around 70% for ± 0.1 accuracy and for observation of the longitudinal force characteristics 80% utilisation is needed. These results are corresponding to results of other authors as discussed in Section 2.2.

The observation of the aligning torque presents most promising opportunity for estimation of low friction, however for the implementation of the estimator first the aligning torque and slip angle estimation has to be implemented. Therefore the implementation of the estimator using the observation of longitudinal force was prioritized. The recursive estimator based on Extended Kalman filter has been implemented for this driving mode. Simulations in Section 4.4.3.2 and Section 4.4.3.3 shown that estimator can identify the tyre-road friction. The condition for accurate estimation is high utilisation of friction. The performance of the estimator is dependant on the tuning of parameters of EKF together with the quality and distribution of the input samples. The estimator can be tuned to improve the performance for particular case, however the distribution of samples (linear or non-linear region of tyre characteristic) in turn depends on the actual tyre-road friction, which shall be estimated. The performance of the estimator deteriorates with increasing noise on the input signals and the negative effect of noise is increased with decreasing number of samples that the estimator gets.

The estimator has been simulated on the real data obtained by braking the investigated vehicle on high- and low-friction surface. On low friction surface the ABS intervenes shortly after the initiation of the braking, which indicates locking the wheels and saturation of the longitudinal tyre forces. In that case the estimator converges to reasonable value of tyre-road friction within time 0.2s from the initiation of the braking. That is approximately in the time when longitudinal tyre force on the investigated tyre first saturates. On high friction the estimator converges to friction corresponding to maximal achieved longitudinal force during the braking and the estimate of friction increase with the increasing longitudinal force. In this case it is not clear whether the tyre is close to the limit or not.

During the processing of the real data it has been found that the resulting force-slip samples - the input samples for the estimator - does not resemble well the expected tyre characteristics. Distortion of the tyre characteristic obtained from the in-vehicle measurements is the reason why the estimator indicates the friction after the maximum of the longitudinal tyre force is reached. Few effects that could be causing the distortion have been identified and respective data processing have been applied in order to improve the quality of the force-slip samples. Within the time of the thesis no satisfactory signal processing has been found. It is probably combination of multiple effects and some effects are named in recommendations for future work.

The estimator theoretically fulfils the requirements for real-time processing, however it has not been implemented in the real-time embedded hardware and thus the performance of the estimator in the field test have not been experimentally validated. Also the estimator reliability and robustness remains unevaluated, since very few validation data has been used.

6.2 Future work

- Processing of the in-vehicle measurements shall be investigated to find the reason of the distortion of the force-slip samples.

Both estimation of longitudinal tyre force and estimation of tyre slip might be affected. The estimation of force may be replicated in the simulation model and all the input quantities may be artificially corrupted to show the effect on the resulting force-slip characteristic. This approach may give some idea on which inputs to the force estimation to focus. The force estimation is surely affected in transients by dynamics of the pneumatic braking system due to position of the brake pressure sensor. Building an observer using mathematical model of the pneumatic system might improve the signal. Additional pressure sensor in the brake cylinder shall be used to validate the observer. Furthermore with only one sensor for both brake cylinders of the front axle the front wheels signals cannot be used for the estimation whenever any ABS or ESP systems intervene. The force estimation is also highly sensitive to the change of the brake factor. The brake factor is affected by many effects, where some can hardly, if only, be taken account in the vehicle, like presence of mud or water on the brake disc that changes the friction between the pads and the disc. The effects of the pneumatic system dynamics and brake factor can be verified by using reference measurement of torque applied on the wheel, for example by using the instrumented wheel rim. Instrumented wheel rim can also validate the estimation of the vertical tyre load. Changing tyre radius might also affect the force estimation. The estimation of slip might be affected by inaccurate linear velocity of the tyre in the contact patch. In this case the readings from vehicle CAN are directly used, that may be affected by changing tyre radius due to changing vertical load.

It is of interest whether the in-vehicle measurements can be realistically improved to better resemble the typical tyre characteristics. If not, than the prerequisite for the friction estimation might be updated, for example to quickly identify the peak tyre force in case of ABS intervention.

- The implementation of the estimator in real-time embedded hardware shall then be done to validate the estimator performance as a true real-time solution.
- The investigation of the required friction utilisation needed for accurate friction estimation by the brush tyre model (shown in Sections 4.2.2 and 4.4.2) may also be done for different tyres in order to provide more general insight to the amount of friction utilisation needed. For example by varying the main parameters of the Magic Formula tyre model and evaluating the required friction utilisation for accurate estimation as shown in Sections 4.2.2 and 4.4.2.
- The observation of the aligning torque presents promising opportunity to estimate the friction on low-friction surfaces. If the previous step confirms that low friction utilisation is needed for different tyre properties, the possibility to estimate the aligning torque from electric power steering measurements shall be further explored - starting with the estimation of the aligning torque in the vehicle.
- Furthermore the evaluation of robustness shall be done, or a mean to provide the information about quality of the estimated value of tyre-road friction.
- A measure of non-linearity briefly introduced in Section 4.4.6 can be further evaluated to a) provide base for adaptive tuning of the EKF and b) tell the architecture whether sufficient excitation has been reached to reliably estimate tyre-road friction.

Bibliography

- [1] REGULATION (EC) No 661/2009 OF THE EUROPEAN PARLIAMENT AND OF THE COUNCIL, concerning type-approval requirements for the general safety of motor vehicles, their trailers and systems, components and separate technical units intended therefor, OJ L 200/1 (2009).
URL <http://eur-lex.europa.eu/legal-content/EN/TXT/PDF/?uri=CELEX:32009R0661>
- [2] U. Kiencke, L. Nielsen, Automotive control systems, 2nd Edition, Springer, Berlin, 2005.
- [3] AB Volvo, Safety as a core value, online (May 2015).
URL <http://www.volvogroup.com/GROUP/GLOBAL/EN-GB/VOLVO%20GROUP/OURVALUES/SAFETY/PAGES/SAFETY.ASPX>
- [4] L. Laine, Reconfigurable Motion Control Systems for Over-Actuated Road Vehicles, Doktorsavhandlingar vid Chalmers tekniska högskola. Ny serie, no: 2641, Department of Applied Mechanics, Chalmers University of Technology, 2007, 242.
- [5] Road vehicles - Vehicle dynamics and road-holding ability - Vocabulary, Stockholm (2011).
- [6] H. B. Pacejka, Tyre and vehicle dynamics, 2nd Edition, Butterworth-Heinemann, Oxford, 2006.
- [7] J. Svendenius, Tire modeling and friction estimation, Phd thesis, Lund University, Lund, Sweden (2007).
URL <http://www.control.lth.se/documents/2007/jsvenPDH.pdf>
- [8] J. Pauwelussen, Essentials of vehicle dynamics, 1st Edition, Butterworth-Heinemann, Oxford, 2014.
- [9] S. Koskinen, P. Peussa, Friction: Final report - public, Tech. rep., Technical Research Centre of Finland (VTT) (2009).
URL http://friction.vtt.fi/FRICTION_FinalReport_D13.pdf
- [10] M. Burckhardt, J. Reimpell, Fahrwerktechnik: Radschlupf-Regelsysteme, Vogel, Würzburg, 1993.
- [11] Sten Löfving Optical sensors, Road eye, Online (2014).
URL <http://www.opticalsensors.se/roadeye.html>
- [12] Road status information, online (April 2015).
URL www.roadstatus.info
- [13] D. Pavković, J. Deur, J. Asgari, D. Hrovat, Experimental analysis of potentials for tire friction estimation in low-slip operating mode, in: SAE technical paper series, SAE International, Warrendale, 2006.
- [14] F. Gustafsson, Slip-based tire-road friction estimation, in: Automatica, Vol. 33, 1997, pp. 1087–1099.
URL <http://linkinghub.elsevier.com/retrieve/pii/S0005109897000034>
- [15] R. Rajamani, G. Phanomchoeng, D. Piyabongkarn, J. Y. Lew, Algorithms for real-time estimation of individual wheel tire-road friction coefficients, in: IEEE/ASME Transactions on Mechatronics, Vol. 17, 2012, pp. 1183–1195.
URL <http://ieeexplore.ieee.org/lpdocs/epic03/wrapper.htm?arnumber=5959213>
- [16] M. Choi, J. J. Oh, S. B. Choi, Linearized recursive least squares methods for real-time identification of tire-road friction coefficient, in: IEEE Transactions on Vehicular Technology, Vol. 62, 2013, pp. 2906–2918.
URL <http://ieeexplore.ieee.org/lpdocs/epic03/wrapper.htm?arnumber=6508885>
- [17] W. R. Pasterkamp, H. B. Pacejka, The tyre as a sensor to estimate friction, in: Vehicle System Dynamics, Vol. 27, 1997, pp. 409–422.
URL <http://www.tandfonline.com/doi/abs/10.1080/00423119708969339>
- [18] C. Ahn, H. Peng, H. E. Tseng, Robust estimation of road friction coefficient using lateral and longitudinal vehicle dynamics, in: Vehicle System Dynamics, Vol. 50, 2012, pp. 961–985.
URL <http://www.tandfonline.com/doi/abs/10.1080/00423114.2012.659740>

- [19] A. Gambier, Real-time control systems, in: 2004 5th Asian Control Conference, IEEE, Piscataway, N.J., 2004, pp. 1024–1031.
- [20] D. G. Manolakis, V. K. Ingle, S. M. Kogon, ebrary (e-book collection), I. Books24x7, Statistical and adaptive signal processing: spectral estimation, signal modeling, adaptive filtering, and array processing, Artech House, Boston, 2005.
- [21] M. S. Grewal, A. P. Andrews, Kalman filtering: theory and practice using MATLAB, 3rd Edition, Wiley-Blackwell, New Jersey, 2008.
- [22] H. B. Pacejka, Tyre and vehicle dynamics, 1st Edition, Butterworth-Heinemann, Oxford, 2002.
- [23] MSC Software Corporation, Adams/Tire 2005 r2 Help (2005).
- [24] Robert Bosch GmbH, Automotive Handbook, 4th Edition, Robert Bosch GmbH, 1996.
- [25] J. Miller, Advanced braking systems for heavy vehicles, Ph.D. thesis, Engineering Department, University of Cambridge (2010).
- [26] L. M. Henderson, Improving emergency braking performance of heavy goods vehicles, Ph.D. thesis, Engineering Department, University of Cambridge (September 2013).
- [27] Joint Committee for Guides in Metrology, Evaluation of measurement data — Guide to the expression of uncertainty in measurement, 1st Corrected Edition (2010).
- [28] Y.-H. J. Hsu, Estimation and control of lateral tire forces using steering torque, Dissertation, Stanford University (March 2009).
- [29] K. Emancipator, M. Kroll, A quantitative measure of nonlinearity, *Clinical chemistry* 39 (5) (1993) 766–772. URL <http://www.clinchem.org/content/39/5/766.full.pdf>

A Definitions of vehicle variables

This appendix explains definitions of vehicle variables used in this thesis report.

A.1 Longitudinal acceleration

According to ISO [5] the longitudinal acceleration is denoted a_X and it is component of total acceleration vector \vec{a} , projected to intermediate axis system. Intermediate axis system (with axis X, Y, Z) is defined as having X, Y axis parallel to the ground plane, with the origin in vehicle reference point (hereby the vehicle CoG is used) and with the X axis along the vehicle undercarriage longitudinal axis. The ground plane is then normal to gravitational vector \vec{g} , therefore parallel to water level. If a vehicle stands on an inclined road, where the inclination angle is according to ISO denoted as λ (positive for vehicle pointing uphill), the vehicle longitudinal acceleration with respect to local road plane is decreased for the influence of road inclination

$$a_{X,road} = a_X \cos \lambda \quad (\text{A.1})$$

Another effect is brought by the component of gravitational acceleration that occurs due to road inclination - $g \sin \lambda$. This affects the measurement of acceleration in not a straightforward way. Common sensor measuring the acceleration works on principle of measurement of the displacement of a mass, that is suspended in the frame of sensor on springs of known stiffness. When such a sensor is accelerated, the mass inside the sensor moves in the direction opposite to the acceleration vector (due to its inertia). Now consider the situation of vehicle driving forward uphill on an inclined road with certain longitudinal acceleration with respect to road $a_{X,road}$. Consider sensor of longitudinal acceleration in the vehicle. This acceleration forces the mass inside the accelerometer in the opposite direction (back relative to vehicle). The mass inside the sensor is also pulled down the slope with the component $g \sin \lambda$. Therefore the measured acceleration is

$$a_{X,IMU} = a_X \cos \lambda + g \sin \lambda \quad (\text{A.2})$$

where $a_{X,IMU}$ denotes the acceleration measured by the vehicle Inertial Measurement Unit (IMU).

The IMU is mounted on the vehicle body that is suspended, which introduces additional effect of vehicle pitch that affects the acceleration measurement. The vehicle pitch θ is by ISO defined as an angle between axis X_V of vehicle body-fixed axis system and X of intermediate axis system [5]. In such definition the road inclination is part of the pitch, therefore to denote the pitch of vehicle sprung body relative to vehicle undercarriage symbol θ_{road} is introduced. Following then holds:

$$\theta = \lambda + \theta_{road} \quad (\text{A.3})$$

If the vehicle has no suspension, than the pitch to road is zero all the time - $\theta_{road} = 0$. The effect of pitch angle on measurement of longitudinal acceleration can then be expressed

$$a_{X,IMU} = a_X \cos \theta + g \sin \theta \quad (\text{A.4})$$

A.2 Tyre slip

A.2.1 Longitudinal slip quantity

Different definitions of tire longitudinal slip can be seen in various sources dealing with the topic. This section is presented to set the slip definitions used in this project. Already standardised definitions will be used wherever possible.

ISO defines longitudinal slip with notation S_X as

$$S_X = \frac{\omega_W - \omega_{W0}}{\omega_{W0}} \quad (\text{A.5})$$

where ω_W is the wheel-spin velocity and ω_{W0} is the reference wheel-spin velocity [5]. Reference wheel spin velocity represents the angular velocity of wheel at free rolling case - where no slip occurs. Slip is positive for driving (accelerating) and negative for braking. Then for full sliding of the locked wheel, i.e. $\omega_W = 0$ the slip is

$S_X = -1$. The slip caused by driving is however not bounded and for vehicle standing still can go to infinity, i.e. $\omega_{W0} = 0 \implies S_X \rightarrow \infty$. Similar definition is introduced in [6] where the topic is extensively discussed including other effects that come into place in general case.

For derivation of the brush model in [6] a *theoretical* slip is introduced and defined as

$$\sigma_x = -\frac{V_{sx}}{V_r} = -\frac{V_{sx}}{V_x - V_{sx}} = \frac{\kappa}{1 + \kappa} \quad (\text{A.6})$$

where κ is called *practical* slip and defined as

$$\kappa = -\frac{V_{sx}}{V_x} = -\frac{V_x - r_e \Omega}{V_x} = -\frac{\Omega_0 - \Omega}{\Omega_0} \quad (\text{A.7})$$

where Ω is actual wheel angular velocity, Ω_0 is wheel angular velocity at free rolling, V_x is longitudinal velocity of wheel centre and r_e is effective rolling radius.

In [8] the *practical* slip is noted as s_x and defined as

$$s_x = -\kappa = \frac{V_{sx}}{V_x} \quad (\text{A.8})$$

Theoretical slip is then noted as ρ with components defined as

$$\rho_x = \frac{V_{sx}}{V_r}, \quad \rho_y = \frac{V_{sy}}{V_r} \quad (\text{A.9})$$

The relation between theoretical and practical slip is then

$$\rho_x = \frac{s_x}{1 - s_x}, \quad \rho_y = \frac{s_y}{1 - s_x} \quad (\text{A.10})$$

Hence while using definitions introduced by Pacejka a positive slip σ_x (or κ) results in positive longitudinal force, a positive slip ρ_x (or s_x) defined by Pauwelussen results in negative longitudinal force.

In ISO standard [5] the tyre longitudinal slip is noted as S_X and defined

$$S_X = \frac{\Omega - \Omega_0}{\Omega_0} \quad (\text{A.11})$$

thus being effectively the same as Pacejka's κ , compare equation (A.11) with equation (A.7).

A.2.2 Lateral slip quantity

It is the deviation between the wheel velocity vector and the vehicle velocity vector at tyre contact point that makes the tyre to introduce the lateral force. Common measure of how much the tyre is loaded in lateral direction is the slip angle α [5, 6].

B Magic Formula tyre model used in VTM

This section contains information gathered from inspection of the PAC2002 Magic Formula tyre model used in VTM and is intended to extend the information provided about the tyre model in Section 3.3.3.1. The tyre model has been subjected to loading in order to obtain and visualise the tyre behaviour to the specific loading. The tyre model has following inputs:

v_{XT}	tyre contact point longitudinal velocity (in wheel plane)
v_{YT}	tyre contact point lateral velocity (\perp to wheel plane)
γ	tyre camber angle
F_{ZT}	tyre vertical load
M_{YT}	driving/braking torque applied on wheel and hence on tyre belt
$\underline{\lambda}$	scaling coefficients for specific tyre-road conditions

and outputs:

F_{XT}	tyre longitudinal force
F_{YT}	tyre lateral force
M_{XT}	tyre overturning torque
M_{YT}	tyre rolling torque
M_{ZT}	tyre aligning torque
S_X	longitudinal slip
$SlipY$	unknown lateral slip quantity, not matching the slip angle
ρ	tyre deflection
R_e	effective rolling radius
ω_w	wheel rotational velocity

In order to get typical sweep characteristics, the tyre is subjected to increasing load (ramp) in longitudinal and lateral direction. The longitudinal slip is introduced by increasing of the driving/braking torque M_{YT} . The lateral slip is in case of Magic Formula described by the slip angle α in terms

$$\sigma_Y = \tan(\alpha) = \frac{v_{YT}}{v_{XT}} \quad (\text{B.1})$$

To achieve the sweep of slip angle a sweep of lateral tyre velocity is introduced to the tyre.

The PAC2002 tyre model is dynamic, that said it reflects the dynamic tyre behaviour like relaxation length. For this reason the input sweep of either σ_X or σ_Y was designed as rather slow, in order to show tyre steady state behaviour. The reason for steady state behaviour is that the brush model in its simple form can only reflect the steady state behaviour. Furthermore the VTM tyre model can reflect the dependency of tyre forces on longitudinal tyre velocity v_{XT} . The velocity has been kept constant $v_{XT} = 10$ m/s in the observations made here.

Truck tyres are more differentiated in their properties to their purpose than it is on passenger vehicles. Therefore different types of tyres are used on single truck. Typical differentiation is based on the fact whether the tyre is used on a steered axle or on a driven axle. In general though, even the steered axle can be driven. However the driven tyres are subjected to very high longitudinal forces because commonly on truck only the one axle is driven and has to accelerate few tens of tonnes into motion. In this appendix only the tyre that is used throughout the thesis is inspected, hereby denoted as *Front tyre*.

B.1 Pure lateral load

Front tyre characteristics under varying vertical load are shown in Figure B.1. Normalised characteristics are then shown in Figure B.2. The cornering stiffness as a slope of the initial linear part of the $F_{YT}-\alpha$ characteristic is load dependent and this (of course non-linear) relation is shown in Figure B.3a. Interesting for the sake of this project may be the dependency of maximum tyre-road friction on the vertical load, which is shown in Figure B.3b. The lateral force characteristic for different values of tyre-road friction coefficient are shown in .

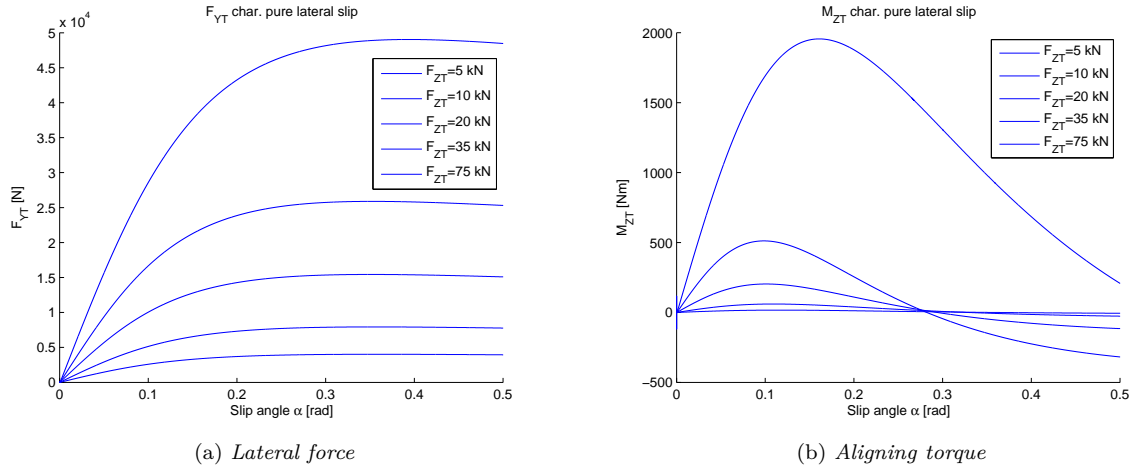


Figure B.1: *Front tyre response to pure lateral slip*

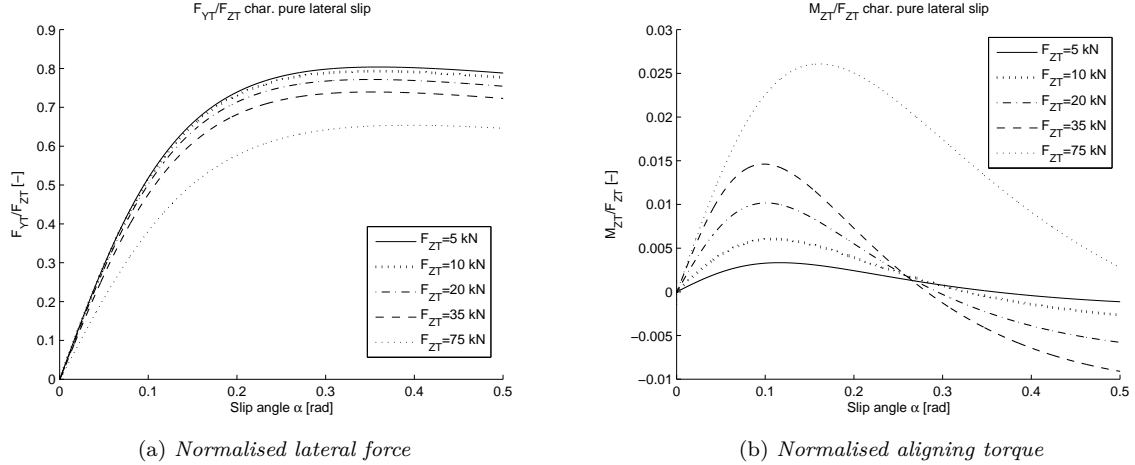
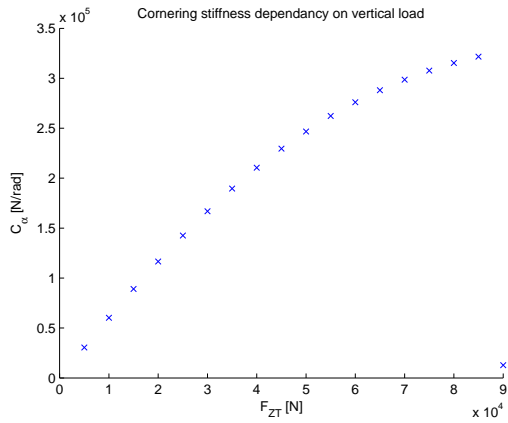
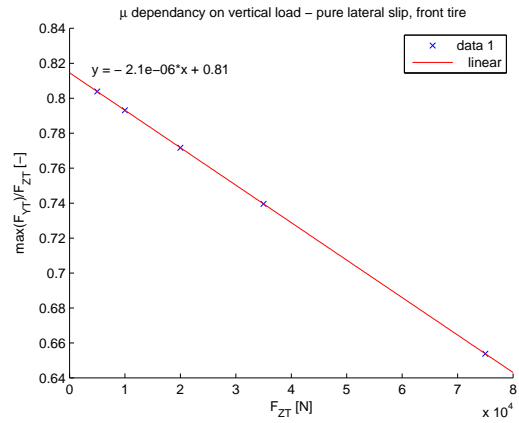


Figure B.2: *Front tyre normalised response at pure lateral slip*



(a) Cornering stiffness dependency on load



(b) Tyre-road friction dependency on vertical load

Figure B.3: Effect of vertical load on cornering stiffness and friction parameter

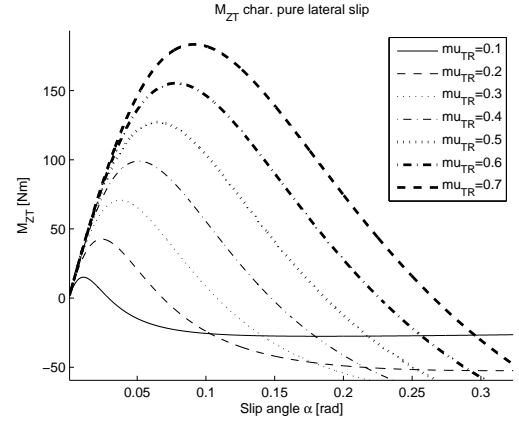
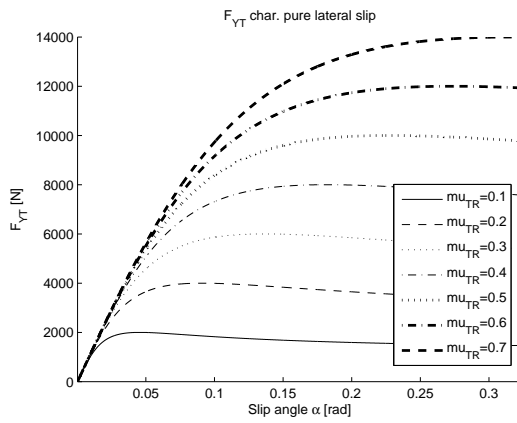


Figure B.4: Lateral force and aligning torque for different tyre-road friction

B.2 Pure longitudinal load

Front tyre longitudinal force characteristics are for the varying vertical load much closer to each other, see Figure B.5. From there one may see that also the change of maximum tyre-road friction coefficient is almost constant.

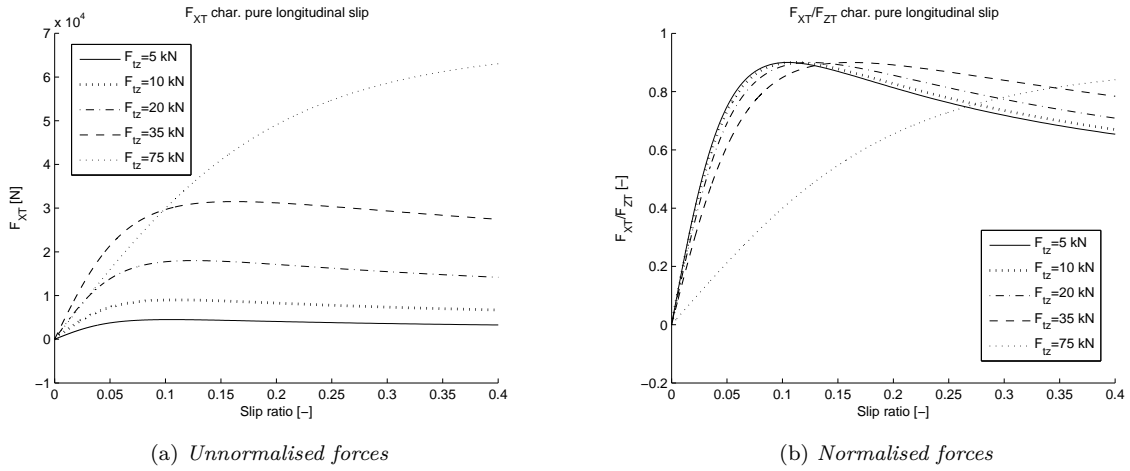


Figure B.5: *Front tyre response to pure longitudinal slip*

The response of front tyre to pure longitudinal slip for constant vertical load and multiple friction levels μ_{T-R} is shown in Figure B.6.

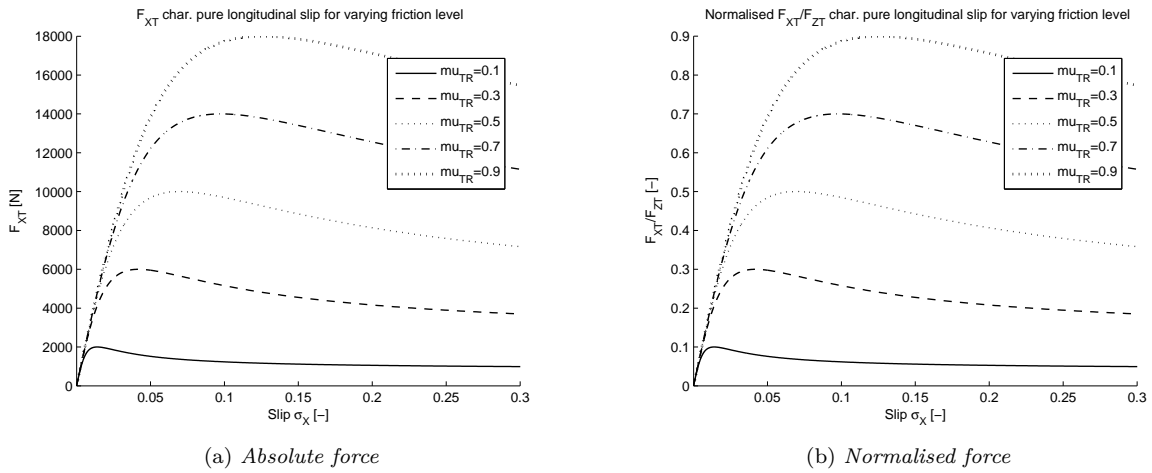


Figure B.6: *Front tyre response to pure longitudinal slip for different μ_{T-R}*

B.3 Combined load

In a combined slip case, the longitudinal force decreases with increasing induced slip angle, as can be seen in Figure B.7. This phenomena is described by so called Kamm's circle. In theory, the total shear force provided by tyre is limited by friction limit times the vertical load. This shear force can be distributed either to longitudinal or to lateral direction. In practice the limit curve is usually not a nice circle, but due to anisotropy of tyre properties in longitudinal and lateral directions it deforms into ellipse. In this case such a graph was obtained and can be seen in Figure B.8.

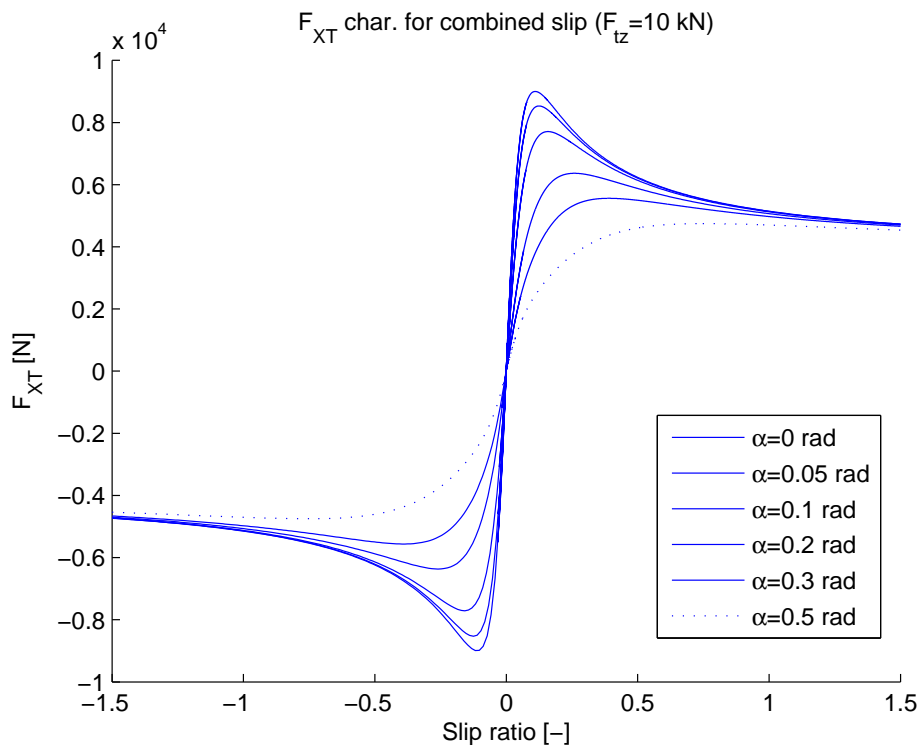


Figure B.7: Front tyre - longitudinal tyre force at combined slip

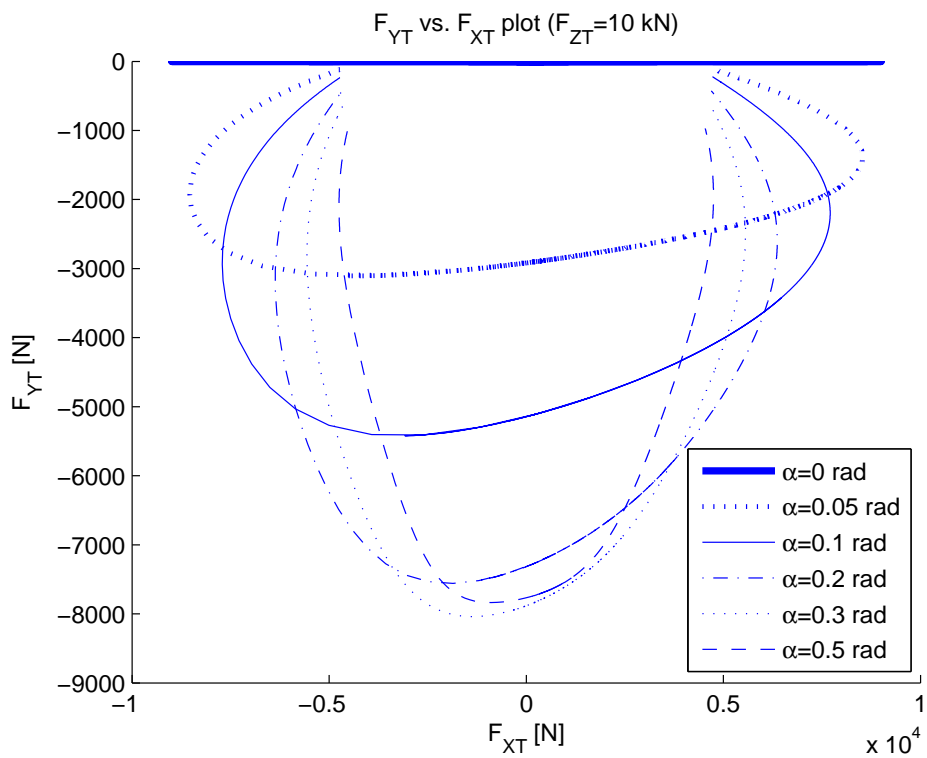


Figure B.8: Front tyre under combined slip - Kamm's circle

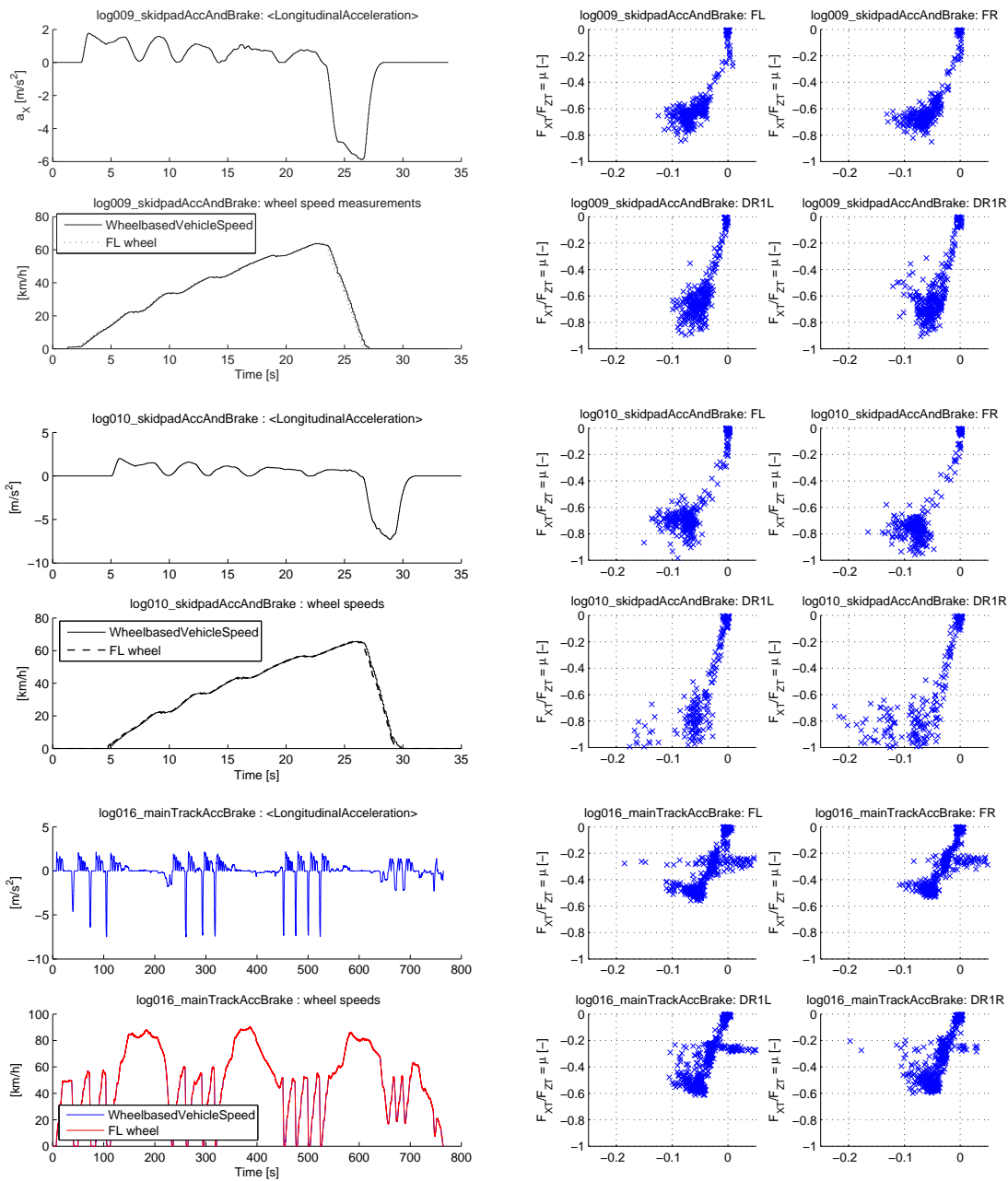
C Results of testing

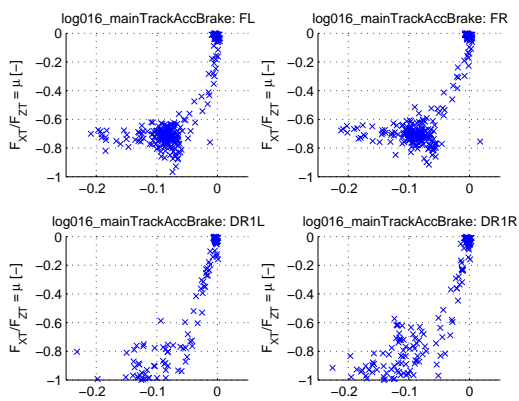
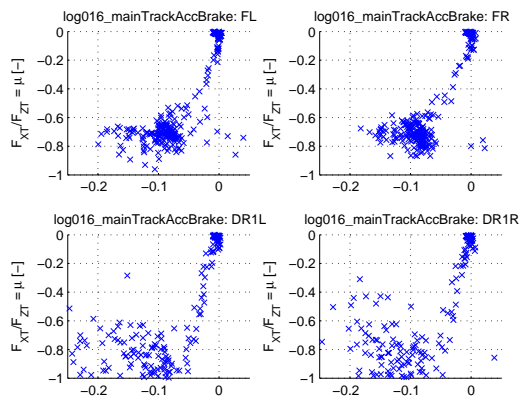
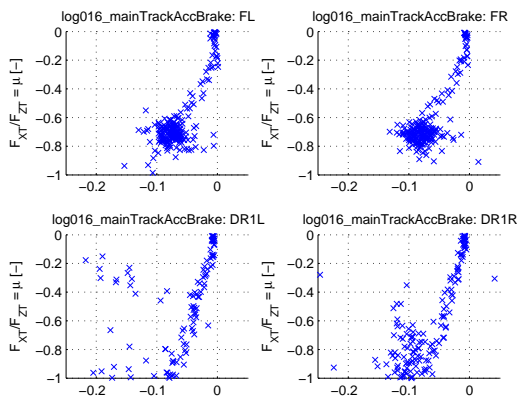
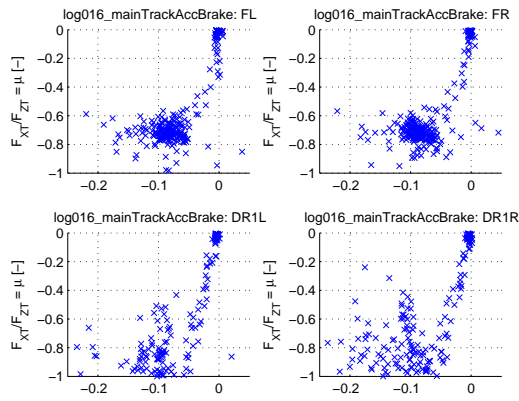
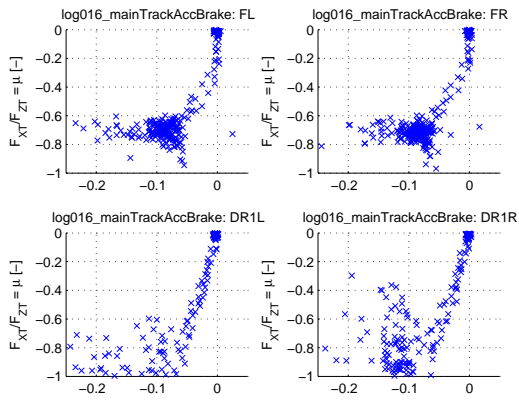
C.1 Intensive braking on dry road

This section gives results of testing that has been conducted in April 8, 2015 on the Volvo's test track. This section further extends the results shown in Section 4.4.5.

Results of individual wheel force estimation with no signal processing

In the following graphs are shown results of the evaluation of individual wheel force-slip characteristics. In this case no signal processing as outlined in Section 4.4.5 is applied. For the plots of force-slip characteristics only the time window of measurement data is used when the braking occurs.





D Documentation to the appended files

Results presented in this thesis report can be reproduced using the files appended in digital form in folder `RT_estimation_of_TR_friction_DATA` folder. The files are MATLAB scripts (*.m files) or Simulink models (*.mdl files). Within the thesis MATLAB R2012b 32bit has been used with respective version of Simulink library. Tree of the appended folder can be seen in Figure D.1. This section provides brief instructions how to work with the appended files. All the script then contain detailed documentation, so it shall be easy for reader to navigate and understand.

Some data cannot be disclosed. This is the case of simulation models of tyre and complete vehicle, which are confidential or subject to license policies. For this reason the data-files containing signals needed within this thesis are enclosed in place of the simulation models.

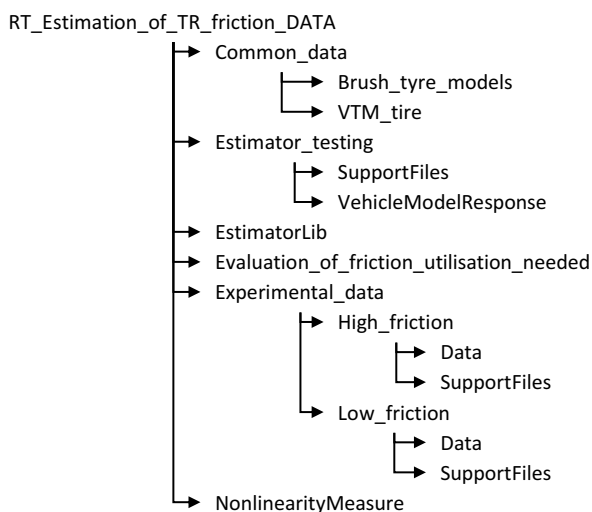


Figure D.1: *Tree of the appended folders*

D.1 Evaluation of friction utilisation needed for accurate friction estimation

This section contain description of files used to evaluate what amount of friction utilisation is needed for accurate estimation of tyre-road friction using the brush tyre model for evaluated driving modes. There are MATLAB script files stored in folder

`Evaluation_of_friction_utilisation_needed`

The folder `Common_data\VTM_tire` contains data-files with responses of tyre to increasing lateral or longitudinal loading at different levels of tyre-road friction. These responses are results of Magic Formula tyre model used by Volvo GTT.

D.1.1 Lateral tyre loading

This section describe code used in Section 4.2, particularly in Section 4.2.2. There are files:

- `Brush_fitting_friction_Fy.m` for evaluation of the needed friction utilisation using the observation of lateral tyre force,

and

- `Brush_fitting_friction_Mz.m` for evaluation of the needed friction utilisation using the observation of aligning torque.

When executed both scripts asks user to specify tyre-road friction μ_{TR} for which the evaluation should be done and then create graphs as shown in Figures 4.4, 4.5, 4.2, 4.3 and 4.6 for lateral force and in Figures 4.8, 4.9, 4.10 and 4.11 for aligning torque.

D.1.2 Longitudinal tyre loading

This section describe code used in Section 4.4, particularly in Section 4.4.2. A file `Brush_fitting_friction_Fx.m` was used to evaluate the required friction utilisation. When executed the script asks user to specify tyre-road friction μ_{TR} for which the evaluation should be done and then creates graphs as shown in Figures 4.13, 4.14, 4.15 and 4.16.

D.2 Implementation of the recursive friction estimation algorithm

This section describes the implementation of the recursive friction estimation algorithms. First the estimator is implemented in MATLAB code, which is described in Section D.2.1. Such implementation is later used for testing the estimator on ideal input, see Section D.3.1. The EKF implementation in MATLAB code then forms basis for implementation of whole estimator in Simulink blocks, described in Section D.2.2. A Simulink implementation is later used in testing the estimator in vehicle simulation model, see Section D.3.2 and for testing on experimental data, see Section D.3.3.

D.2.1 EKF estimator in MATLAB code

The estimator based on Extended Kalman Filter (EKF), described in 4.4.3.1 is implemented using a MATLAB function

`Estimator_testing\EKF_JP.m`

The function implements the steps that EKF execute in each iteration as described in Section 2.4.2. The inputs to the function are:

Thesis notation	MATLAB notation	Description
f_{XT}	<code>Fxnorm</code>	normalised longitudinal tyre force
S_X	<code>SlipX</code>	longitudinal tyre slip
c_{x0}	<code>cx0</code>	last ¹ estimate of the normalised slip stiffness parameter
μ_0	<code>mu0</code>	last estimate of the friction parameter
$\mathbf{P}(k-1 k-1)$	<code>P_last</code>	last error covariance matrix
\mathbf{Q}	<code>Q</code>	process noise covariance matrix
\mathbf{R}	<code>R</code>	measurement noise covariance matrix

and the outputs then

Thesis notation	MATLAB notation	Description
$c_{x,est}$	<code>cx_est</code>	updated estimate of slip stiffness parameter
μ_{est}	<code>mu_est</code>	updated estimate of friction parameter
$\mathbf{P}(k k)$	<code>P_upd</code>	updated error covariance matrix
-	<code>err</code>	error between model response and measured response
$\mathbf{K}(k)$	<code>K</code>	Kalman gain

The estimates ($c_{x,est}$, μ_{est}) and the updated error covariance matrix ($\mathbf{P}(k|k)$) are then used in next iteration of the EKF as the respective input.

D.2.2 EKF estimator in Simulink

The friction estimator as discussed in 4.4.3.3 is implemented in Simulink model

`Estimator_testing\MuEstimator_braking.mdl`

which represent isolated friction estimator together with the switching logic, specialised for the Strong braking driving mode. The model contain sub-block

`Brake_mode_switching_logic`

where the conditions for running the estimator, given in 4.4.3.3 by equation (4.21), equation (4.22) and equation (4.23), are implemented.

Within the sub-block

`Main_mu_estimator_CondUpd`

is then implemented the friction estimator itself. The sub-block contains two parallel sub-blocks that execute exclusively, one corresponding to the state when the estimator should update (`Run_estimator`) and one corresponding to state when the estimator does not update and hold the values of estimates and error covariance for next iteration (`Hold_values`). Within the `Run_estimator` block the EKF procedure is implemented using the same MATLAB function as discussed in D.2.1. The `Hold_values` block passes the estimates and error covariance matrix unchanged to next iteration.

Whole simulation model of the estimator process the input signals `Fxnorm_in`, `SlipX_in`, `vx_in` (corresponding to variables f_{XT} , S_X , v_X) in discrete steps, thus simulating the situation when the estimator processes new samples of the input signals online.

D.3 Testing performance of the estimator

This section describes files used to test the estimator and obtain results of its performance as shown in 4.4.3 and Section 4.4.5. All the cases discussed in this section have files within folder

`Estimator_testing`

unless otherwise stated.

D.3.1 Performance with ideal input from single tyre simulation

File

`EstimatorTest_Ideal_input.m`

tests the estimator performance on a response of a single tyre under constant vertical load, as described in 4.4.3.2. The tyre response ($f_{XT} - S_X$ samples) to increasing load in pure longitudinal direction is loaded from data file

`Common_data\VTM_tire\PAC2002_PureLong_multi_muTR@Fzt2e4N.mat`

This data file contains response of the tyre for 5 levels of tyre-road friction $\mu_{TR} = [0.1 \ 0.3 \ 0.5 \ 0.7 \ 0.9]$ and the particular set is selected using index given by the variable `muselected`. The default value is `muselected=5` which selects $\mu_{TR} = 0.9$. The file then decrease the number of samples of the original dataset to better reflect expected number of samples in reality. The file then simulates the recursive estimator by iterative feeding by the tyre response samples. The recursive friction estimator implementation is in detail described in Section D.2.1.

D.3.2 Performance within the full vehicle model

The performance of the estimator within the vehicle model as described in Section 4.4.3.3 was tested using file

`EstimatorTest_VehicleModel.m`

The model of the vehicle is replaced by dataset with logged signals from the vehicle model. Different datasets corresponding to different drive cases are available in the folder

`VehicleModelResponse`

The drive case is described by following values:

`vx0` velocity of the vehicle when the braking is initiated,

`Pcyl_demand` demanded value of pressure in the brake cylinders,

`tau` time constant of the brake actuator (representing how fast the brake torque rises),

`muSim` scaling factor of the road friction.

These 4 values are contained in the name of the dataset files. Within the script different drive cases can be selected by uncommenting the respective line loading one of the dataset files.

Setting of the parameters of the estimator can be changed using variables P11, P22, Q11, Q22 and R as discussed in Section 4.4.3.1. The results shown in Section 4.4.3.3 can be reproduced when using the same drive case and the EKF parameters that are shown in annotation of the graphs showing results of the estimator, e.g. Figure 4.24b.

When executed, the script shows relevant graphs of the drive case:

- vehicle velocity and acceleration,
- applied brake torque,
- normalised longitudinal tyre force f_{XT} evolution in time,
- tyre response characteristic $f_{XT}-S_X$.

and prepares input signals for one selected tyre (Front Left tyre in this case) and calls the simulation model of the estimator, which was described in Section D.2. The simulation model represents online processing of the input samples by the friction estimator. After the simulation is finished the results of the estimator are plotted as shown in Section 4.4.3.3. The results of the estimator are then shown in graphs comparing input samples and online brush model fit, as in Figure 4.24a, and the evolution of the estimates, as in Figure 4.24b.

D.3.2.1 Adding noise to the inputs of the estimator

The results of the estimator performance on the input signals with added noise as described in Section 4.4.3.4 were obtained using

```
EstimatorTest_VehicleModel_AddNoise.m
```

script. Like in the previous section this script loads signals from the simulation of the vehicle model and adds noise to the signals that are inputs for the estimator, namely the normalised longitudinal tyre force f_{XT} and the slip S_X . Selection of the drive case is the same as described in previous section. The power of noise can be set with lines

```
SlipX_noise_STD=0.003; %standard deviation of the slip noise  
Fxnorm_noise_STD=0.01; %standard deviation of the Fxnorm noise
```

as explained in Section 4.4.3.4. The script then prepares input signals with noise and calls the simulation model of the estimator, which was described in Section D.2, and then shows the result of the estimator performance in graphs as shown in Section 4.4.3.4. Again the setting of the parameters of the estimator can be changed using variables P11, P22, Q11, Q22 and R as discussed in Section 4.4.3.1.

D.3.3 Performance on experimental data

The estimator performance on experimental data is tested using the Simulation model of the estimator, described in Section D.2.2, where the inputs for the estimator are obtained from testing of the vehicle. Processing the in-vehicle measurements to obtain input signals for the estimator is described in Section D.5.1 and Section D.5.2. The scripts described later in this section require results of the experimental data processing in the MATLAB Workspace, therefore first the script processing the experimental data must be executed, then the corresponding script calling the simulation of the estimator.

The scripts for testing the estimator on the test data,

```
EstimatorTest_OnTestData_LowMu.m  
EstimatorTest_OnTestData_HighMu.m
```

prepare the input signals, call the simulation model of the estimator and then show the results of the estimator in graphs as shown in Section 4.4.5.1. With the default values each of the scripts reproduces the results presented in Section 4.4.5.1 and Section 4.4.5.2. As in previous sections the parameters of the estimator can be changed using variables P11, P22, Q11, Q22 and R as discussed in Section 4.4.3.1.

D.4 Measure of non-linearity evaluation

Files related to the concept of Measure of Nonlinearity (MoN), discussed in Section 4.4.6, are stored in folder `NonlinearityMeasure`

The script

`MoN_analyse.m`

evaluates the concept of MoN to identify the non-linear region of the tyre response on different levels of tyre-road friction μ_{TR} . The friction levels can be specified by variable `muTR`. The script creates a force-slip samples using the simple brush tyre model, and then simulates functionality of recursive algorithm that evaluates the MoN. The Recursive least square algorithm as described in Section 4.4.6 with recursive evaluation of MoN, given by equation (4.44), are implemented within the MATLAB function `MoNfcn_rel.m`. The `MoN_analyse.m` script then plots a graph with comparison of tyre characteristics and resulting MoN, both for different levels of tyre-road friction.

D.4.1 Evaluation on signals with added noise

To analyse the concept of MoN on the signal with added noise the script

`MoN_analyse_w_noise.m`

has been used. In the script the tyre characteristic is again obtained by a simple brush model. A tyre-road friction and slip stiffness of the tyre characteristic can be set by variables `muTR` and `cx_in`. A noise is added both to force and slip samples and the power of the noise is specified by standard deviations of the random white noise using variables `Fxnorm_noise_STD` for slip, `SlipX_noise_STD` respectively. There are three functions evaluating:

1. MoN in absolute values, without normalisation to the friction level, therefore following equation (4.43) (function `MoNfcn.m`)
2. relative MoN, following equation (4.44), applied on noisy input samples (function `MoNfcn_rel_cx_lim.m`)
3. relative MoN applied on noise-free input samples (function `MoNfcn_rel.m`)

In the function that is evaluating the MoN on the noisy force-slip samples the limitation of slip stiffness estimate, discussed in Section 4.4.6, is implemented, where the limits are given by input parameter `cx_limits`. The script iterates over the input samples from zero slip to point of maximum tyre force and simulates recursive evaluation of the MoN. Finally the results are shown in graphs similar to those shown in Section 4.4.6, e.g. in Figure 4.49. Since the noise is random, the graphs can look a little different in every execution of the script.

D.5 Experimental data processing

This section describe the files used to load, process and visualise experimental data shown in Section 4.4.5. The respective files of this section are located in the folder

`Experimental_data`

D.5.1 Braking on high friction

This section describes processing of test data obtained by braking on high friction surface, discussed in 4.4.5 and especially in Section 4.4.5.1. Related files are located in the sub-folder

`High_friction`

A script

`Extract_force_slip_data.m`

loads the measurement data from testing, process them and visualise results, where the key result is the graph with force-slip ($f_{XT} - S_X$) samples. The signals are loaded to workspace automatically by calling a script

`\Data\LoadSignals.m`

In this script user can select which set of data to load by uncommenting respective lines of code, as described within the script. In total 3 data sets are available. Default values are set set such as to reproduce results shown in Section 4.4.5.1, particularly in Figure 4.37.

D.5.1.1 Brake pressure processing

Comparison of different brake pressure signal processing discussed in Section 4.4.5 is done using script

`Compare_pbr_processing.m`

This script loads the signals to Workspace using the script

`\Data\LoadSignals.m`

and the results of the processing shown in Section 4.4.5 are obtained with default values of the script. The script has two sections corresponding to either brake pressure low-pass filtering or adding pure time delay, denoted in the script by section headings:

```
%% process the data – LP filter
```

and

```
%% process the data – Pure time delay
```

Consequently by uncommenting the content of the respective section the respective processing is applied and shown in graphs. Only one section can be uncommented at a time for correct operation.

D.5.2 Braking on low friction

This section describes processing of test data obtained by braking on high friction surface, discussed especially in Section 4.4.5.2. Related files are located in the sub-folder

`Low_friction`

A script

`Extract_force_slip_data.m`

loads the measurement data from testing, process them and visualise results, where the key result is the graph with force-slip ($f_{XT} - S_X$) samples. Executing this script will reproduce results shown in Section 4.4.5.2. The signals are loaded to workspace using

`\Data\LoadSignals.m`

and in this case only one data-set is available.

D.5.3 Uncertainty evaluation and sensitivity analysis

This section discuss the files used for analysis of uncertainty and sensitivity of force and slip estimation, as discussed in Section 4.4.4.3. The analysis has been done on the test data from high friction, therefore related files are stored in the sub-folder

`High_friction`

The script

`EvaluateUncertainty.m`

requires previous execution of script from Section D.5.1 to have the required signals loaded in MATLAB Workspace. If the scripts are executed with default values the results shown in Section 4.4.4.3 are reproduced, where the respective values are also printed into MATLAB Command Window. The notation of variables is straightforward.

If the evaluation of uncertainty has to be done on different data set, then the time for averaging input quantities as per lines

```
%% select time window for averaging the input quantities
TAvgStart=27;
TAvgStop=29;
IndAvg=TAvgStart*100:TAvgStop*100;
```

has to be changed to match the time window of some steady state braking situation. Similarly the analysis can be performed for different wheel of the truck by changing the value of variable `WhSel`, where 1 = FL wheel, 2 = FR wheel, 3 = DR1L wheel,..., 8 = TAR wheel.

The sensitivity analysis is done using the same script. Respective sections of the script are documented within the code. Result of the sensitivity analysis are the graphs shown in Section 4.4.4.4.